

ADA083264

The work reported in this document was performed at Lincoln Laboratory, a center for research operated by Massachusetts Institute of Technology. This work was sponsored by the Defense Advanced Research Projects Agency under Air Force Contract #19528-60-C-0672 (AFPA Order 3724).

This report may be reproduced to satisfy needs of U.S. Government agencies.

The views and conclusions contained in this document are those of the author and should not be interpreted as necessarily representing the official policies, either expressed or implied, of the United States Government.

This technical report has been reviewed and is approved for publication.

FOR THE COMMANDER

*Raymond E. Linnelle*  
Raymond E. Linnelle, Lt. Col., USAF  
Chief, SAC Lincoln Laboratory Project Office

MASSACHUSETTS INSTITUTE OF TECHNOLOGY  
LINCOLN LABORATORY

PATTERN DEGRADATION OF SPACE FED PHASED ARRAYS

*J. RUZE*  
*Division 3*

PROJECT REPORT SBR-1

5 DECEMBER 1979

Approved for public release; distribution unlimited.

LEXINGTON

MASSACHUSETTS

ABSTRACT

The far field pattern degradation of space fed phased arrays suitable for a space based radar is examined. The effects considered are:

Structural;

- 1) Axial lens surface distortions,
- 2) Uniform radial thermal expansion,
- 3) Axial and lateral feed displacements,

Electrical;

- 1) Element phase and amplitude excitation errors,
- 2) Failed elements.

An introductory section discusses the size, cost, and weight penalties of low sidelobe designs. The final section presents a method of phase compensation or coherence of large axial lens distortions.

Accession For	
NTIS GRA&I	<input checked="" type="checkbox"/>
DDC TAB	<input type="checkbox"/>
Unannounced	<input type="checkbox"/>
Justification	
By _____	
Distribution/ _____	
Special Access Codes	
Dist	Avail and/or special
P	

CONTENTS

ABSTRACT	iii
1. INTRODUCTION	1
2. NATURE OF IDEAL RADIATION PATTERNS	3
3. PRACTICAL LIMITATIONS ON ANTENNA SIDELOBES	11
3.1 Antenna Spatial Distortions	11
3.2 Aperture Blockage	12
3.3 Aperture Excitation Errors	13
3.4 Failed Elements	16
4. DISTORTION SENSITIVITY OF DIVERS ANTENNAS	19
5. COMPUTATION OF ANTENNA PATTERNS	23
6. AXIAL DISTORTIONS	26
6.1 Bowl	26
6.2 Linear Fold	31
6.3 Quadratic Fold	38
6.4 Quadratic Astigmatism	52
6.5 Sinusoidal Astigmatism	64
6.6 Eight and Sixteen Gore	75
6.7 Half Linear Fold	105
7. RADIAL DISTORTIONS	113
7.1 Uniform Thermal Expansion	113
8. FEED DISPLACEMENT	117
8.1 Axial	117
8.2 Lateral	118
9. THREE DIMENSIONAL ARRAYS AND PHASE COMPENSATION	119

10. CONCLUSIONS	129
10.1 Electrical and Structural Defects	129
10.1.1 Electrical	129
10.1.2 Structural	129
10.2 Phase Compensation	130
ACKNOWLEDGMENTS	132
REFERENCES	133
APPENDIX	134
A-1 Axial Displacements	134
A-2 Radial Displacements	136

## 1. INTRODUCTION

Recently interest has been expressed in a large aperture Space Based Radar for earth surveillance. There is general agreement that such a structure should consist of a space fed phased array. There are significant advantages to this type of antenna namely:

- 1) The antenna beam can be electronically scanned over the earth's field of view.
- 2) The structural tolerances of a space fed lens are at least an order of magnitude greater than a corporate fed phased array or a reflect array.
- 3) A space feed is a very efficient means of element excitation compared to a corporate feed when a large number of elements are involved. It is frequently used in large ground base installations requiring two dimensional beam scanning.
- 4) Monopulse operation is readily obtained by use of an appropriate monopulse feed. This is obtained essentially without beam distortion whereas a corporate feed requires separate sum and difference illumination functions to obtain low sidelobes in the sum and difference modes.

Radar system studies have indicated that the probable frequency of operation would lie in the region from L to X band. Depending on frequency and satellite altitude the antenna diameter may range from 30 to 100 meters. Present requirements are that it be space transportable by one space shuttle load and that the structure be self deployable. Such a structure must be extremely

light weight and will be subject to thermal and station keeping stresses. Such stresses will create distortions of the planar lens surface.

It is the purpose of this memorandum to calculate the radiation patterns of a space fed array subject to various array distortions. As these distortions are not presently known divers canonical distortions have been assumed. The normal modes of a circular membrane at first suggested themselves.<sup>[1]</sup> However, these are not particularly applicable as our antenna may not be rigidly clamped at the rim. Instead, various possible simple distortions were used. Undoubtedly, the motion of the space antenna will be very complex being a superposition of the simple types assumed. The computer program employed is flexible so that when the structurally computed strains are known they can be inserted.

It is believed that this handbook of antenna patterns will prove useful to structural and thermal analysts and also for radar clutter calculations.

## 2. NATURE OF IDEAL RADIATION PATTERNS

It is planned that on transmission a uniformly illuminated aperture be used to take advantage of the entire available aperture and the power available from the element transmitters in the active array. Neglecting for the present all losses, aperture errors and blockage such an aperture has a gain of  $\left(\frac{\pi D}{\lambda}\right)^2$ ; a HPBW of  $1.02 \lambda/D$  radians; a first sidelobe of 17.6 dB; and a theoretical sidelobe envelope that has a power decay of:

$$p(u) = \frac{8}{\pi} \frac{1}{u^3} \approx \frac{2.55}{u^3} \quad (1)$$

where

$$u = \frac{\pi D}{\lambda} \sin \theta \quad (2)$$

" $\theta$ " being the angle off beam peak and  $D/\lambda$  the antenna diameter in wavelengths.

Of interest is where the sidelobe envelope attains isotropic (0 dBi) or the -10 dBi level. For the uniform illumination considered these levels occur at the angles defined by:

$$\sin \theta_0 = 0.932 \left(\frac{\lambda}{D}\right)^{1/3} \approx \sqrt[3]{\text{HPBW}} \quad (3)$$

$$\sin \theta_{-10} = 2.01 \left(\frac{\lambda}{D}\right)^{1/3} \approx 2 \sqrt[3]{\text{HPBW}} \quad (4)$$

So that for typical HPBW's under consideration we have the table

<u>HPBW</u>	$\frac{+ \theta}{- \theta}$	$\frac{+ \theta}{- \theta} -10$
1° (0.0175 r)	15°	31°
0.1° (0.00175 r)	6.9°	13.8°

We note that depending on orbit, for uniform illumination, a good part of the earth's FOV is above isotropic levels.

For the receive mode a low sidelobe illumination taper is desired to suppress ECM interference. For computation purposes a truncated Gaussian function of the form

$$f(r) = e^{-2r^2} \quad (5)$$

has been used. This illumination has an edge taper of -17.4 dB and an aperture efficiency of 76% so that the gain is:

$$G = 0.7616 \left( \frac{\pi D}{\lambda} \right)^2 \approx \frac{3}{4} \left( \frac{\pi D}{\lambda} \right)^2 \quad (6)$$

and the

$$\text{HPBW} = 1.25 \lambda/D \text{ radians} \quad (7)$$

The first sidelobe is about -34 dB and the sidelobe decay rate is

$$p(\theta) = \frac{0.25}{u^3} \quad (8)$$

That is a sidelobe envelope 10 dB below the uniform case and we have the corresponding table for the isotropic and -10 dBi levels:

<u>HPBW</u>	<u><math>\pm \theta_0</math></u>	<u><math>\pm \theta_{-10}</math></u>
$1^\circ (0.0175 \text{ r})$	$5.4^\circ$	$11.7^\circ$
$0.1^\circ (0.00175 \text{ r})$	$2.5^\circ$	$5.4^\circ$

We can summarize this data in the following table

Illumination	Uniform	$e^{-2r^2}$
Gain	$\left(\frac{\pi D}{\lambda}\right)^2$	$0.76 \left(\frac{\pi D}{\lambda}\right)^2$
HPBW (radians)	$1.02 \lambda/D$	$1.25 \lambda/D$
Rim Taper	0 dB	-17.4 dB
First Sidelobe	-17.6 dB	-34 dB
Sidelobe Decay (power)	$2.55/u^3$	$0.25/u^3$
Isotropic Level $\theta_0^\circ$		
HPBW = $1^\circ$	$15^\circ$	$5.4^\circ$
HPBW = $0.1^\circ$	$6.9^\circ$	$2.5^\circ$
-10 dBi Below Isotropic Level		
HPBW = $1^\circ$	$31^\circ$	$11.7^\circ$
HPBW = $0.1^\circ$	$13.8^\circ$	$5.4^\circ$
Relative Antenna Area For Same HPBW	1.0	1.50

These theoretical results are of interest as they set the limits on antenna performance. Although the tapered illumination has lower sidelobes it requires a 50% increase in antenna area for the same HPBW or resolution - with a corresponding increase in the number of elements, modules, etc.

Aperture illuminations can be theoretically designed to yield any specified sidelobe level. In Fig. 1 we plot the increase in the number of elements required for a specified HPBW for the frequently used circular Taylor distribution<sup>[2]</sup> against the desired near-in sidelobe level. The near-in sidelobe level is of special importance as it is subject to earth based ECM. The parameter  $\bar{n}$  determines the number of equal height sidelobes, subsequent sidelobes decay from this design value. It is evident that low sidelobe design - near isotropic level - requires larger arrays with their corresponding increase in cost and weight. Thinned arrays are not applicable for this application as they have relatively high far-out sidelobe levels and low array gain.

Figures 2 and 3 show the theoretical patterns for the uniform and the assumed Gaussian distribution with their asymptotic fall-off indicated.

The reader may wonder why we did not use an illumination function for which some optimum properties are claimed, such as the Taylor Circular Distribution. The truncated Gaussian was chosen due to analytic and computer convenience. The Taylor

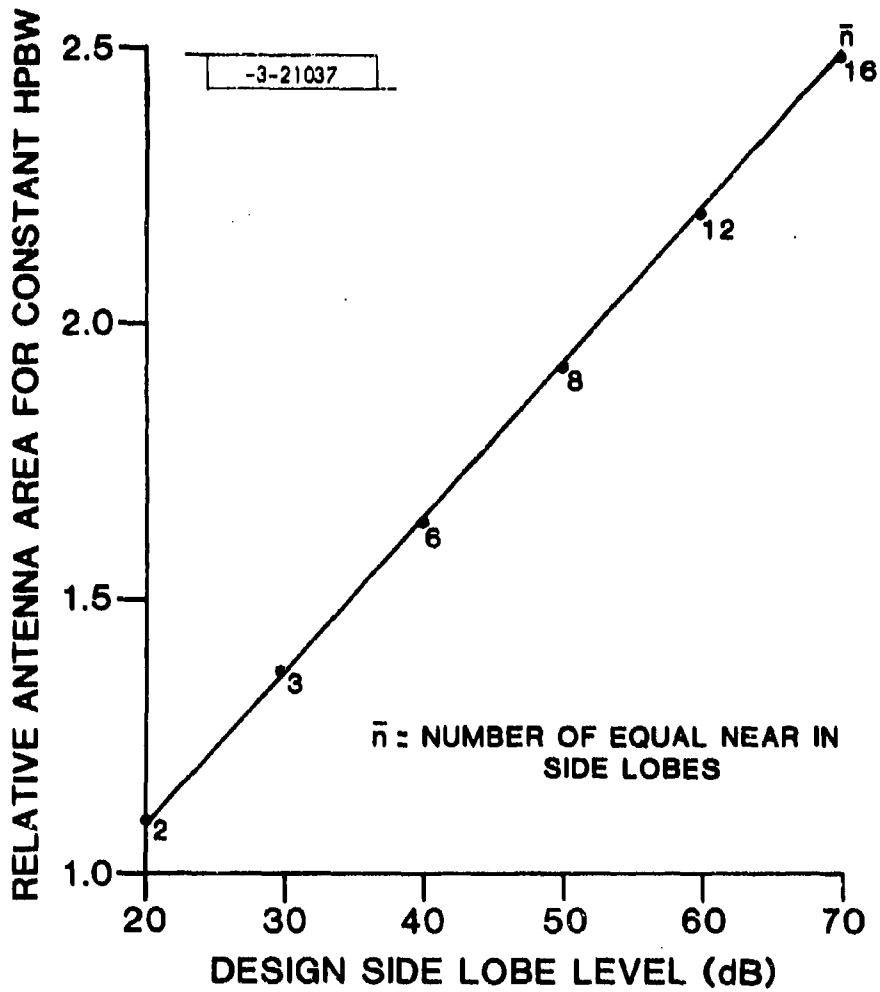


Fig. 1. Relative increase in area (number of elements, cost, and weight) for specified design sidelobe levels. Circular Taylor taper used.

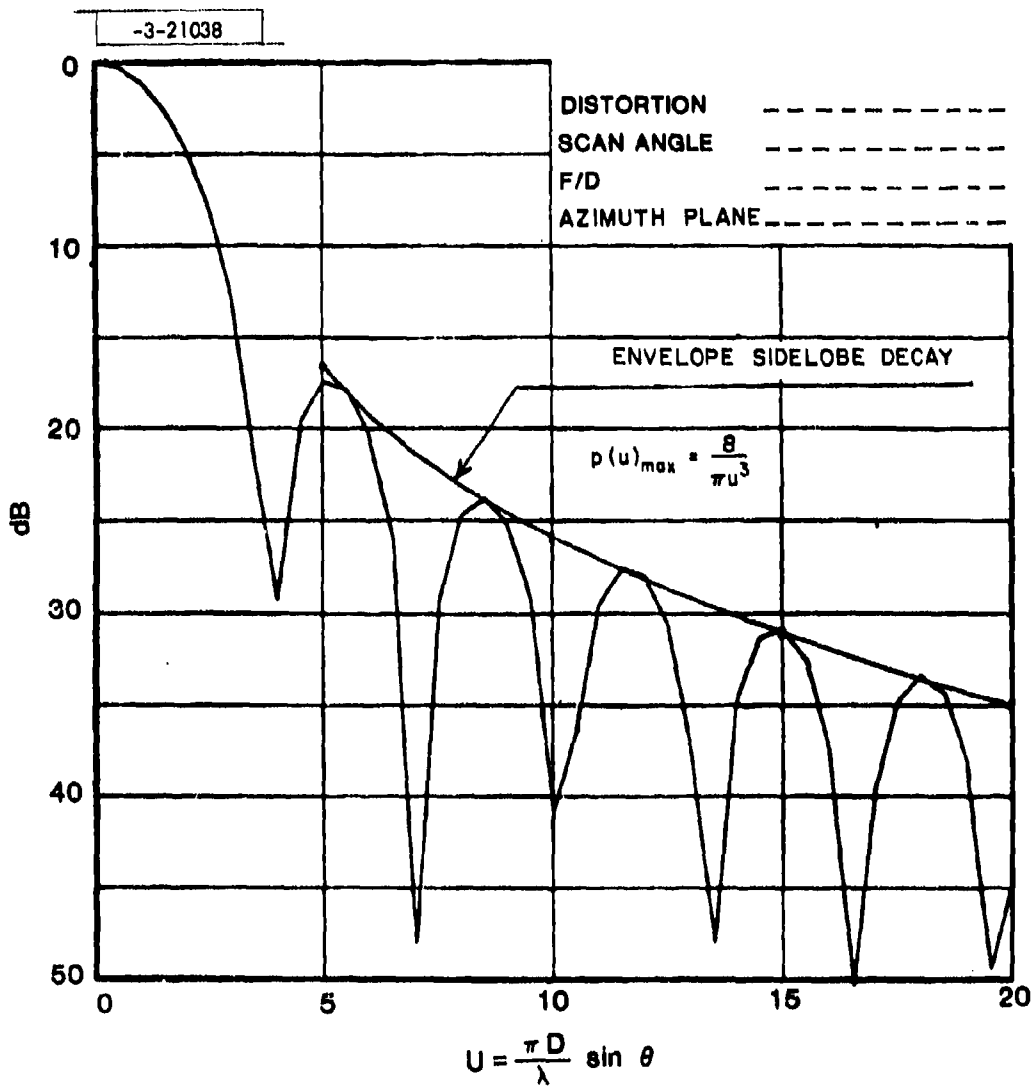


Fig. 2. Radiation pattern of space fed array uniform illumination  $f(r) = 1$ .

-3-21039

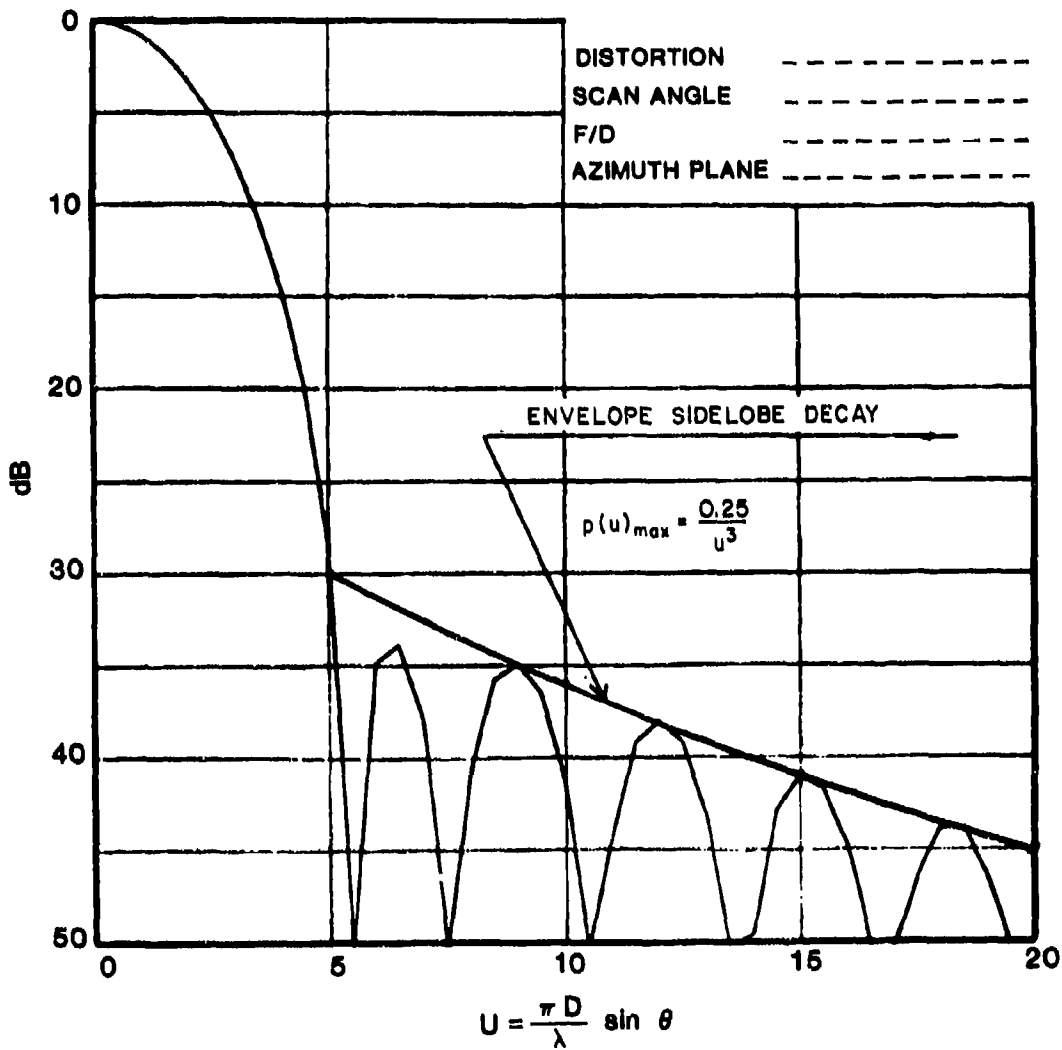


Fig. 3. Radiation pattern of space fed array Gaussian taper  $f(r) = e^{-2r^2}$ .

circular function yielding the same HPBW and gain has about a 4 dB lower first sidelobe; however, the first 5 sidelobes are of the same strength (-38 dB). Whereas with the truncated Gaussian the fifth sidelobe has already decayed to -43 dB. It was, therefore, concluded that for this degree of sidelobe suppression there was no significant advantage of either of these forms for these calculations or for the constructed antenna.

### 3. PRACTICAL LIMITATIONS ON ANTENNA SIDELOBES

#### 3.1 Antenna Spatial Distortions

It is expected that antenna surface distortions, whether we have a reflect array, corporate or space fed phase array, will have a low spatial frequency or that they may be considered smooth in wavelength measure. Distortions caused by structural or thermal strains will then occupy large portions of the antenna aperture and due to their long spatial period, will degrade the antenna pattern principally in the vicinity of the main beam and the first few sidelobes, leaving the far-out sidelobe region essentially undisturbed.

As the magnitude of the distortions is increased the pattern degradation further increases and also spreads out in angle. The latter is due in part to the shorter spatial period due to the removal of module  $2\pi$  from the phase front and also due to higher order terms in the expansion of the phase function.

### 3.2 Aperture Blockage

Some of the proposals for a large space fed array included an axial feed support (unipod). Such a support will not only block the center portion of the array but also, if of large diameter, disturb the primary pattern of the feed. It is believed that a strut feed support to the rim of the array will be desirable. As the effect on the feed primary pattern is not readily calculable feed support aperture blockage was not included in these calculations.

Another form of aperture blockage, not included, is the presence of seams and hinges, necessary for space deployment. The effect is similar to that of strut blockage in a parabolic reflector.

We have also assumed that the array elements are placed on a uniform square grid. This is not possible with a gore type of construction as the elements must be fitted into the available space.

There is no doubt that the above factors will further degrade the antenna pattern especially in the low sidelobe region. However, our neglect is not without its benefit as it places the pattern degradation due to spatial distortion in evidence.

### 3.3 Aperture Excitation Errors

The pattern of a constructed array, outside of the main beam and first few sidelobes, bears little relation to the theoretically desired pattern. The reason for this is that we have not achieved our theoretical aperture distribution in our model. The radiation pattern, in the low sidelobe region, is determined not by our theoretical aperture distribution but by the aperture excitation errors.

Nevertheless, if the aperture excitation plus errors are known the pattern can be computer calculated. This is generally not the case and recourse is made to estimates of the errors and statistical methods. Based on some reasonable statistical assumptions it can be shown that the average sidelobe level referred to the beam peak is

$$\overline{\text{SLL}} = \frac{\overline{\phi^2} + \overline{\Delta^2} + (1-P)}{\eta PN} \quad (9)$$

where

$\overline{\phi^2}$  = mean square phase error (radians)

$\overline{\Delta^2}$  = mean square fractional amplitude error

(1-P) = fraction of failed elements

N = number of independent elements.

P = fraction of elements active

$\eta$  = aperture illumination efficiency

As the gain of the array for half wavelength spaced elements is " $n\pi PN$ " the average sidelobe level referred to the isotropic level is:

$$\overline{SLL}_o = \pi [(1-P) + \overline{\phi^2} + \overline{\Delta^2}] \quad (10)$$

Equations (9) and (10) give statistical average levels. The peak sidelobe level may be as much as 10 dB above the average value. Whether this peak value occurs for a given array depends on the number of samples taken - that is pattern cuts, frequencies and scan angles.

Fig. 4 shows the phase and amplitude tolerance required for a -10 dBi average and peak sidelobe level. We note that to achieve an average SLL due to excitation errors we require a  $10^\circ$  rms phase only tolerance or a 1.5 dB rms amplitude only tolerance. Combinations of phase and amplitude errors may be obtained from these curves. For a guaranteed -10 dBi peak sidelobe we require about one third of these values. The excitation error sidelobes must be added to those due to the theoretical excitation. In the far sidelobe region the latter are negligible for a tapered aperture.

It may appear that to achieve an average SLL of -10 dBi would not be too difficult as we require only about  $7^\circ$  rms phase error and a 1 dB amplitude error (if phase and amplitude errors are equally divided). However, a four bit phase shifter has a

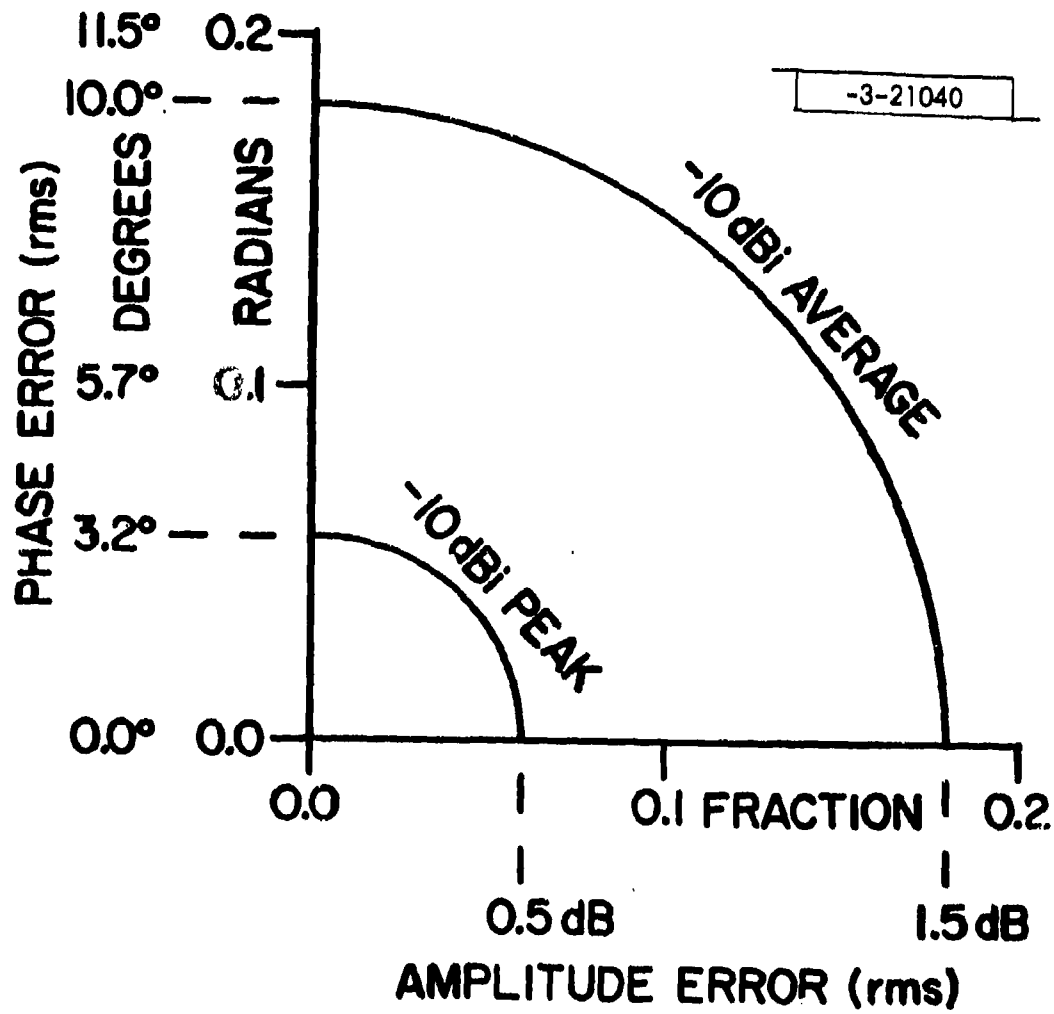


Fig. 4. Phase and amplitude tolerance required for -10 dBi average and peak sidelobe level.

bit quantization error of 6.5 degrees rms, a typical manufacturing error of 5 degrees rms, to which must be added line length errors, measurement errors, module errors, mismatch errors, mutual coupling errors etc.

Typical ground based optically fed phase arrays have average SLL of -5 to -8 dBi in the distant sidelobe region.

### 3.4 Failed Elements

In any spaced based array the number of failed elements must be considered. Equations (9) and (10) show this effect on the average sidelobe level on the assumption that the failed elements do not radiate and are randomly located.

Fig. 5 shows this effect for elements located on a half wave spaced grid for an array with no amplitude and phase errors for the remaining active elements. We note that to achieve a -10 dBi average sidelobe level only 3% element failure is allowable and 30% failure yields isotropic levels.

Fig. 5 is also applicable to purposely thinned arrays. We note that element thinning is not applicable for low sidelobe design and Fig. 5 indicates that for highly thinned arrays the sidelobe level approaches the gain of one element which for our half wave grid spacing is  $P_i(+5 \text{ dBi})$ .

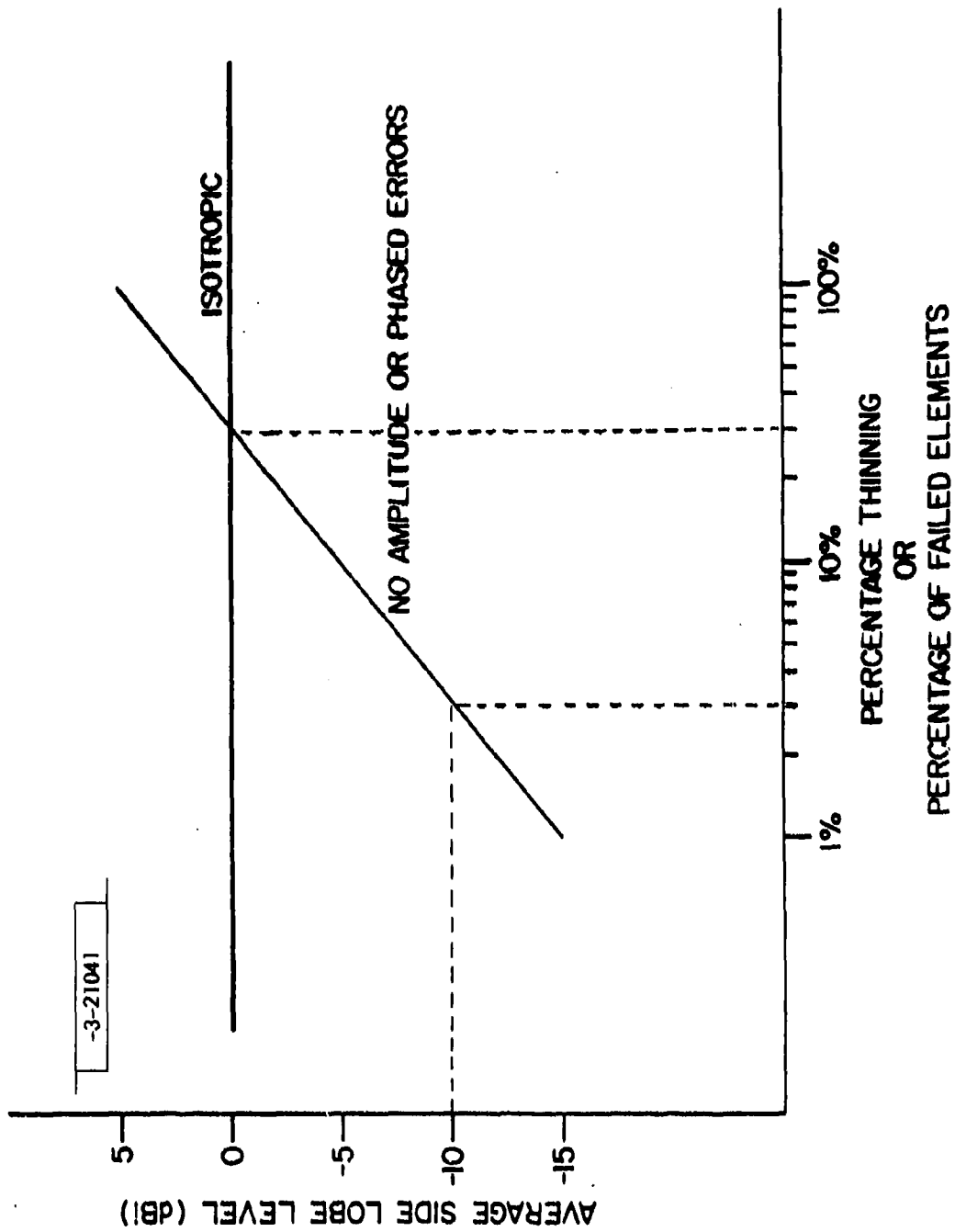


Fig. 5. Effect of failed elements or element thinning on average sidelobe level.

The pattern degradation discussed in this section is cumulative - that is the effects of:

- a) lens surface distortion
- b) aperture blockage
- c) element excitation errors
- d) failed elements

must be added to the theoretical level as an incoherent power addition. The element statistical sidelobes ("c" and "d" above) do decrease with observation angle but for the half wave element spacing this effect varies only as the element pattern; about as the cosine square of the angle off boresight.

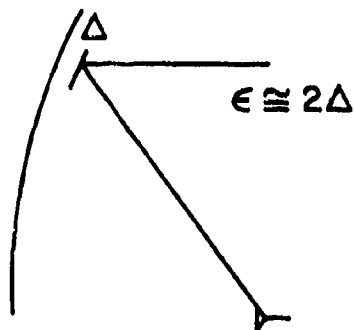
#### 4. DISTORTION SENSITIVITY OF DIVERS ANTENNAS

Fig. 6 shows three common antenna systems; a parabolic reflector, a corporate fed phased array, and a space fed phased array.

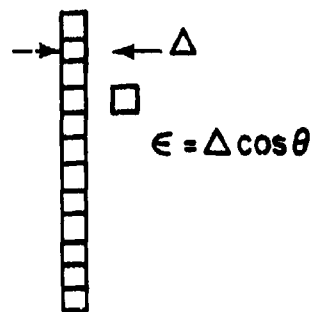
If the parabola's surface is distorted from the desired parabolic shape by an amount " $\Delta$ " the path length error created in the emerging wavefront approaches " $2\Delta$ ".

In contrast a similar distortion of a corporate fed phase array creates a path length error of only " $\Delta \cos \theta$ " where " $\theta$ " is the angle of observation or scan angle. A corporate fed phased array, in addition to its wide angle scanning capabilities, is less sensitive to surface distortion by a factor better than two than a reflector.

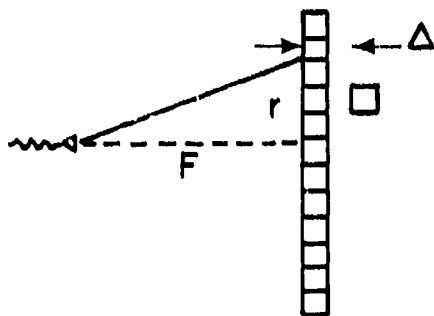
For a phased array with a large number of elements a corporate feed becomes inconvenient as each element must be fed by a transmission line with its inherent ohmic losses. It is common, in such cases, to employ a "space" or "optical" feed. Here the array consists of three layers; a backside comprising receptors (dipoles, waveguides, etc.) illuminated by a horn feed axially located at a focal distance, " $F$ ", a radiating or outside layer of radiators and a isolating layer or metal ground plane. The corresponding receptors and radiators are connected by a network whose function is to transfer power between the two layers



REFLECTOR



CORPORATE FED ARRAY



SPACE FED LENS

$$\epsilon \cong \Delta \left[ \frac{(r/2f)^2}{2} - 2 \sin^2 \frac{\theta}{2} \right]$$

$$f = F/D$$

-3-21042

Fig. 6. Axial distortion susceptibility of various antenna systems.

and to provide the necessary phase shifts to steer the radiated beam. The networks or "modules" may be passive (phase shifters only) or active (pre-amplifiers and transmitters additional).

The path length error, " $\epsilon_a$ " caused by an axial displacement, " $\Delta a$ " of a section of a space fed phase array is (derivation in Appendix A-1)

$$\epsilon_a = \Delta a \left[ \cos\theta - \frac{1}{\sqrt{1 + (r/2f)^2}} \right] \quad (11)$$

where  $\theta$  is the observation angle

$f$  is the f-number =  $F/D$

$r$  is the aperture radial coordinate, normalized to unity at the rim.

The second term of Equation 2 reduces the path length error, in fact phase array distortions that occur at the radial distance " $r_0$ " cause no main beam degradation at a scan angle given by

$$\tan \theta_0 = r_0/2f \quad (12)$$

Axial distortions at other radial distances will still degrade the main beam at  $\theta_0$ , or distortions at  $r_0$  will degrade the beam at scan angles other than  $\theta_0$ .

This form of axial error compensation considerably decreases the susceptibility of a space fed phased error to axial distortions and consequently permits larger distortions.

The compensating effect is quite complex and cannot be simply predicted as it depends on the position and magnitude of the distortion, the illumination excitation, the scan angles involved, and the "f" number of the system. However, as a round rule of thumb the space fed array is about one tenth as sensitive to axial distortion as a corporate fed array.

Further insight into the behavior of the compensating axial error can be seen from an approximate form of Eq. 11 obtained by expanding the radical:

$$\epsilon_a = \Delta_a \left[ \frac{1}{2} \left( \frac{r}{2f} \right)^2 - 2 \sin^2 \frac{\theta}{2} \right] \quad (13)$$

where we have retained only the dominant term. For zero scan angle we have

$$\epsilon_a = \Delta_a \left[ \frac{1}{2} \left( \frac{r}{2f} \right)^2 \right] \quad (14)$$

where it is evident that the path length error is reduced from the corporate fed value by the bracketed term, attaining a maximum value of one eight at the rim for an F/D=1.0. We note that the center element of the array produces no path length error when displaced for an broadside beam. This can be seen, physically, from Fig. 6.

A reflect array has the same susceptibility to axial distortion as a reflector and, therefore, commands no advantage.

## 5. COMPUTATION OF ANTENNA PATTERNS

Antenna patterns were computed basically by evaluating the integral

$$g(\theta, \phi) = \int_A f(r) e^{ju[x \cos \phi + y \sin \phi]} e^{j\epsilon_a(x,y)} dx dy \quad (15)$$

where  $(\theta, \phi)$  are the observation coordinates

$f(r)$  the illumination function, assumed real and circularly symmetric;

$$u = \frac{\pi D}{\lambda} \sin \theta$$

$x, y$  are the array coordinates normalized to unit radius

$\epsilon_a$  the path length error caused by the array distortions in radians

The integration is over the circular aperture so that points where  $x^2 + y^2 > 1$  are excluded.

For computer calculations the integration must be replaced by a summation

$$g(u, \phi) = \sum_i \sum_j f(r_{ij}) e^{ju[x_{ij} \cos \phi + y_{ij} \sin \phi]} e^{j\epsilon_a(x_{ij}, y_{ij})} \quad (16)$$

All patterns are normalized by the beam peak with no path length error.

Patterns are plotted in dB below beam peak. Zero dB then represents the no error on axis gain

$$G_o = \eta \left( \frac{\pi D}{\lambda} \right)^2 \quad (17)$$

This procedure resulted in sets of patterns plotted in universal coordinates, (u, dB). The "u" coordinate can be converted to spatial degrees if the antenna diameter and wavelength are known.

No element pattern is indicated in Eq. 15 as the HPBW's under consideration are in the tenths of degrees. For the scanned patterns the dB indicated should be reduced by

$$20 \log (\cos \theta)$$

which amounts to 0.54 dB for the 20 degrees scan angle usually employed.

The summation indicated in Eq. 16 was performed on a uniformly spaced square grid with 64 intervals on a principal diameter, a total of about 3200 points.

When the array is scanned to the angle  $(\theta_0, \phi_0)$  the elements must be phased according to:

$$\psi_{ij} = \frac{2\pi D}{\lambda} \sin \theta_0 [x_{ij} \cos \phi_0 + y_{ij} \sin \phi_0] \quad (18)$$

We calculated the pattern in the plan of scan where Eq. 16 becomes:

$$G(u, \phi_0) = \sum_i \sum_j f(r_{ij}) e^{j(u-u_0)[x_{ij} \cos \phi_0 + y_{ij} \sin \phi_0]} e^{j\epsilon_a(x_{ij}, y_{ij})} \quad (19)$$

the pattern abscissa is then  $(u-u_0)$  or distance from the beam peak in sine space. This procedure of presenting the data in selected " $\phi_0$ " planes was judged more illuminating than two dimensional contour plots. Although contour plots are more complete their generation was just not possible in view of the available computer time and the large amount of data presented.

Even with this reduction judgement had to be exercised as to what was to be plotted. The parameters generally used were:

taper function,  $f(r) = e^{-2r^2}$

scan angle  $\theta = 0,20^\circ$

f-number F/D - 1.0, 1.414, 2.0

distortion (axial and radial)

pattern cuts (as deemed significant but in the plane  
of scan)

## 6. AXIAL DISTORTIONS

Axial distortions, that is displacement of the elements normal to their planar positions are probably the most common to be experienced. They would occur due to incomplete deployment, thermal strains, station keeping torques, etc.

Although some radial displacement will accompany any axial displacement in a structure with some connection these are considered as second order effects and are neglected in this section

### 6.1 Bowl

Here we consider the lens surface distorted into a bowl, that is the planar surface becomes:

$$z = ar^2 \quad (20)$$

where "a" is the rim displacement.

Fig. 7 shows the planar surface and Fig. 8 the bowl distortion.

Fig. 9 shows the pattern degradation for various values of rim displacement for a corporate fed phased array; indicating that only about a quarter wave rim displacement is allowable. These curves can also be used for a reflector if the displacements are halved.

Fig. 10 shows a comparable curve for a space fed lens with a "f" number of unity and at a scan angle of zero. We note the marked decrease of distortion susceptibility of the optically

-3-21044

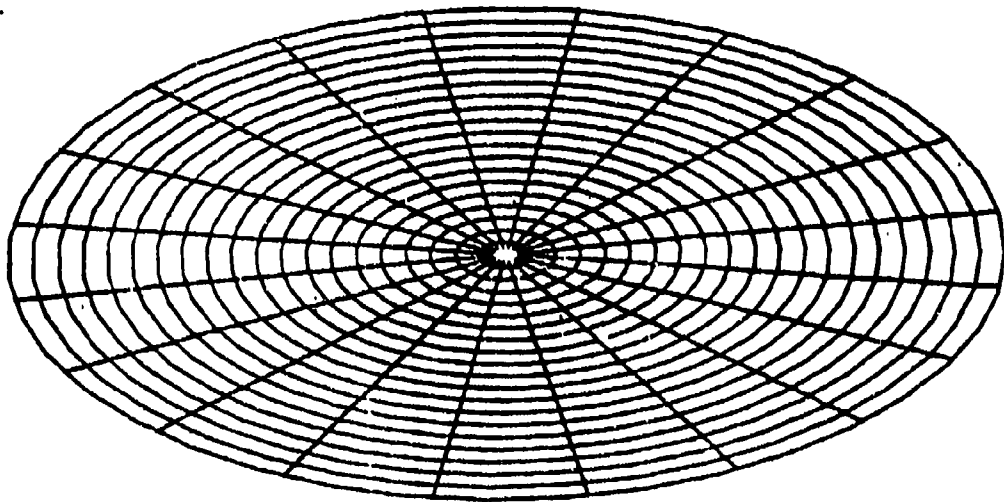


Fig. 7. Undistorted planar array.

-3-21045

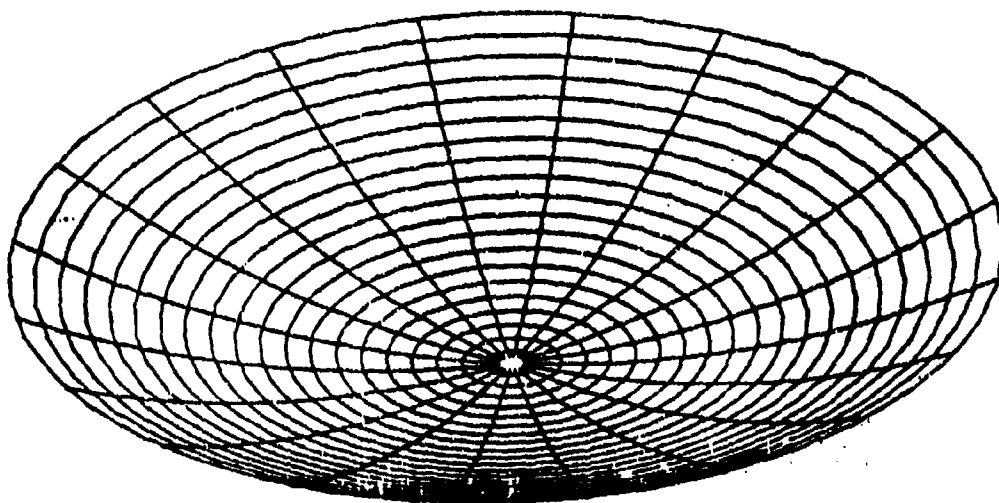


Fig. 8. Bowl distortion  $z = ar^2$ .

-3-21046

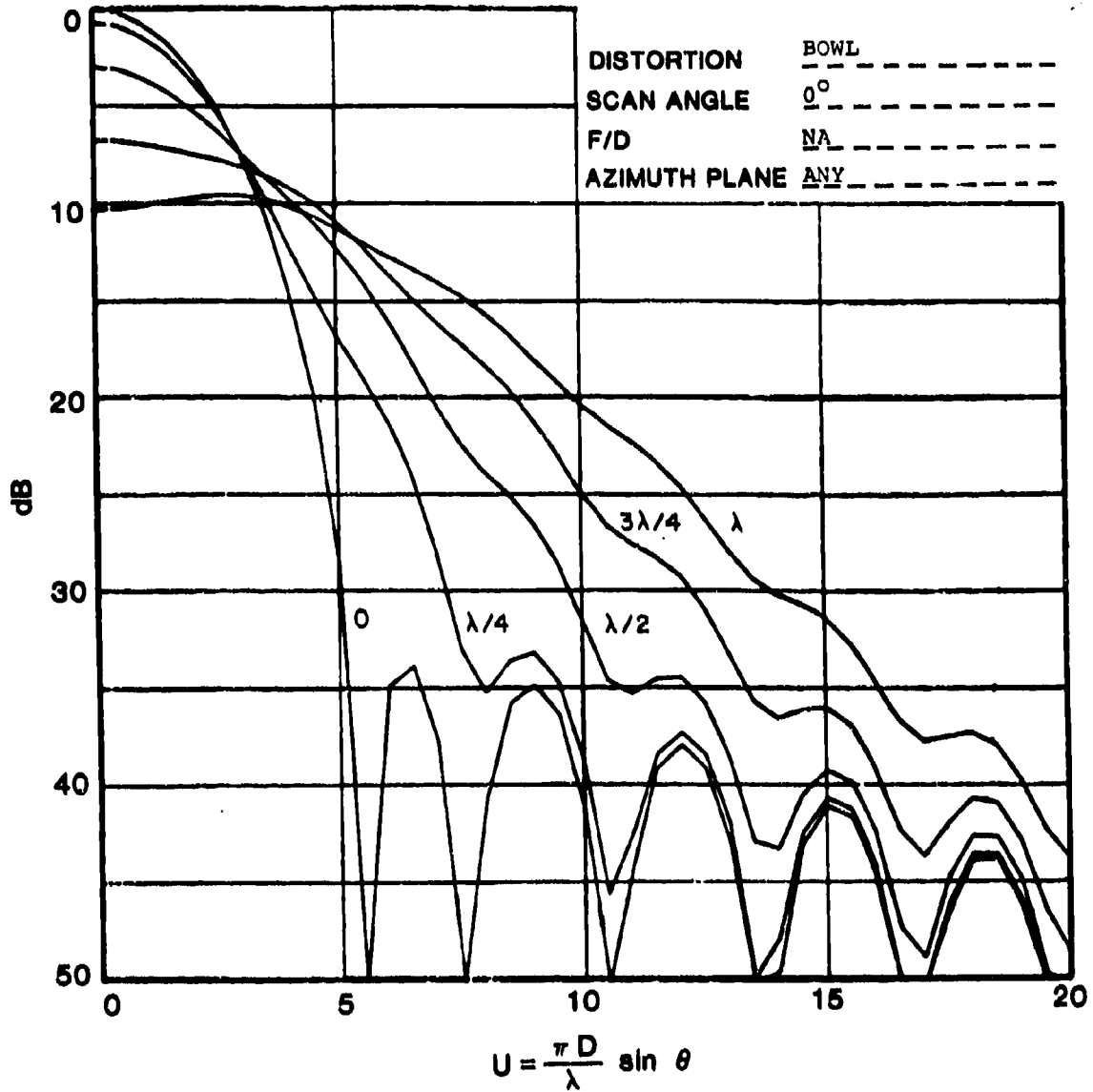


Fig. 9. Radiation patterns of corporate fed array  
Gaussian taper  $f(r) = e^{-2r^2}$ .

-3-21047

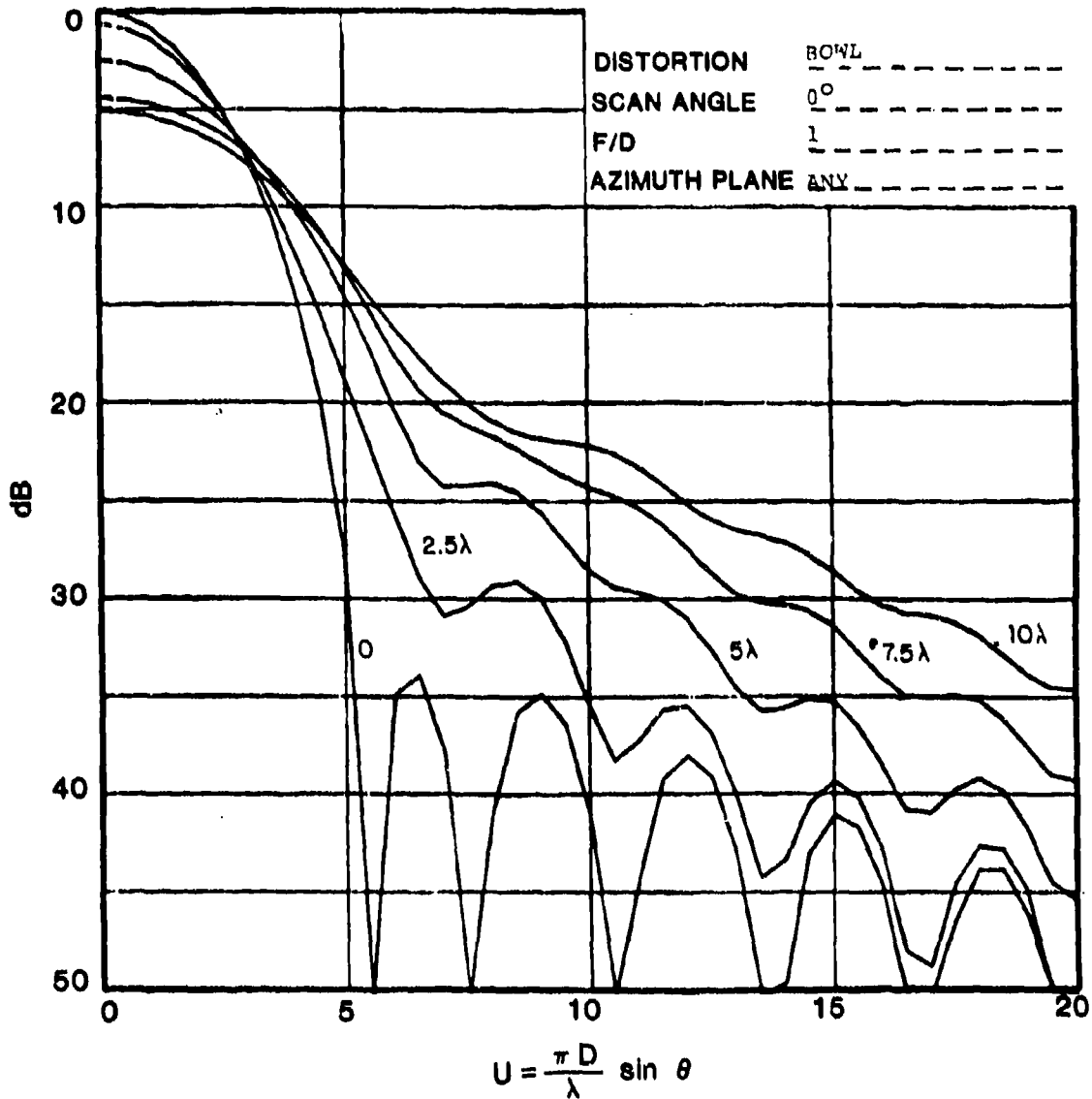


Fig. 10. Radiation patterns of space fed array  
Gaussian taper  $f(r) = e^{-2r^2}$ .

fed structure where a 2.5 wavelength rim displacement is tolerable.

Fig. 11 same as Fig. 10 but scanned to 20 degrees. We note the different shape of the degraded antenna patterns. This is due to the compensating nature of the path length errors. With

$$\Delta a = ar^2$$

we have from Eq. 13

$$\epsilon_a = a \left[ \frac{1}{2} \frac{r^4}{(2f)^2} - 2 r^2 \sin^2 \frac{\theta}{2} \right] \quad (21)$$

where we have a quadratic and a fourth order aberration that tend to compensate.

Fig. 12 and 13 are the same as Fig. 10 and 11 except that the "f" number is 1.414. We note that the compensation is more complete in Fig. 13.

Fig. 14 and 15 are the same as Fig. 12 and 13 except that the "f" number is 2.0. We have obviously over-compensated for this scan angle and "f" number. The smaller "f" number is preferred.

## 6.2 Linear Fold

This is a distortion where the space fed array is bent along a diameter. The distortion is portrayed graphically in Fig. 16 and is represented mathematically by:

$$z = z|y| \quad (22)$$

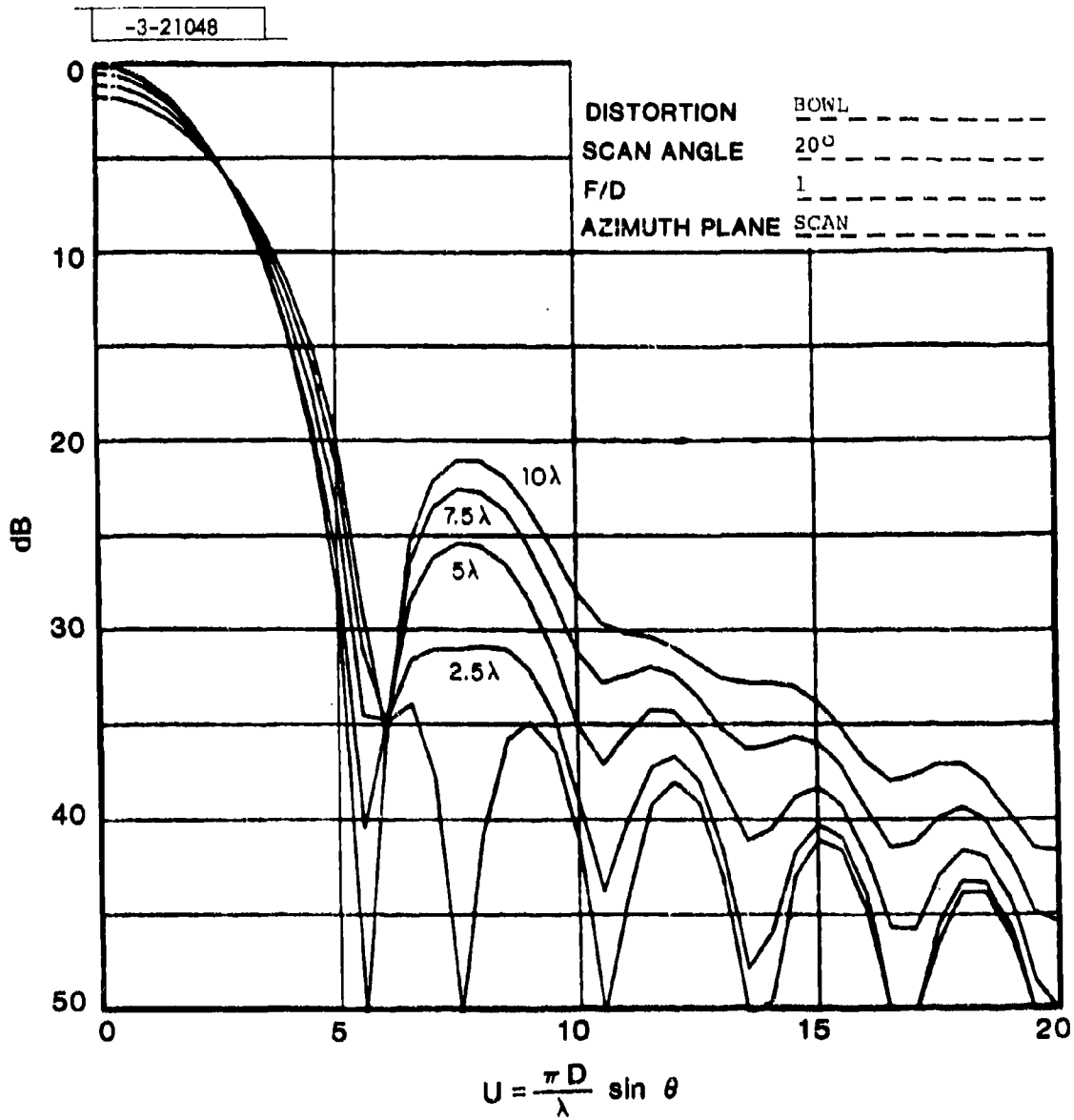


Fig. 11. Radiation patterns of space fed array  
 Gaussian taper  $f(r) = e^{-2r^2}$ .

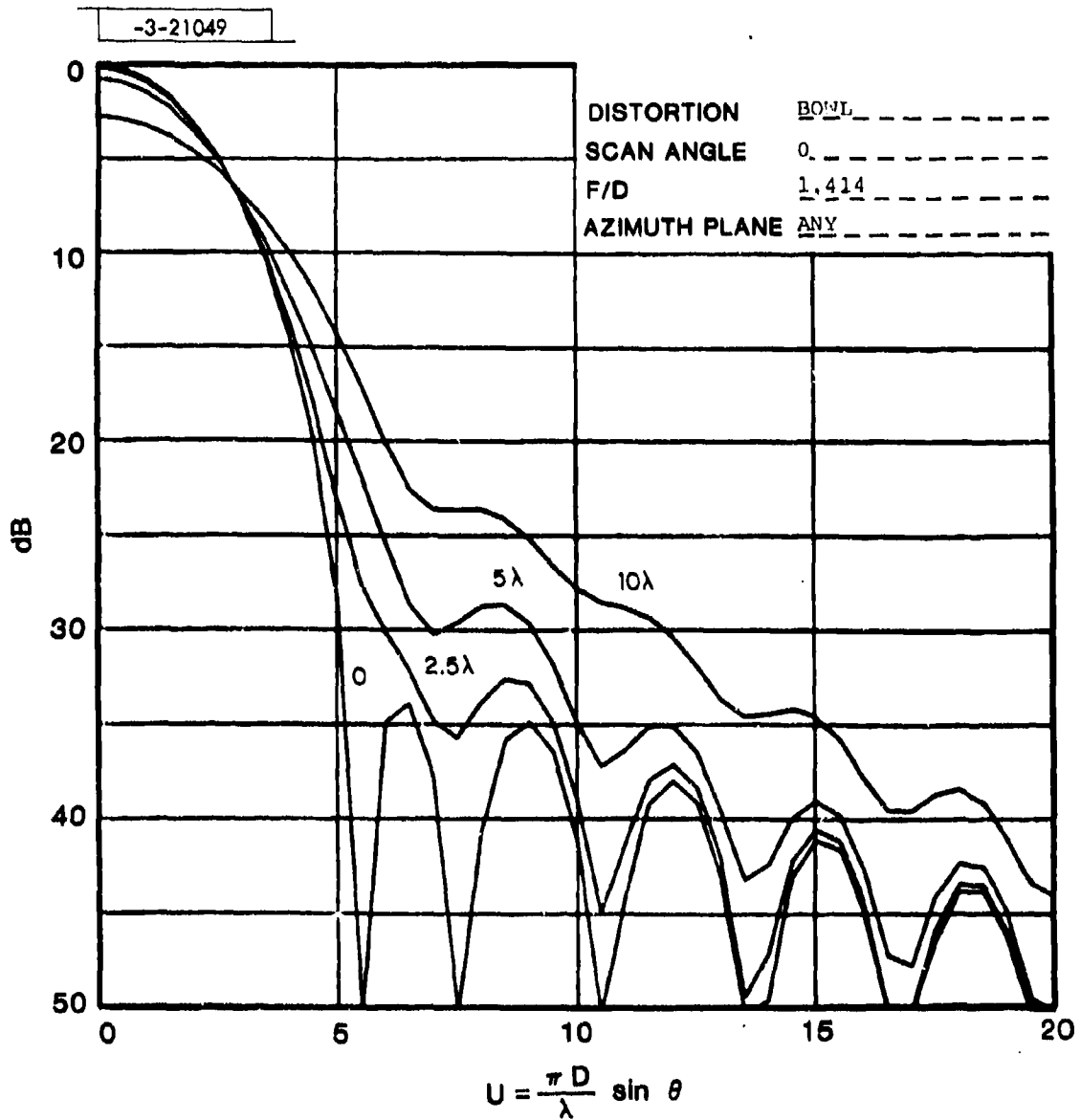


Fig. 12. Radiation patterns of space fed array Gaussian taper  $f(r) = e^{-2r^2}$ .

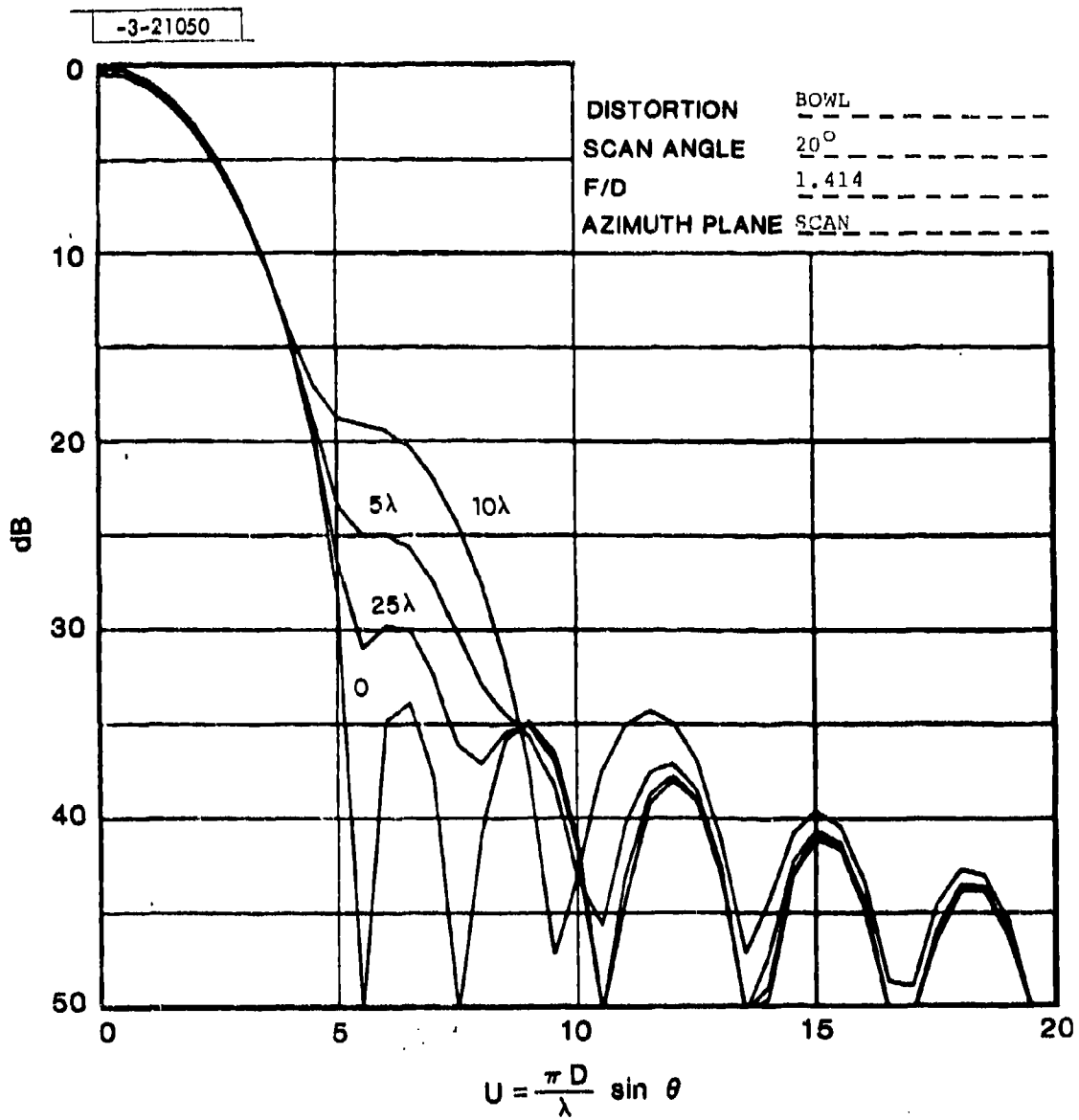


Fig. 13. Radiation patterns of space fed array Gaussian taper  $f(r) = e^{-2r^2}$ .

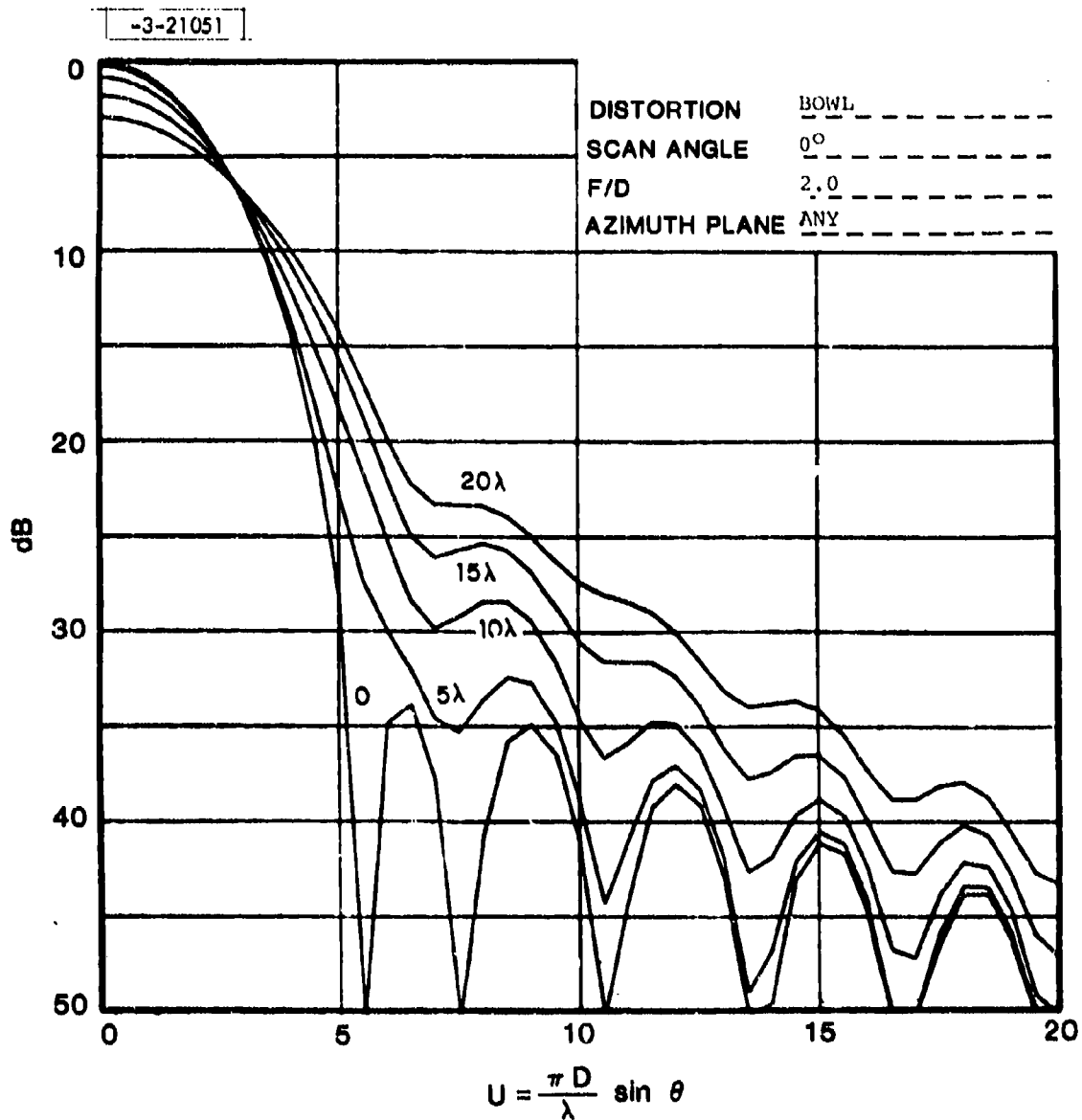


Fig. 14. Radiation patterns of space fed array Gaussian taper  $f(r) = e^{-2r^2}$ .

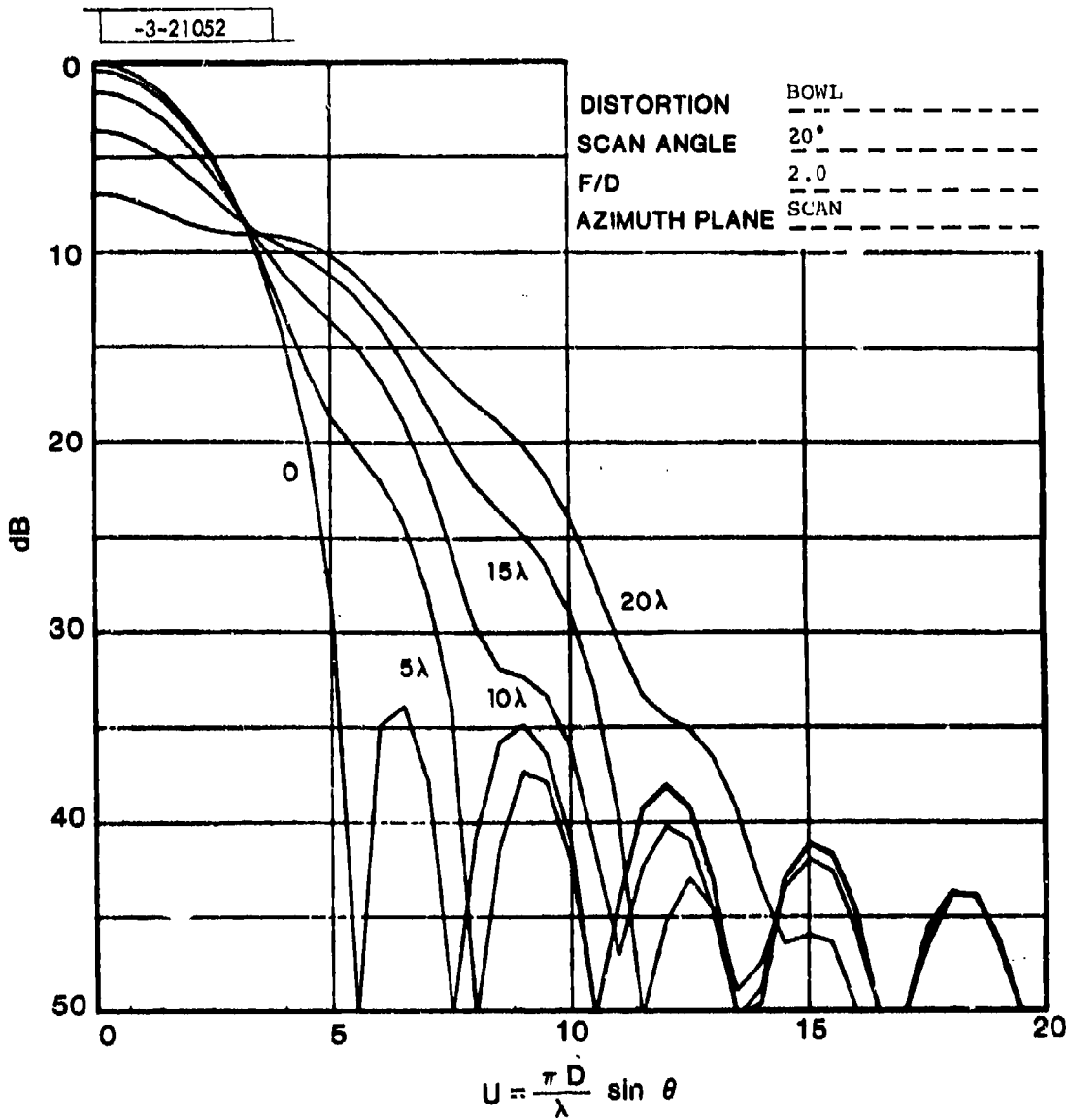


Fig. 15. Radiation patterns of space fed array Gaussian taper  $f(r) = e^{-2r^2}$ .

-3-21053

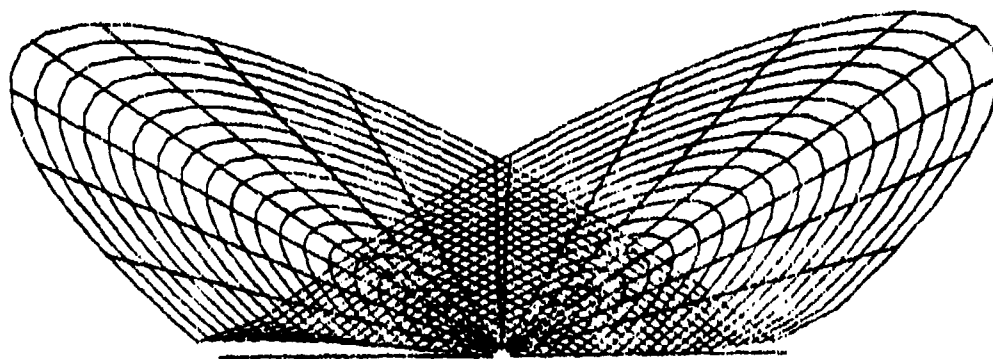


Fig. 16. Linear fold distortion  $z = a|y|$ .

As we no longer have azimuthal symmetry the pattern degradation will be different in various azimuth cuts.

Fig. 17, 18, and 19 show the degradation of the broad-side beam in the " $\phi$ " = 0, 45<sup>o</sup> and 90<sup>o</sup> azimuth cuts for a unity "f" number. The large differences between these cuts can be explained by collapsing the phase error excitation on the line of the cut taken. The tolerance criteria will then be determined by the worse cut, namely, Fig. 19. The axial gain reduction is, obviously the same for all azimuthal cuts.

Fig. 20, 21, and 22 are the same as the previous three except that the beam is scanned 20 degrees in the direction of the azimuth cut taken.

Figs. 23-28 inclusive are the same as the previous six except that the "f" number has been increased to 1.414.

### 6.3 Quadratic Fold

This distortion is similar to the linear fold except that the displacement from the diameter varies in a quadratic manner. It is shown graphically in Fig. 29 and mathematically represented by

$$z = ay^2 \quad (23)$$

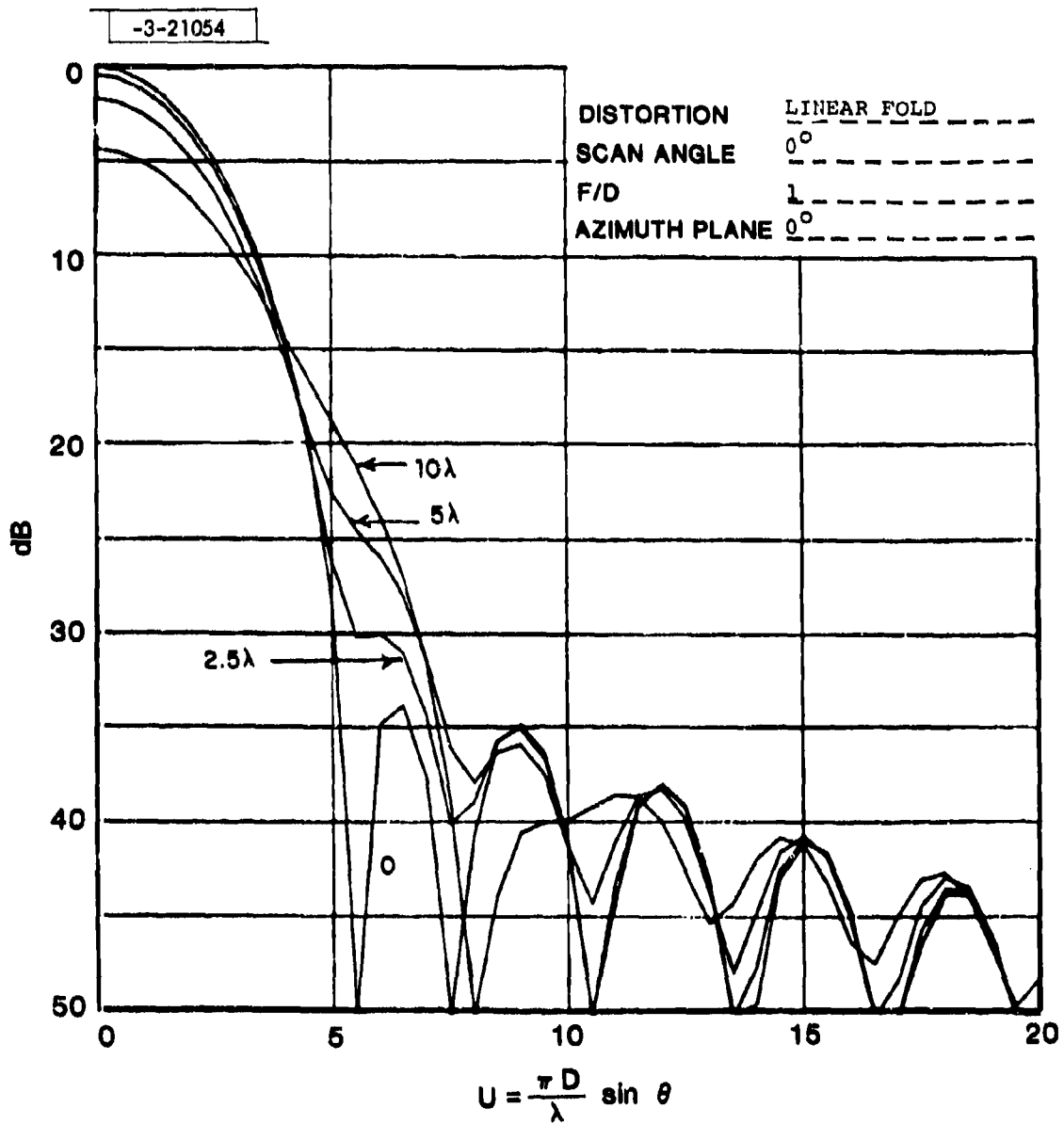


Fig. 17. Radiation patterns of space fed array Gaussian taper  $f(r) = e^{-2r^2}$ .

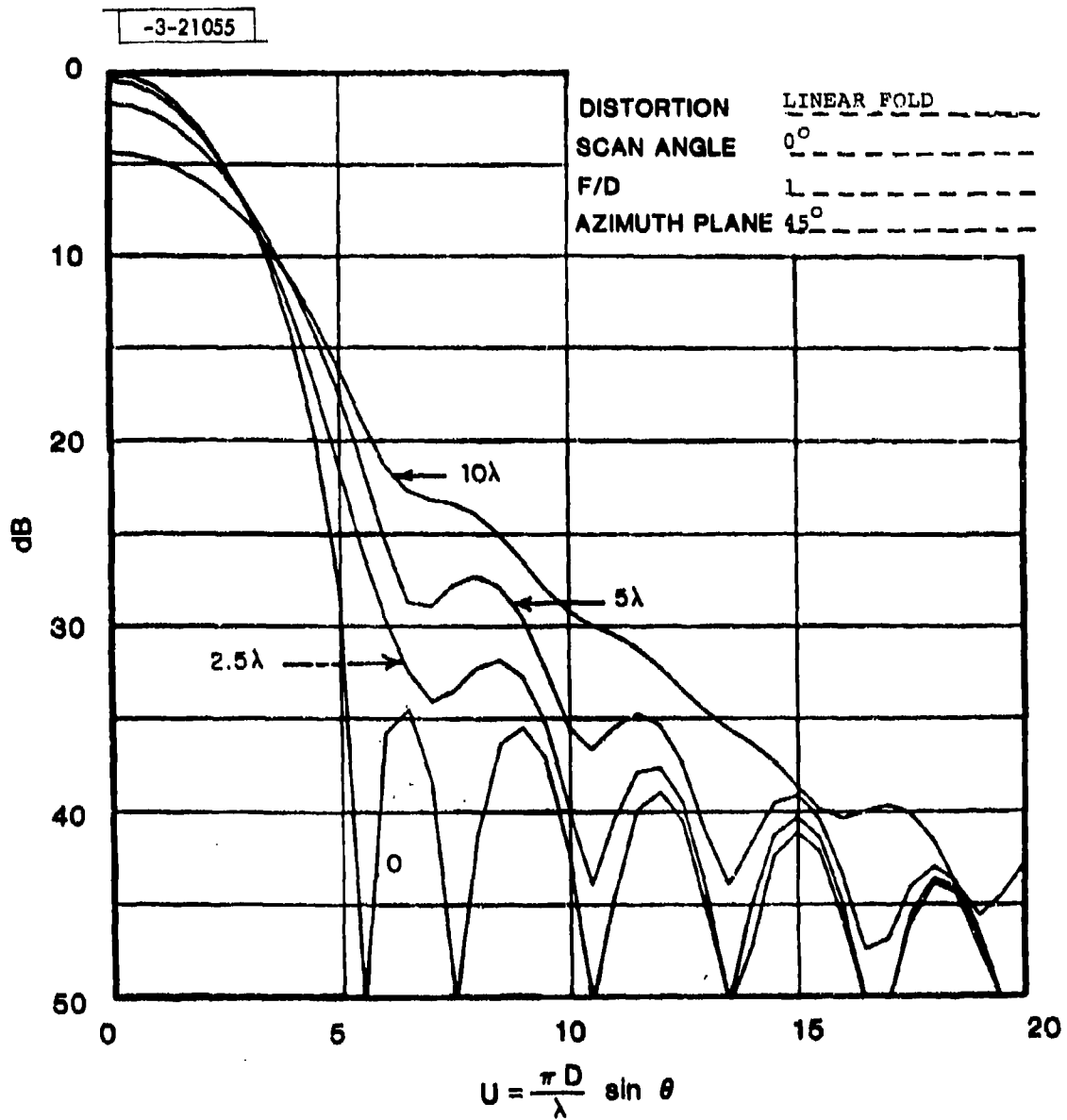


Fig. 18. Radiation patterns of space fed array Gaussian taper  $f(r) = e^{-2r^2}$ .

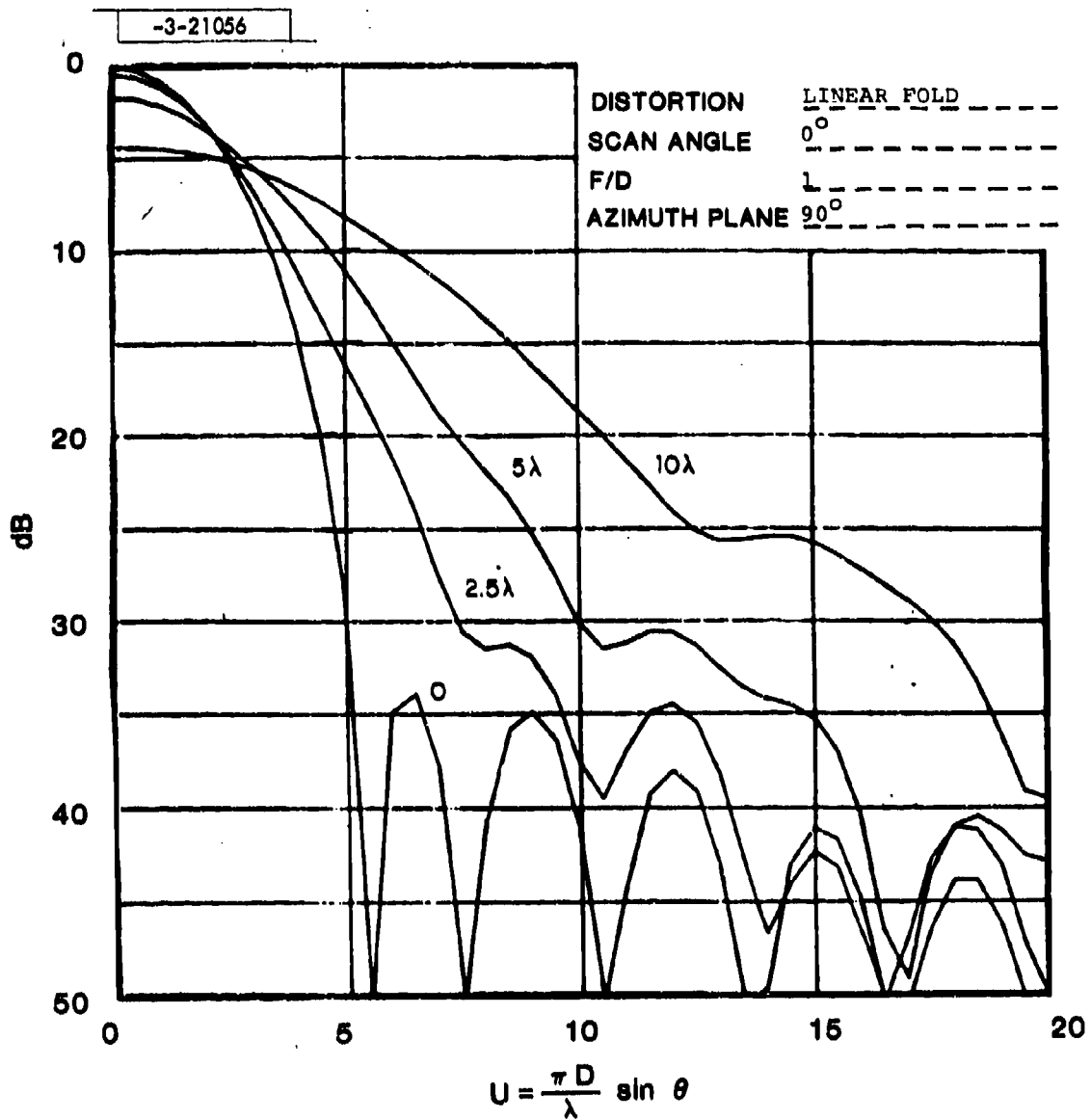


Fig. 19. Radiation patterns of space fed array Gaussian taper  $f(r) = e^{-2r^2}$ .

-3-21057

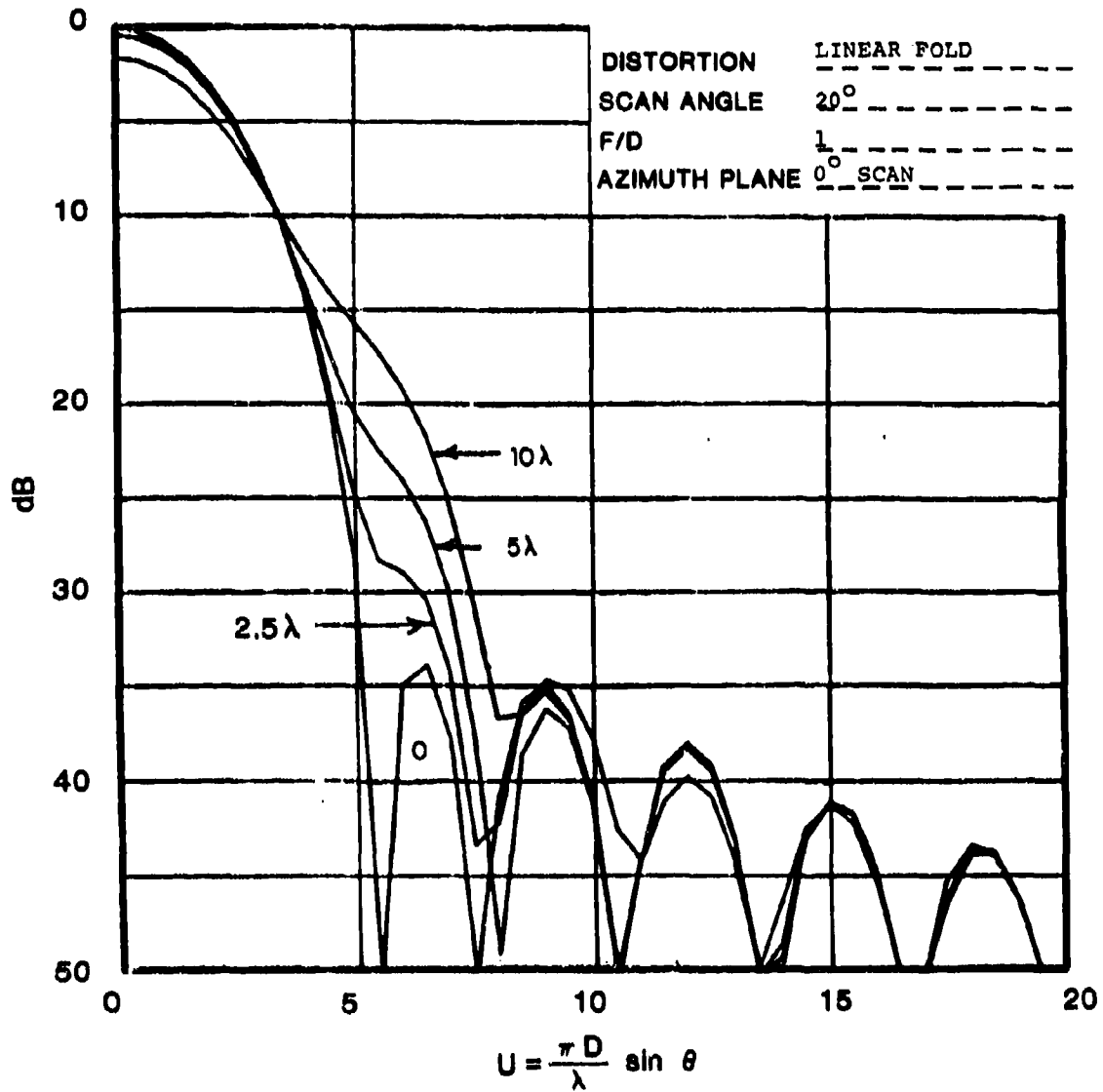


Fig. 20. Radiation patterns of space fed array Gaussian taper  $f(r) = e^{-2r^2}$ .

-3-21058

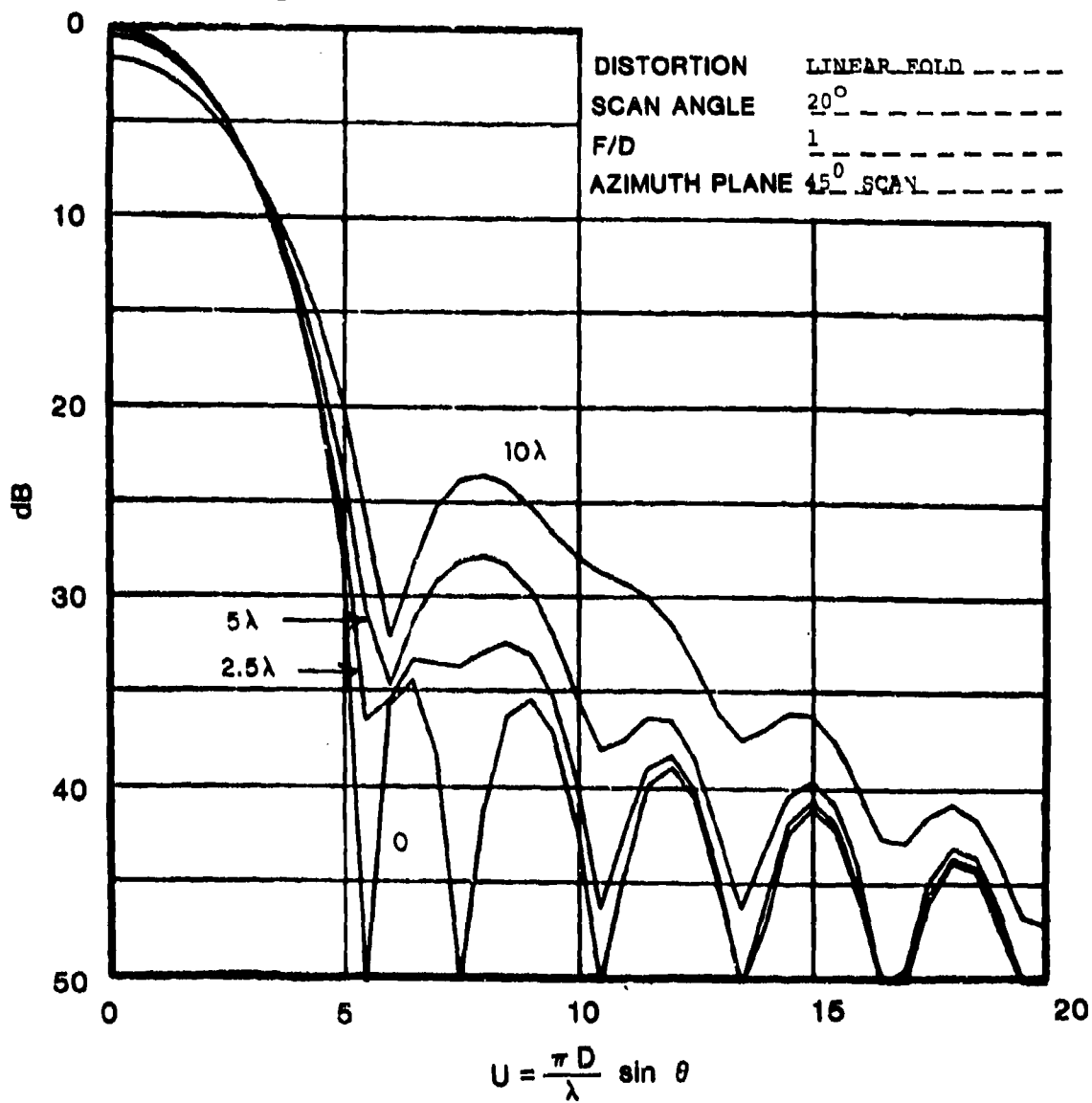


Fig. 21. Radiation patterns of space fed array Gaussian taper  $f(r) = e^{-2r^2}$ .

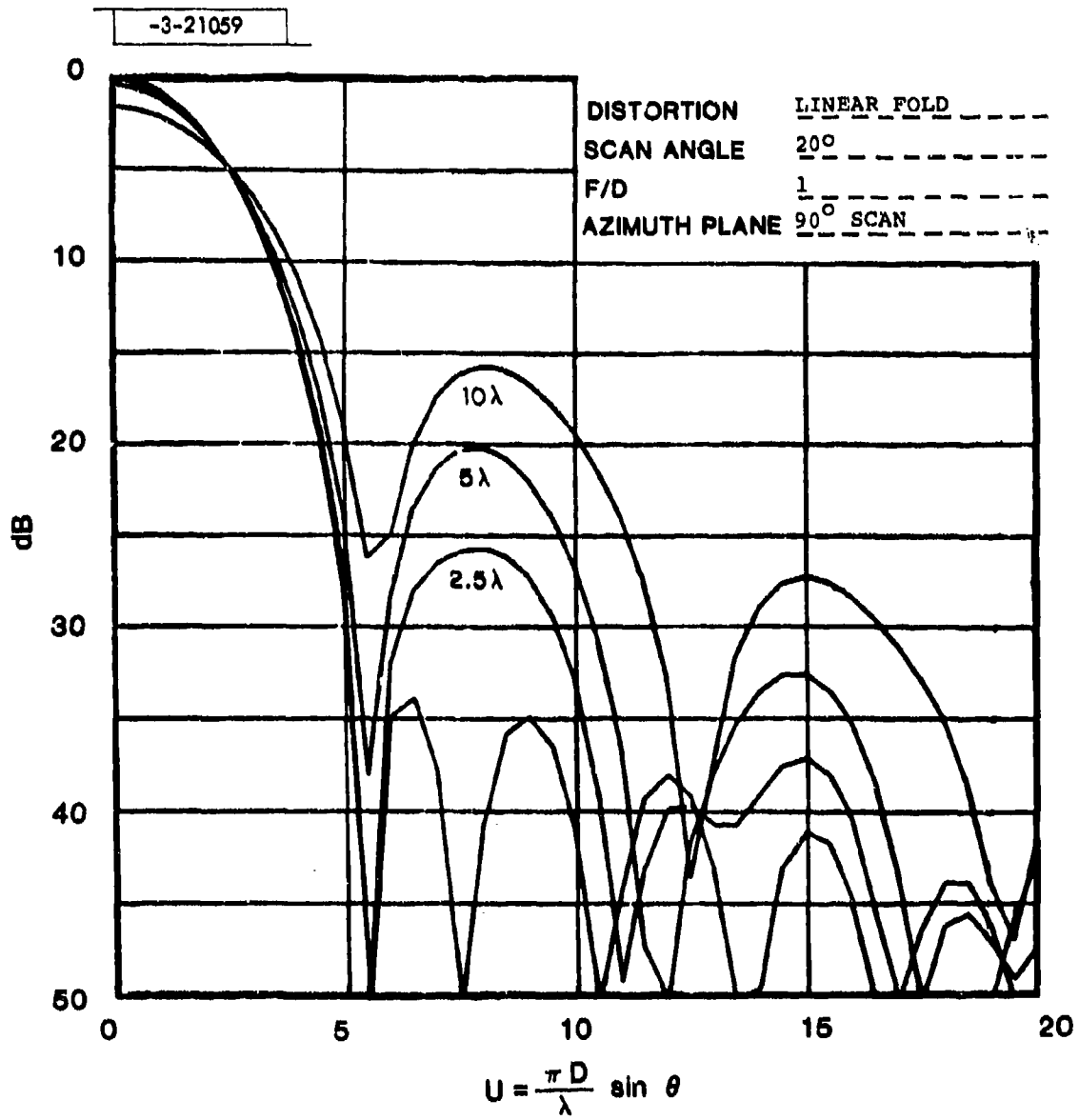


Fig. 22. Radiation patterns of space fed array Gaussian taper  $f(r) = e^{-2r^2}$ .

-3-21060

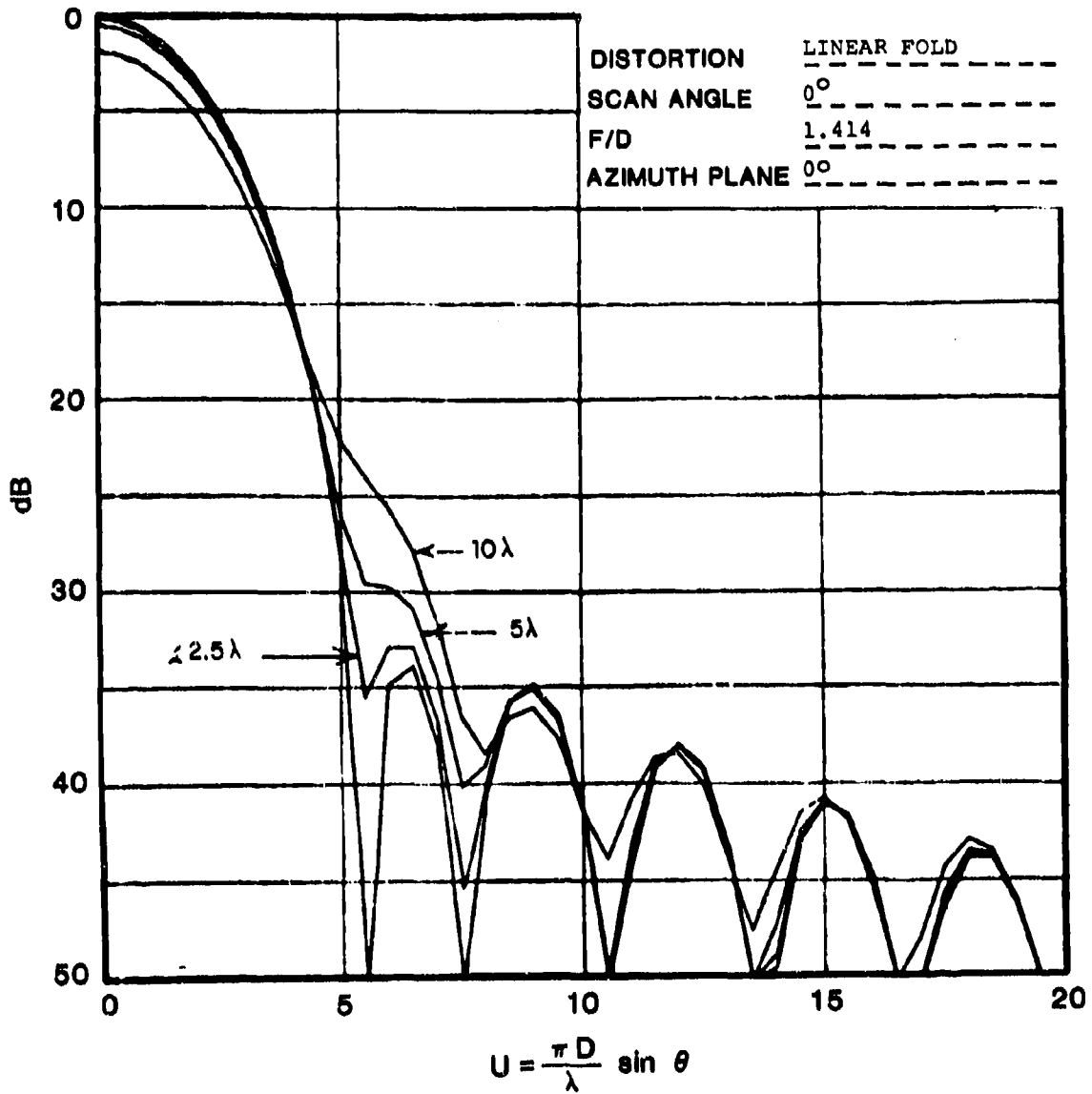


Fig. 23. Radiation patterns of space fed array Gaussian taper  $f(r) = e^{-2r^2}$ .

-3-21061

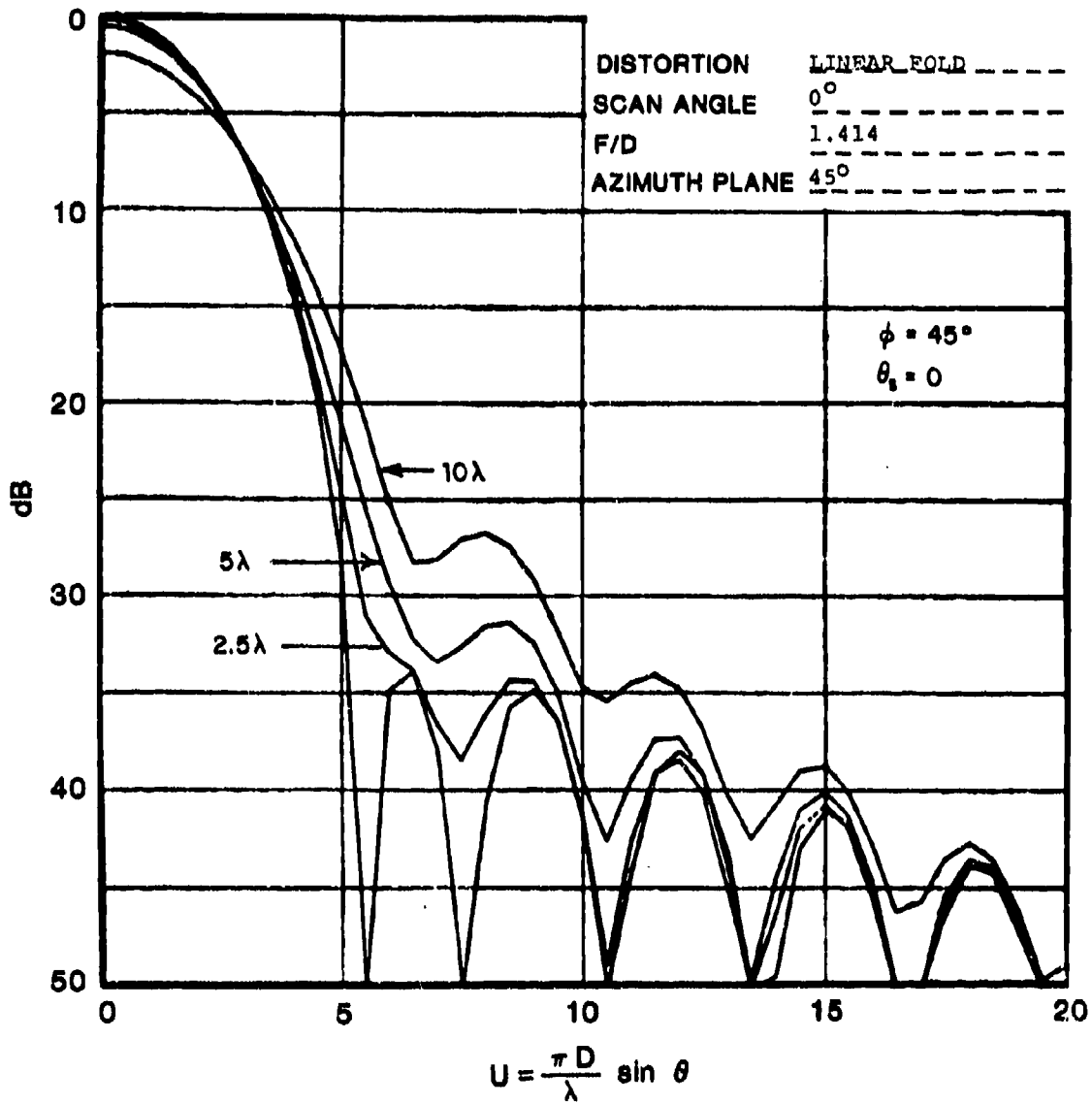


Fig. 24. Radiation patterns of space fed array Gaussian taper  $f(r) = e^{-2r^2}$ .

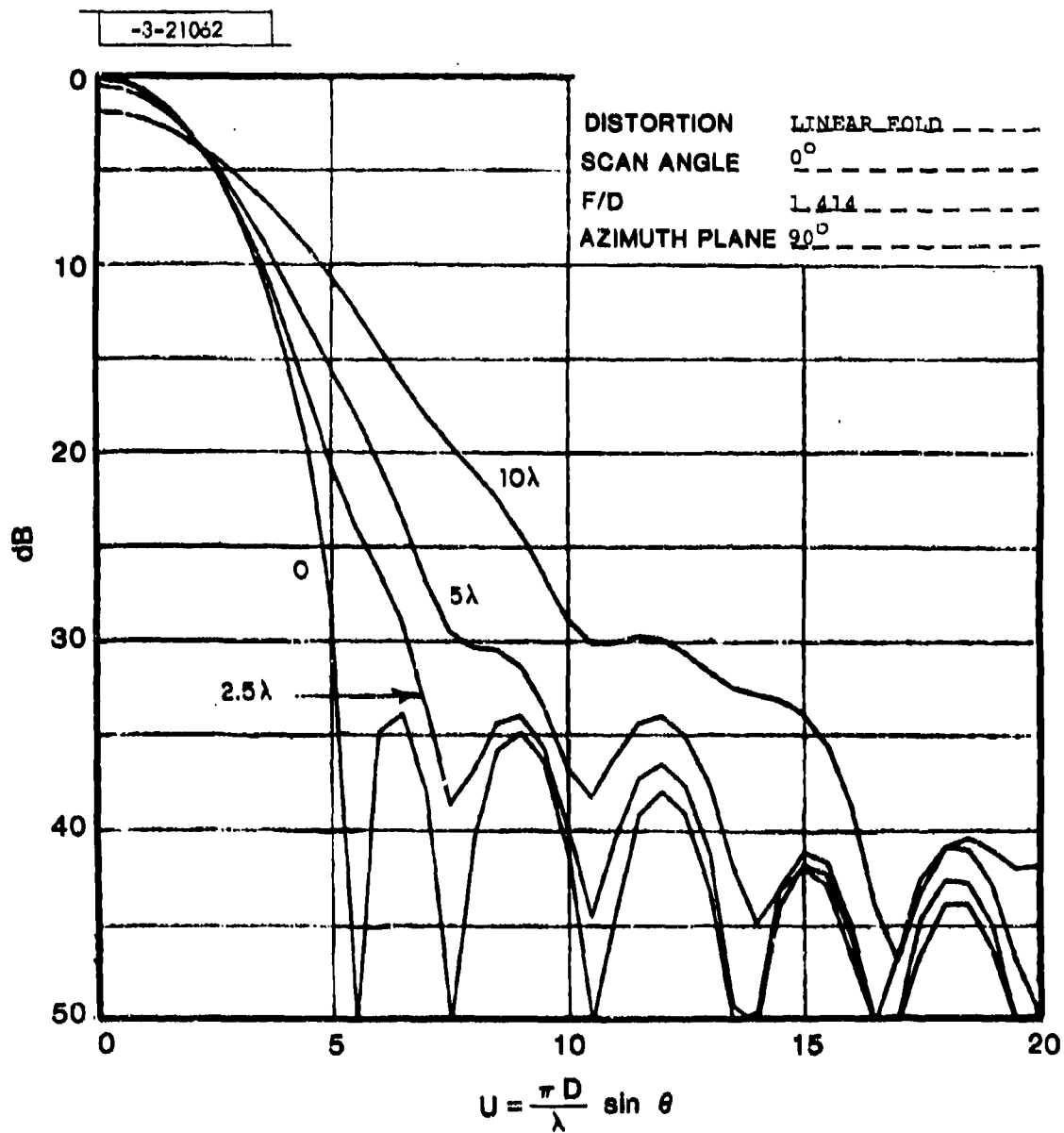


Fig. 25. Radiation patterns of space fed array Gaussian taper  $f(r) = e^{-2r^2}$ .

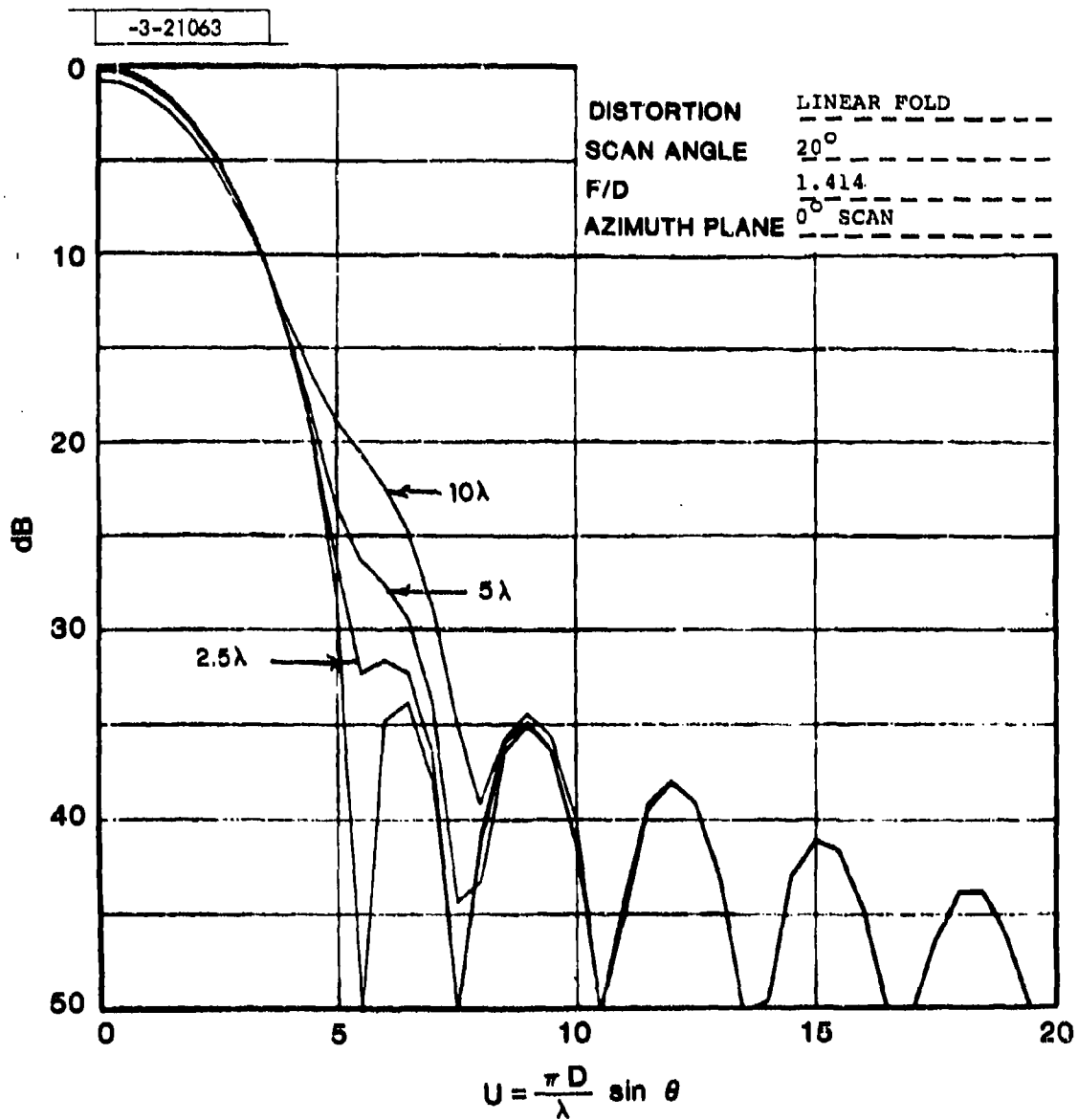


Fig. 26. Radiation patterns of space fed array Gaussian taper  $f(r) = e^{-2r^2}$ .

-3-21064

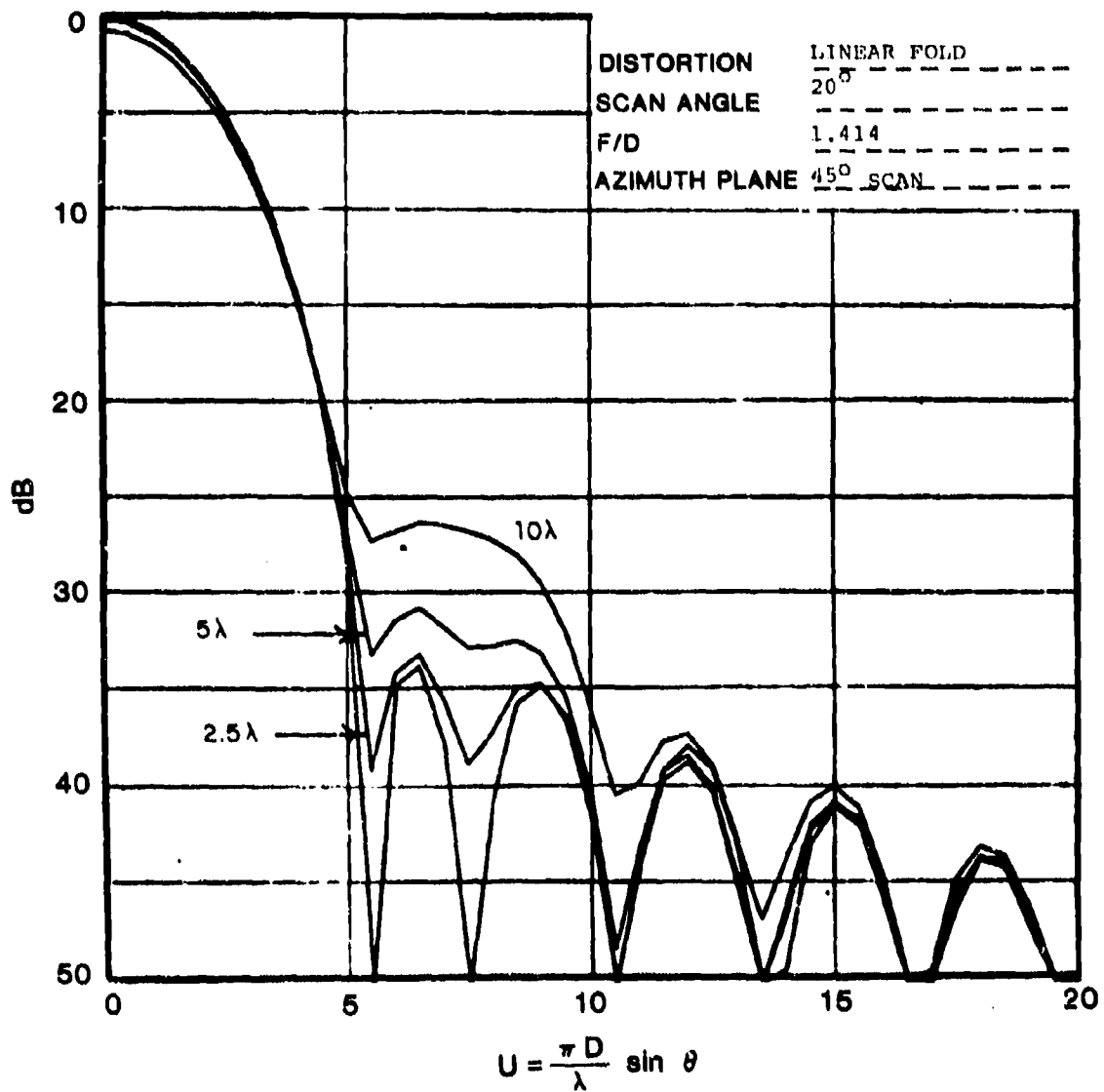


Fig. 27. Radiation patterns of space fed array Gaussian taper  $f(r) = e^{-2r^2}$ .

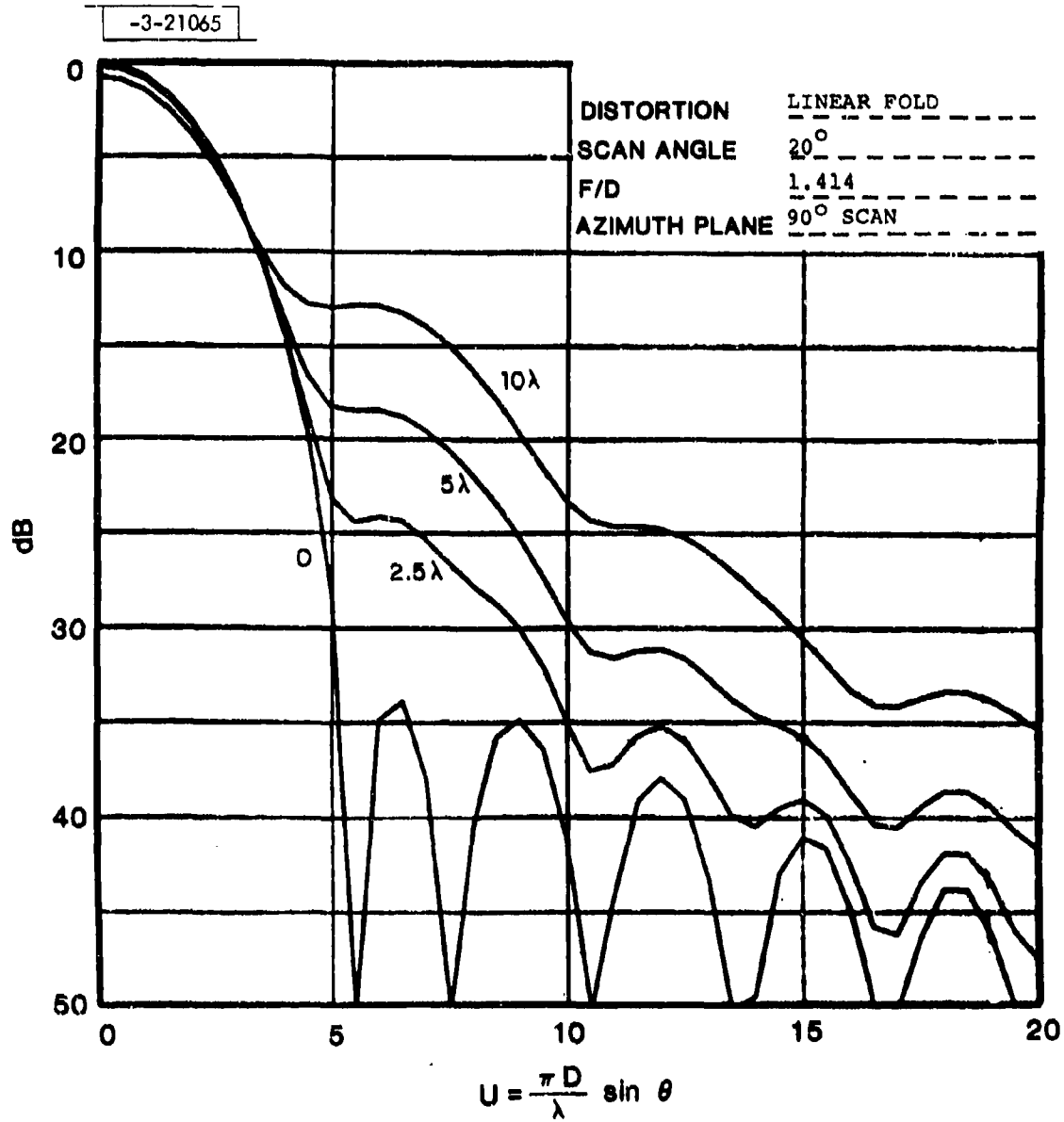


Fig. 28. Radiation patterns of space fed array Gaussian taper  $f(r) = e^{-2r^2}$ .

-3-21066

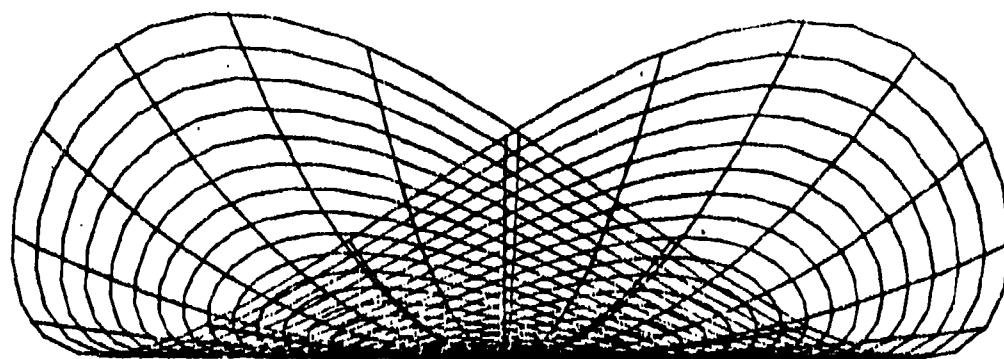


Fig. 29. Quadratic fold  $z = ay^4$ .

Fig. 30-35 inclusive show the pattern degradation in the three azimuth cuts ( $\phi = 0, 45, 90^\circ$ ) for a broadside beam and one scanned to  $\theta = 20^\circ$ . This distortion is more benign than the linear fold as regions of high illumination have smaller displacements for the same rim displacement. Only the case for unity "f" number was calculated.

#### 6.4 Quadratic Astigmatism

This is a distortion called astigmatism in optics, characterized by having different focal lengths in the two principal planes. It is shown graphically in Fig. 36. We see that the lens is bent upward in one principal plane and downward in the orthogonal plane. This distortion is represented mathematically by:

$$z = ar^2 \cos 2\phi \quad (24)$$

There are two azimuthal cuts of interest, namely  $\phi = 0$  and  $\phi = 45^\circ$ . Succeeding 45 degree cuts will have identical patterns.

Fig. 37 and 38 show these two cuts for a broadside beam. Fig. 39 and 40 for the beam scanned to  $20^\circ$  in the direction of the cut taken. All with unity "f" number.

Comparison of Fig. 37 with Fig. 10 (bowl distortion) indicates that the astigmatic degraded patterns have higher sidelobes but smaller gain loss for the same rim distortion.

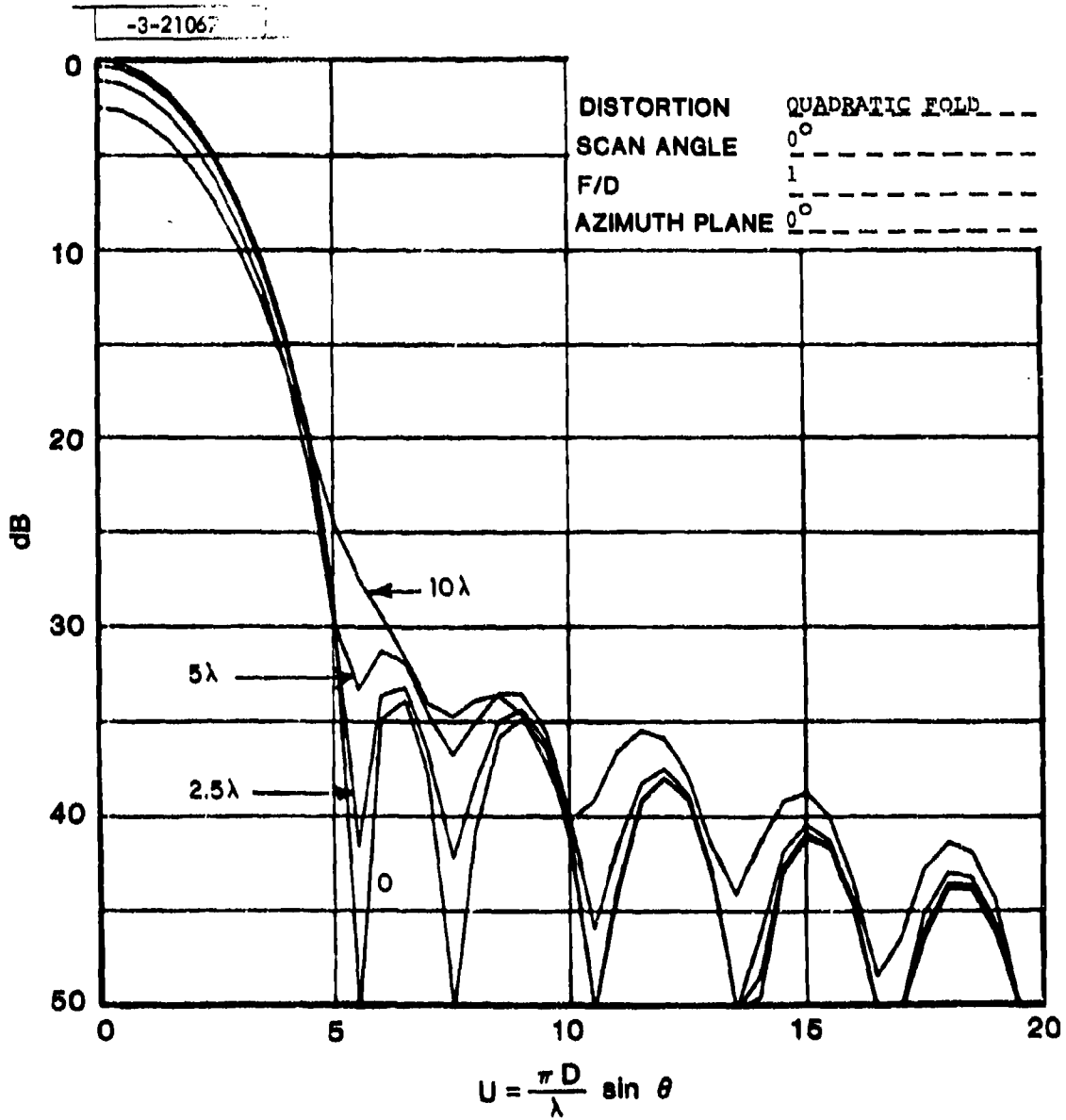


Fig. 30. Radiation patterns of space fed array Gaussian taper  $f(r) = e^{-2r^2}$ .

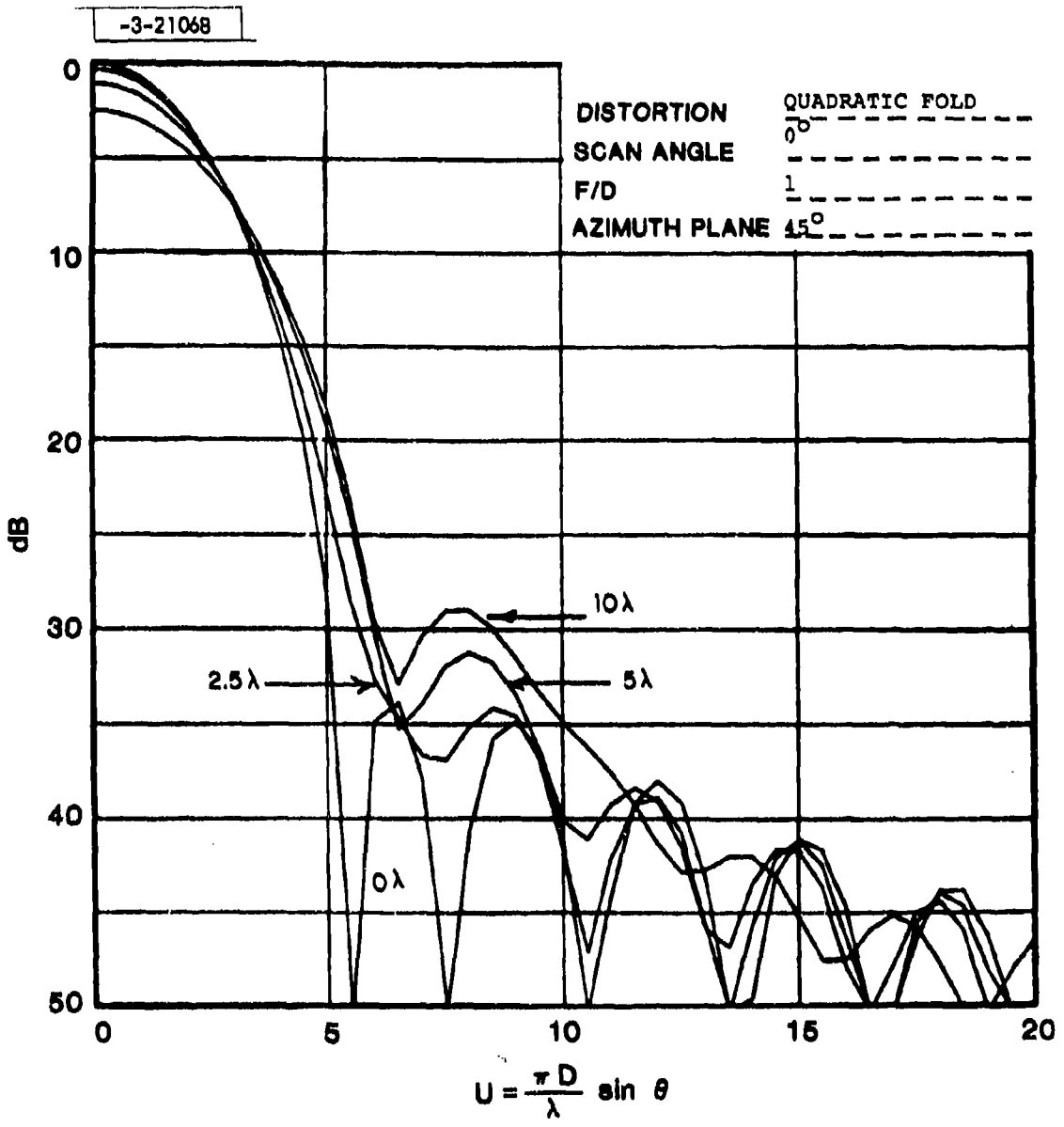


Fig. 31. Radiation patterns of space fed array Gaussian taper  $f(r) = e^{-2r^2}$ .

-3-21069

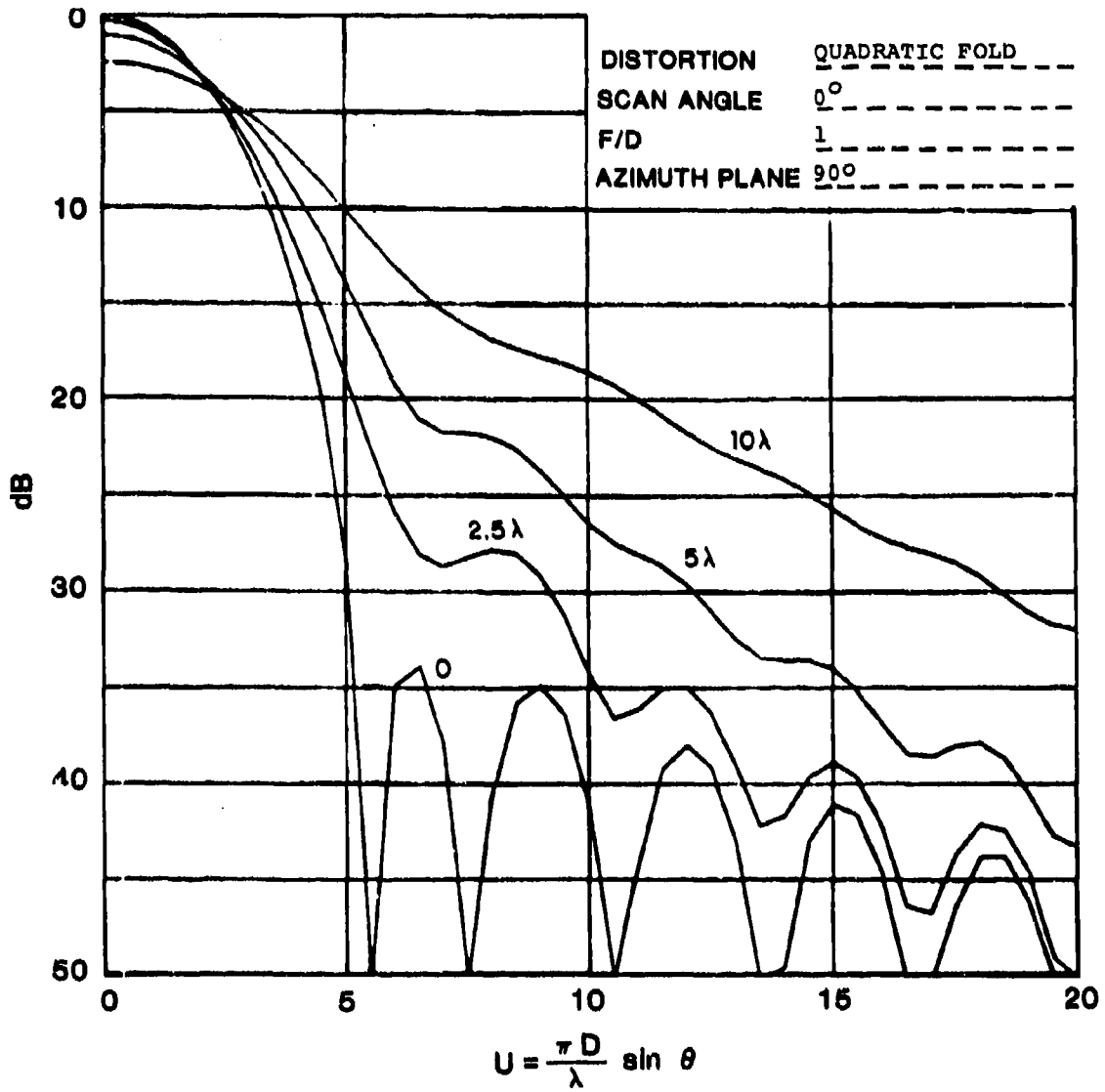


Fig. 32. Radiation patterns of space fed array Gaussian taper  $f(r) = e^{-2r^2}$ .

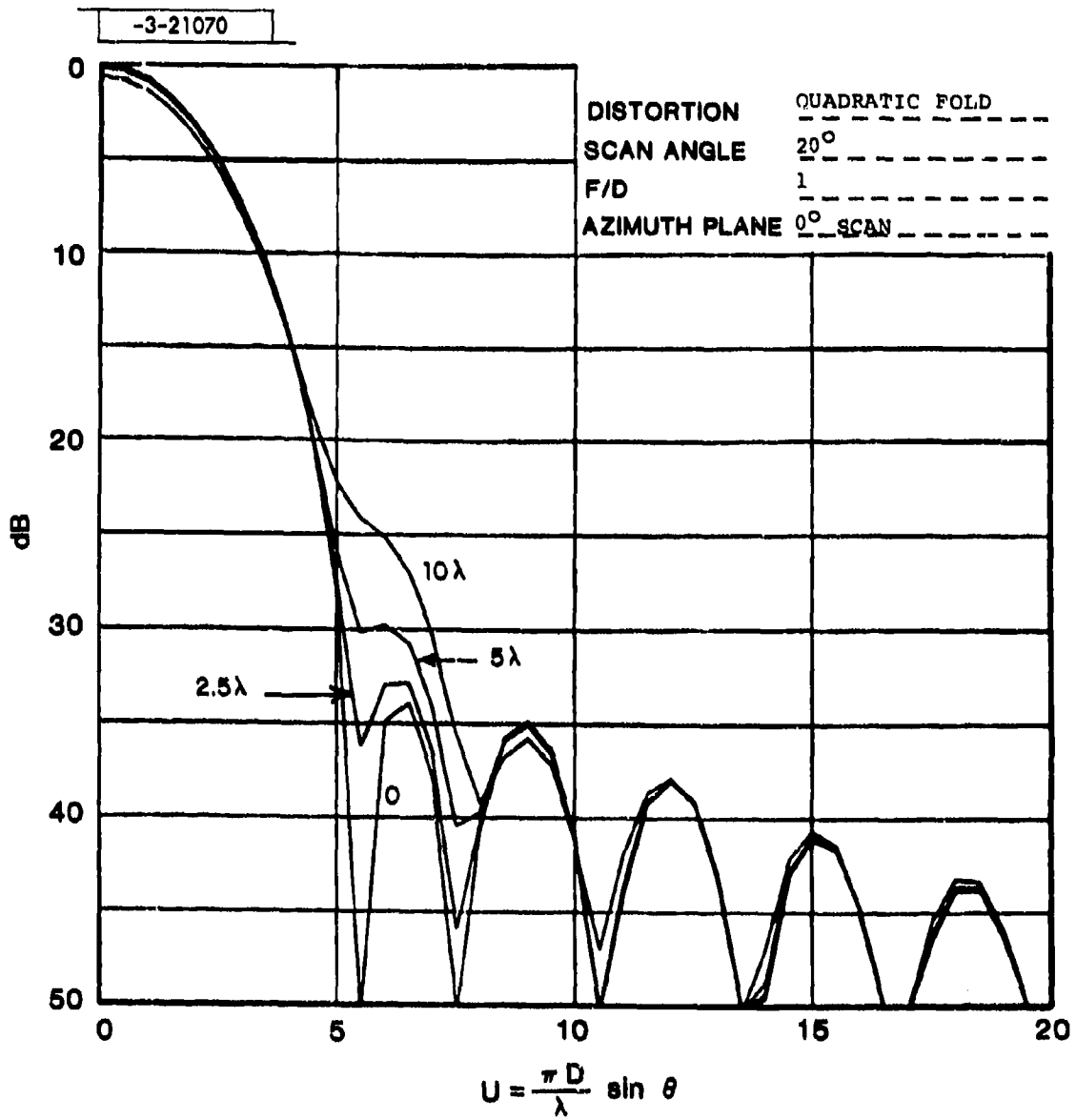


Fig. 33. Radiation patterns of space fed array Gaussian taper  $f(r) = e^{-2r^2}$ .

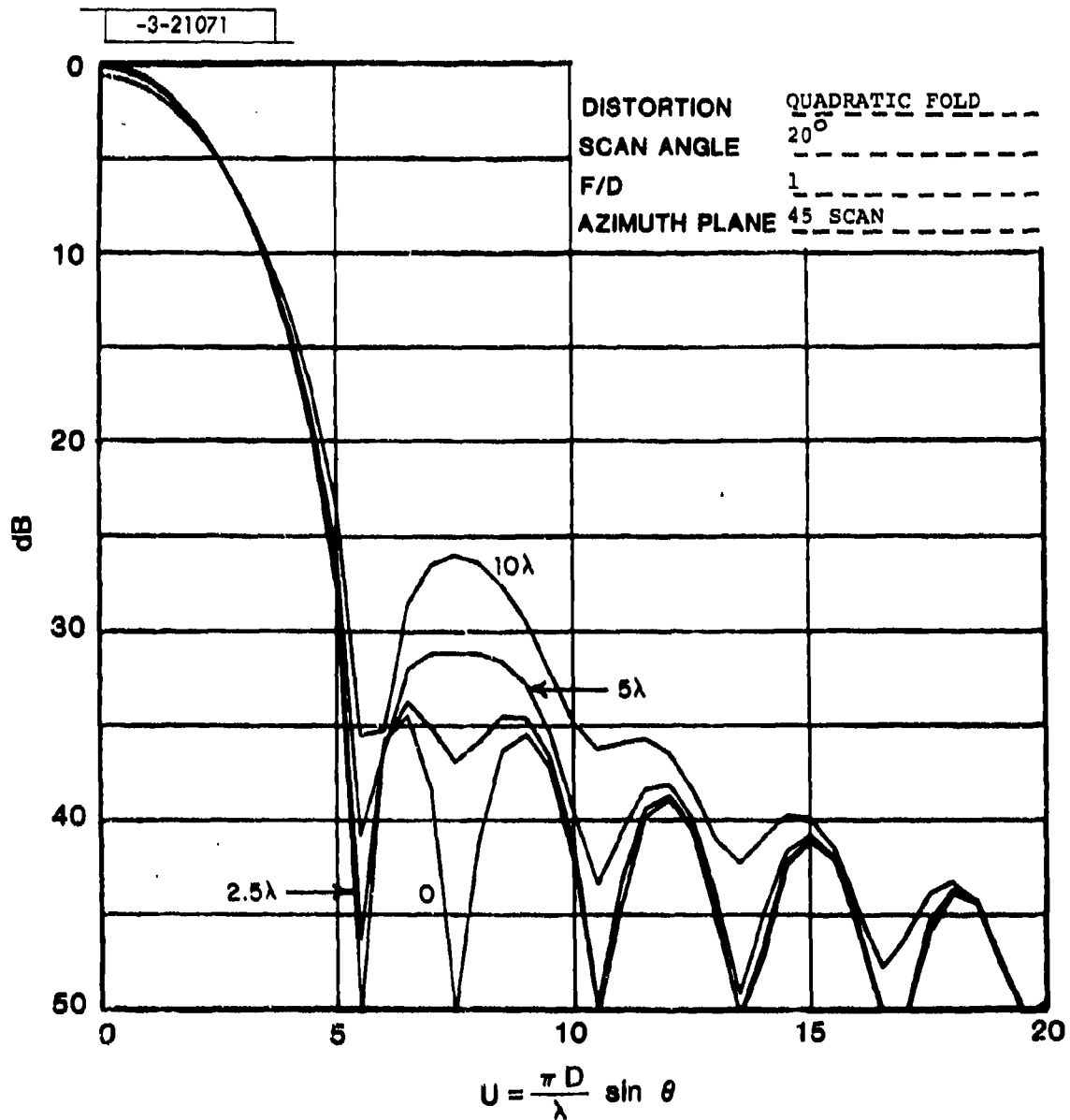


Fig. 34. Radiation patterns of space fed array Gaussian taper  $f(r) = e^{-2r^2}$ .

-3-21072

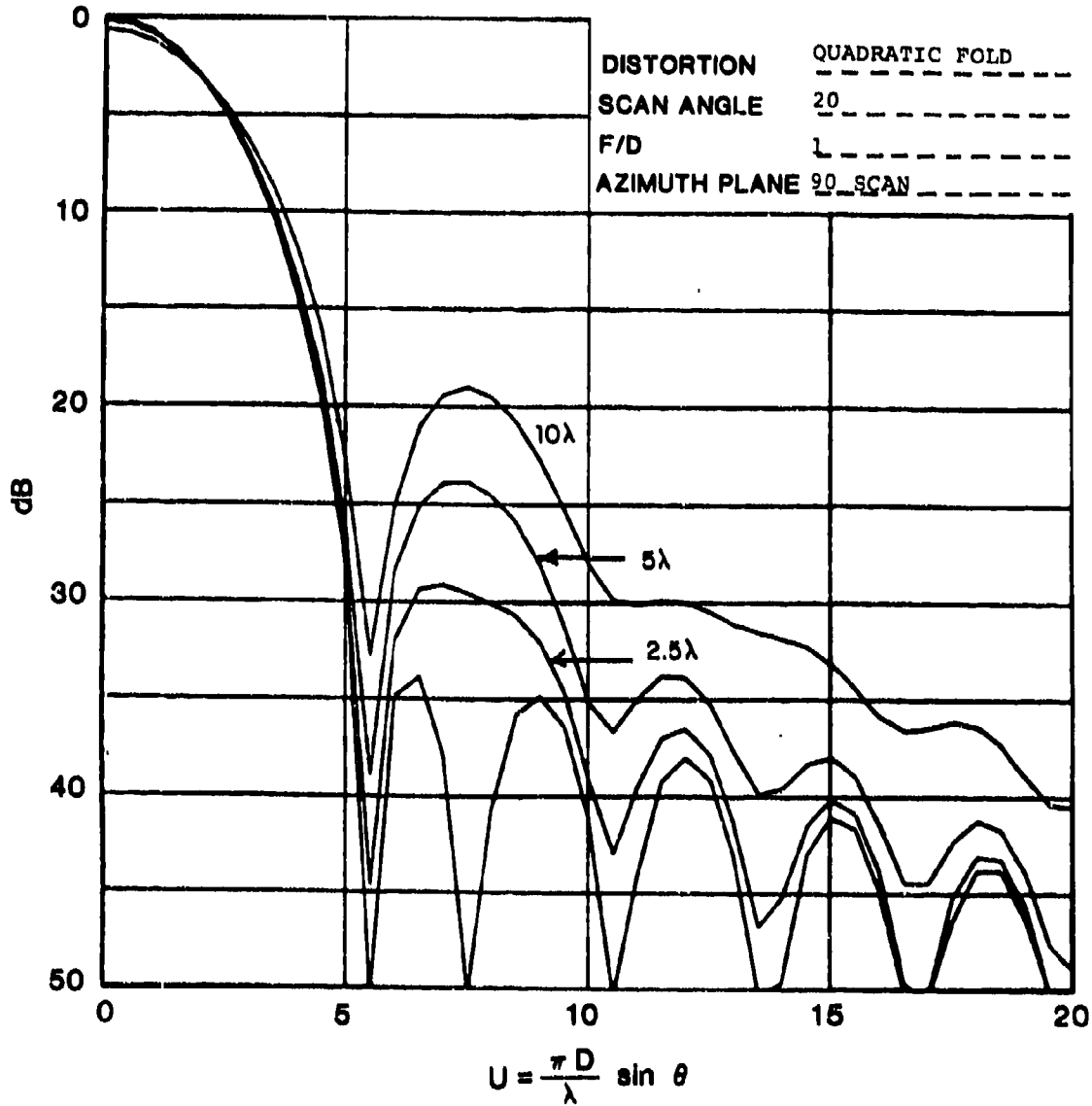


Fig. 35. Radiation patterns of space fed array Gaussian taper  $f(r) = e^{-2r^2}$ .

-3-21073

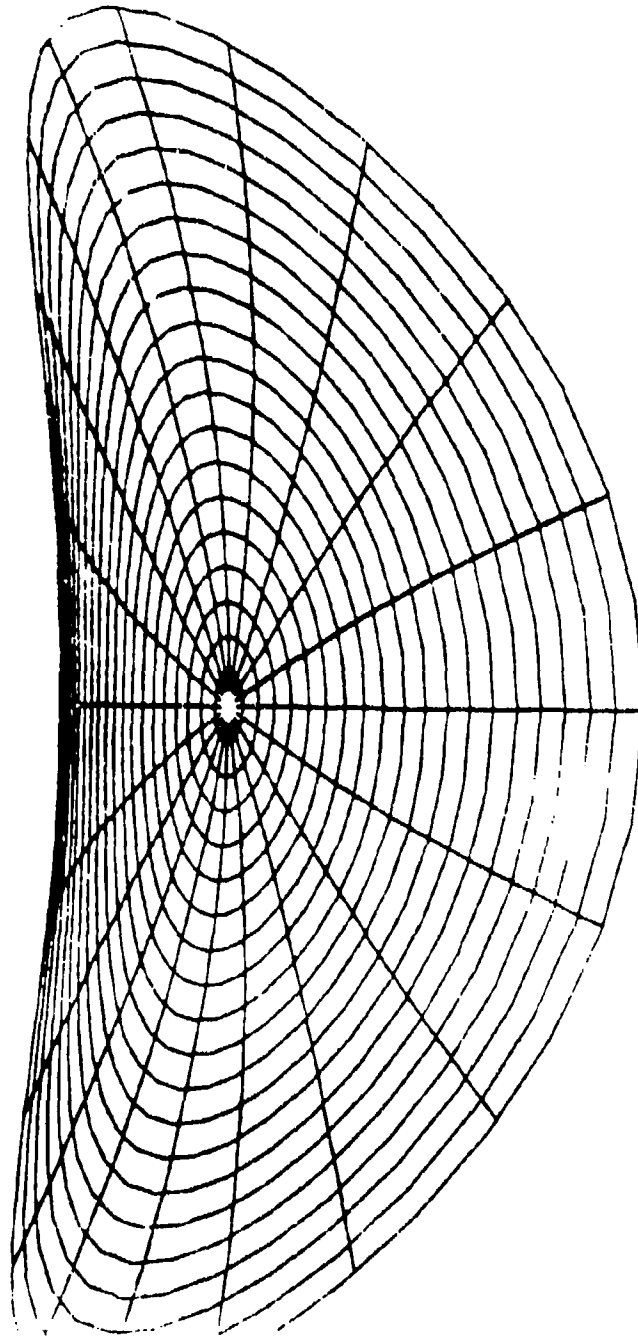


Fig. 36. Quadratic astigmatism  $z = ar^2 \cos 2\phi$ .

-3-21074

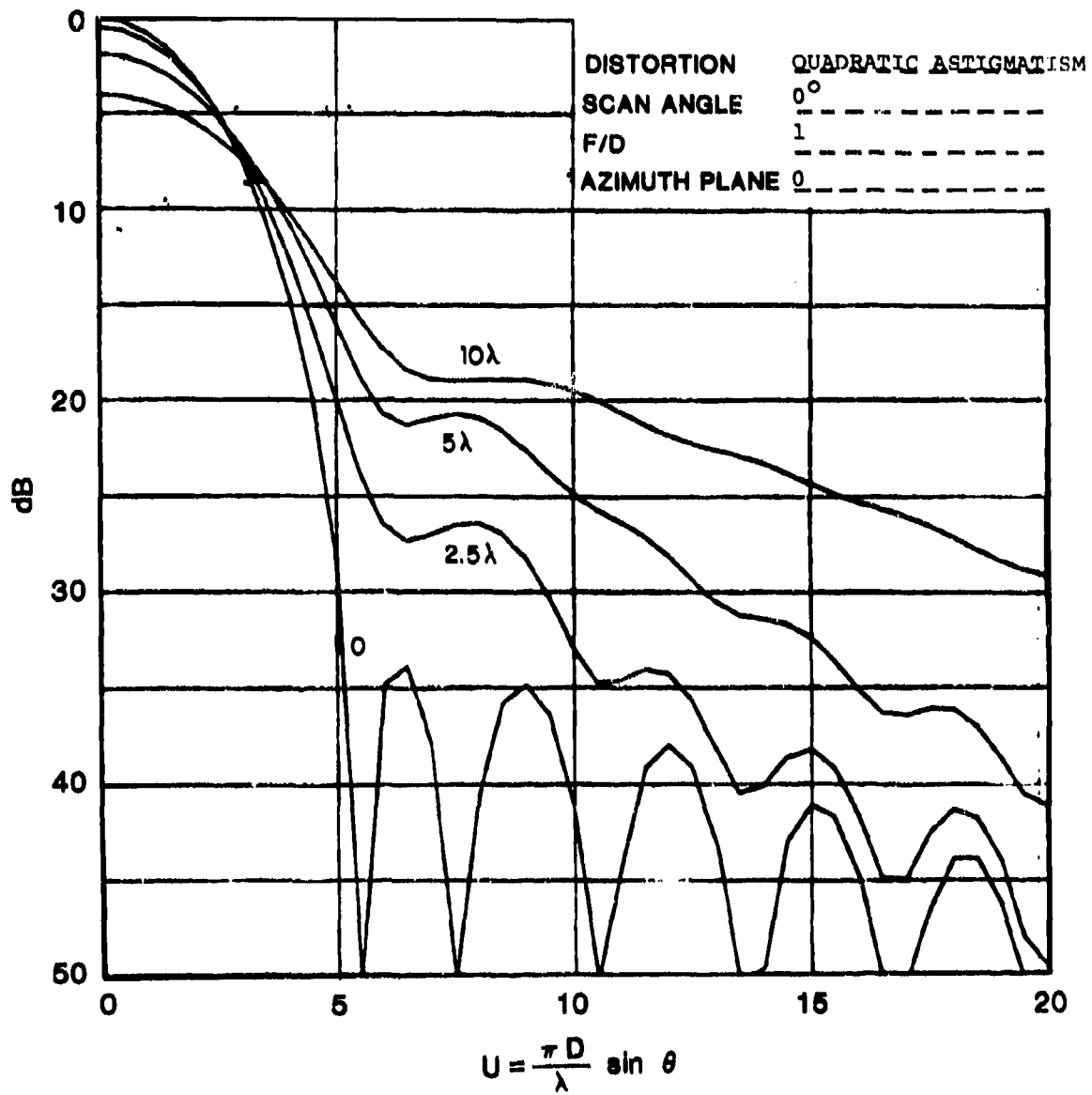


Fig. 37. Radiation patterns of space fed array Gaussian taper  $f(r) = e^{-2r^2}$ .

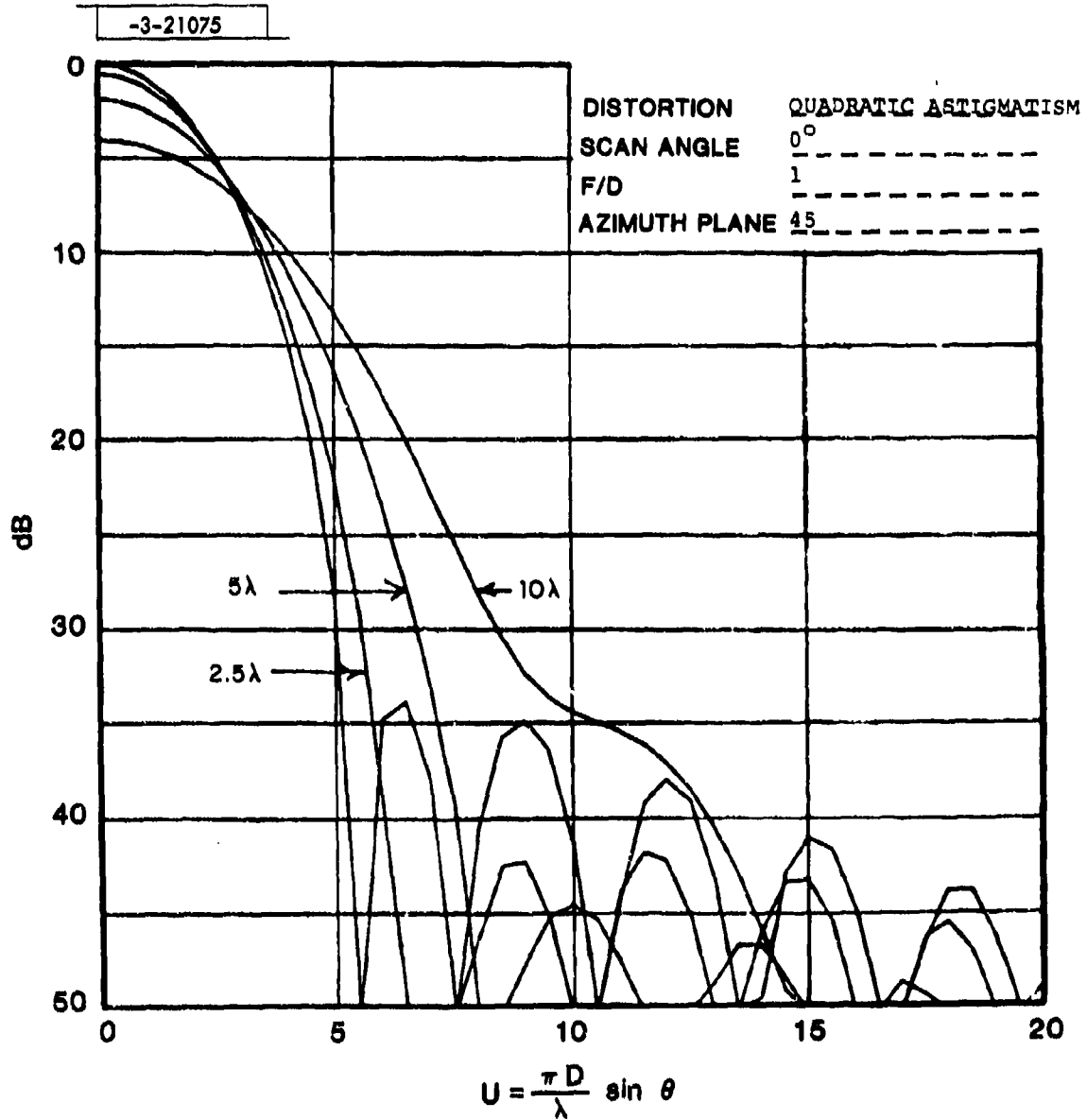


Fig. 38. Radiation patterns of space fed array Gaussian taper  $f(r) = e^{-2r^2}$ .

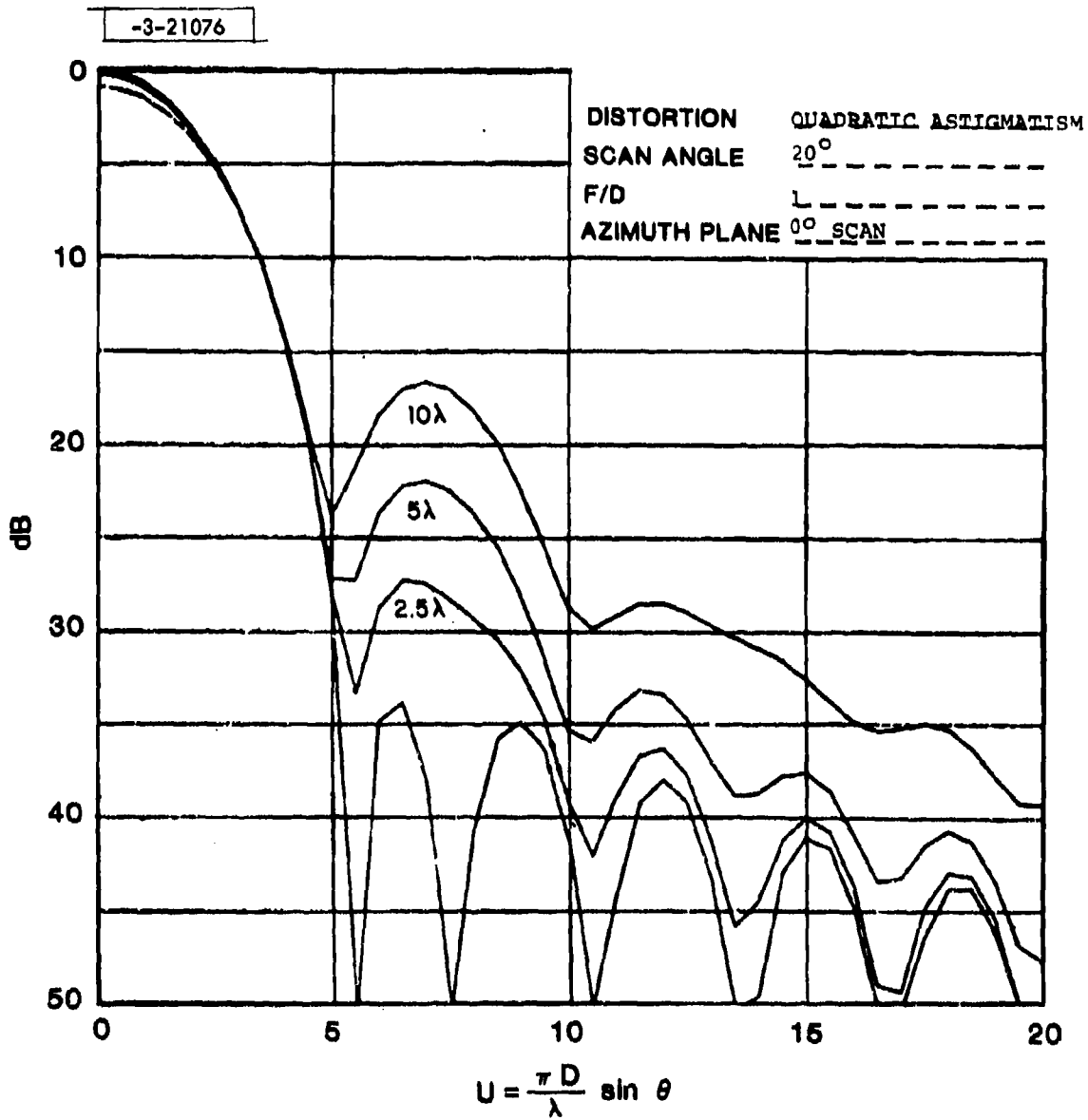


Fig. 39. Radiation patterns of space fed array Gaussian taper  $f(r) = e^{-2r^2}$ .

-3-21077 ]

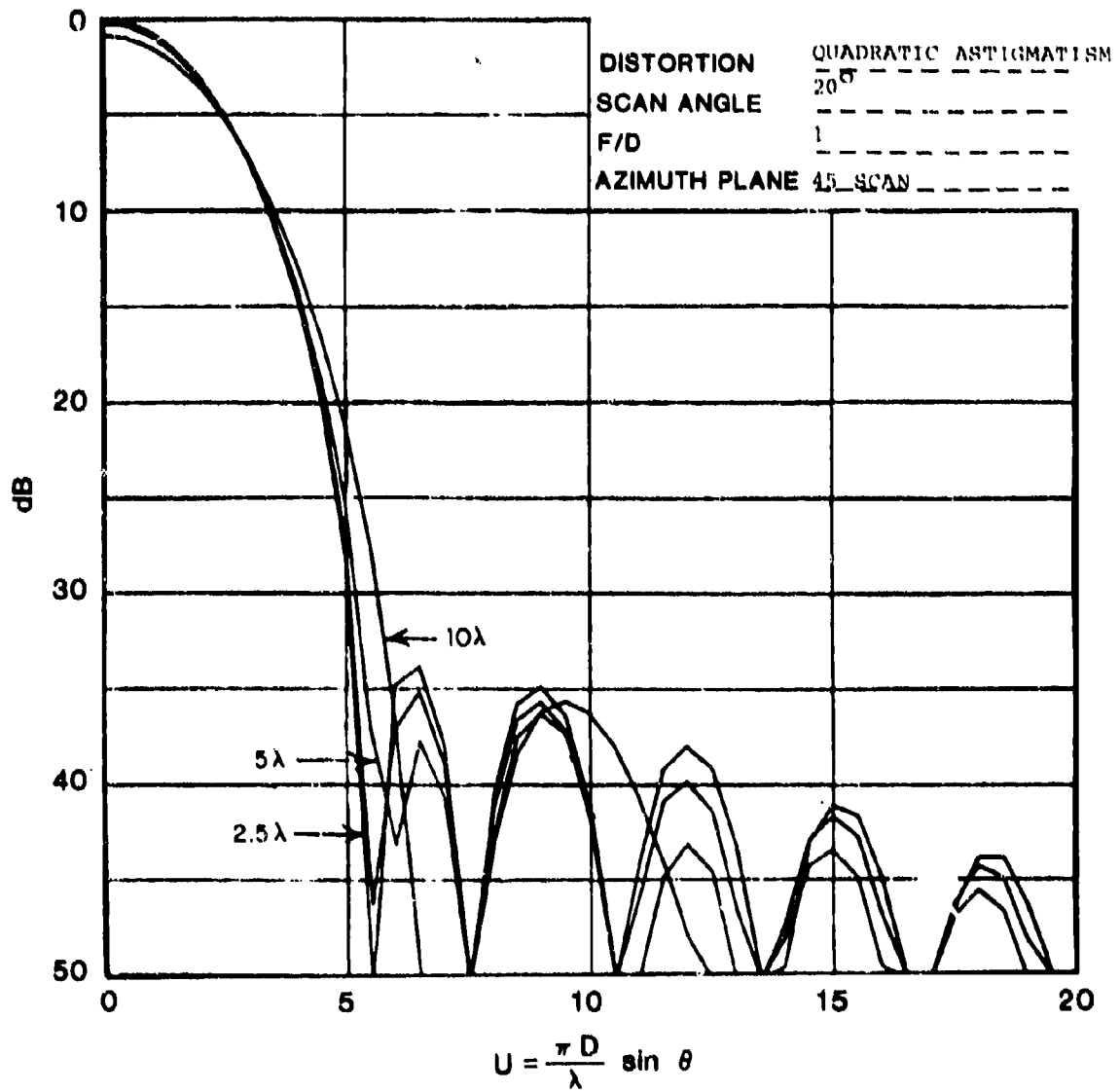


Fig. 40. Radiation patterns of space fed array Gaussian taper  $f(r) = e^{-2r^2}$ .

This can be explained by the fact that the astigmatic distortion has a larger peak to peak distortion creating higher sidelobes in certain cuts, whereas the gain loss depends on the mean square path length error which is smaller for astigmatism as the  $45^\circ$  planes (seam planes) are not displaced.

#### 6.5 Sinusoidal Astigmatism

For want of a better name we call the distortion represented by

$$z = a[\sin k\pi r] \cos 2 \phi \quad (25)$$

sinusoidal astigmatism, as it is astigmatic as far as the azimuth coordinate is concerned but with a radial sinusoidal variation. We would expect the pattern degradation to be greater for this type of distortion than for those considered previously as now, depending on the parameter "k", regions of high distortion move toward the center of the array.

Fig. 41 shows graphically Eq. 25 for "k = 1/2" where greatest distortion occurs at the rim.

Figs. 42-45 inclusive show the radiation patterns for the two planes of interest ( $\phi = 0, 45^\circ$ ) for the broadside beam and one scanned to 20 degrees. All for unity "f" number.

Fig. 46 shows graphically Eq. 25 for "k = 1.0". Here the rim is undistorted. Figs. 47-50 inclusive show the corresponding patterns.

-3-21078

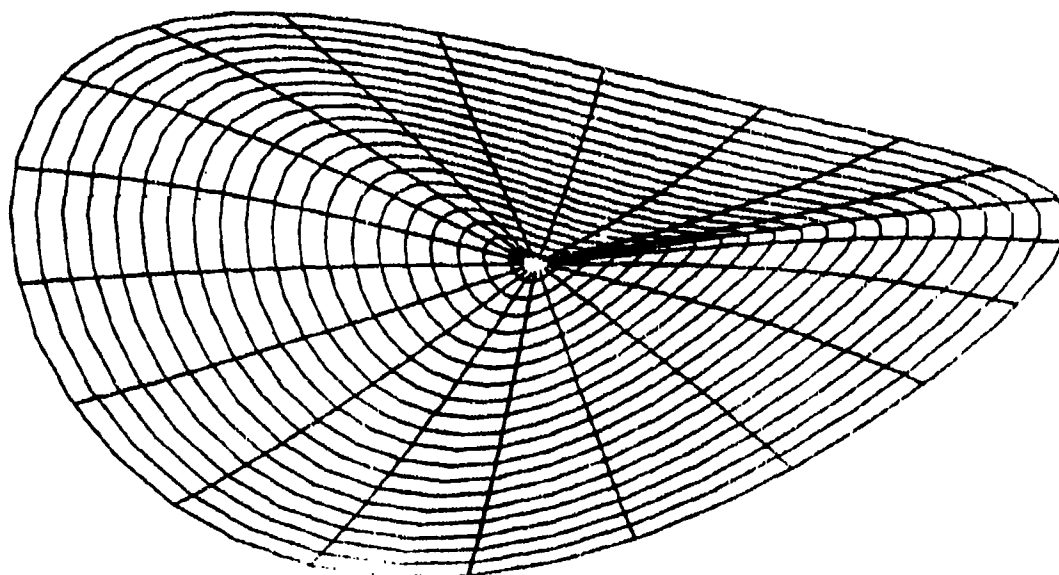


Fig. 41. Sinusoidal astigmatism ( $k = 1/2$ )  $z = a(\sin \frac{\pi}{2} r) \cos 2\phi$ .

-3-21079

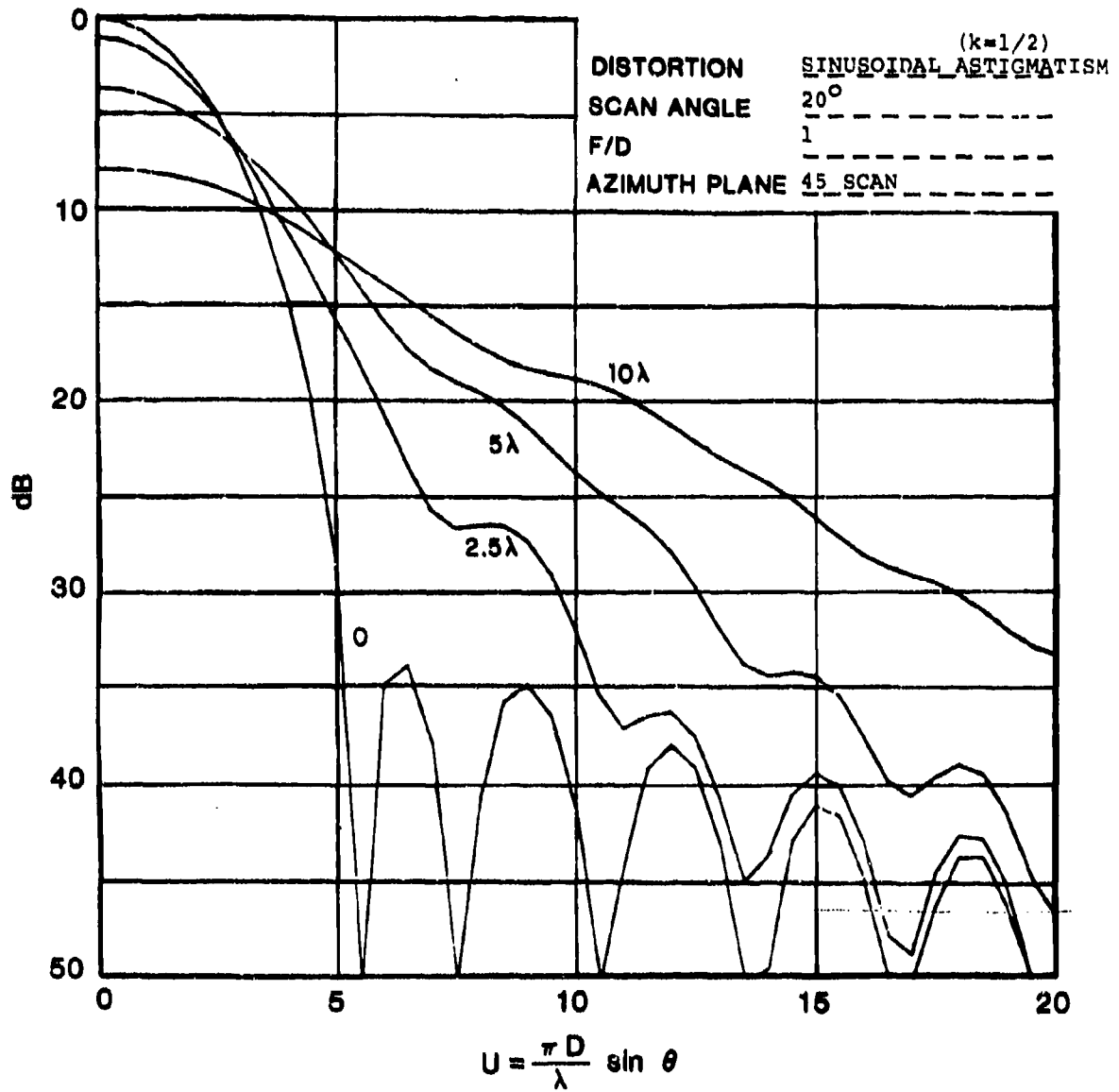


Fig. 42. Radiation patterns of space fed array Gaussian taper  $f(r) = e^{-2r^2}$ .

-3-21080

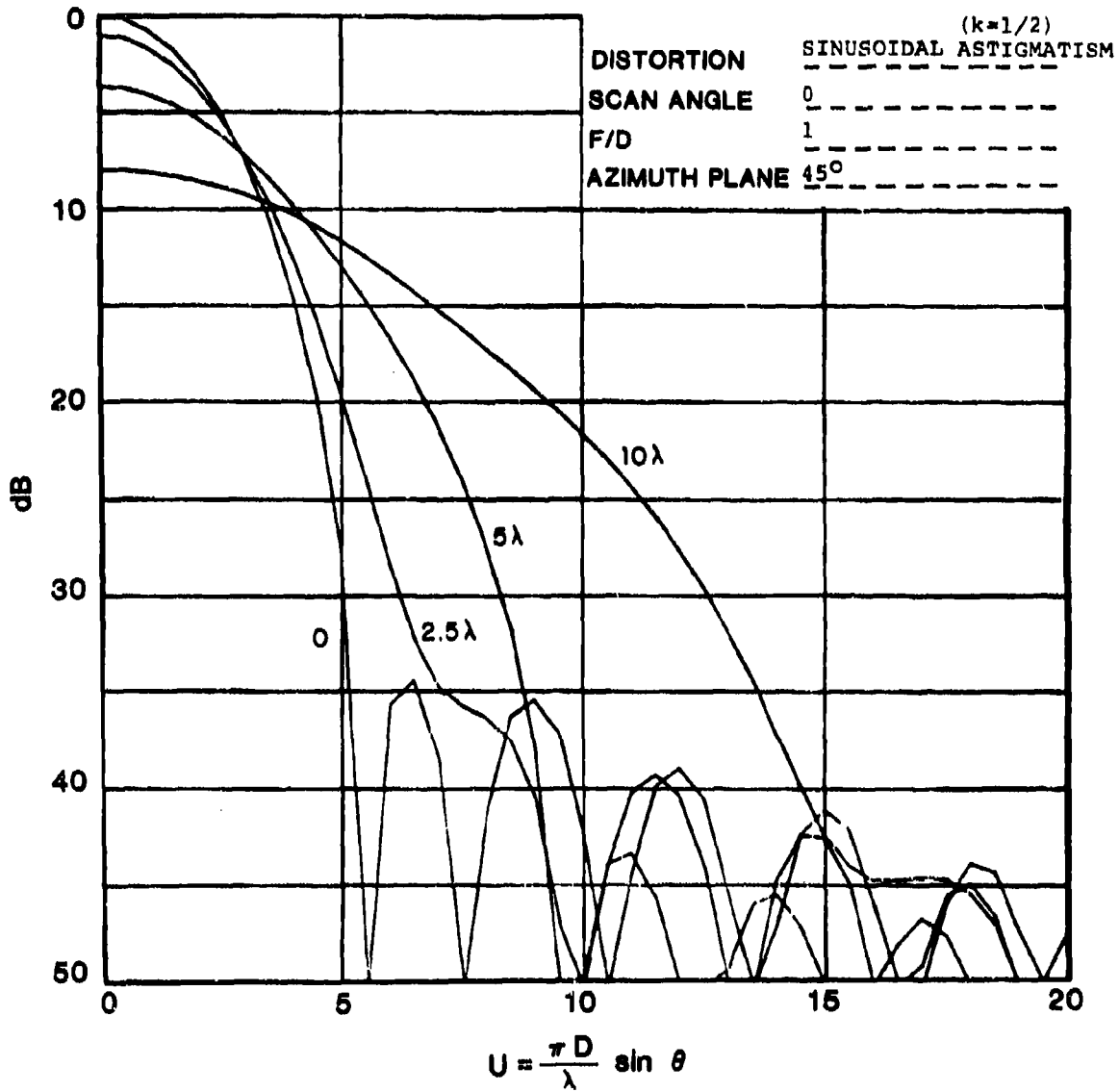


Fig. 43. Radiation patterns of space fed array Gaussian taper  $f(r) = e^{-2r^2}$ .

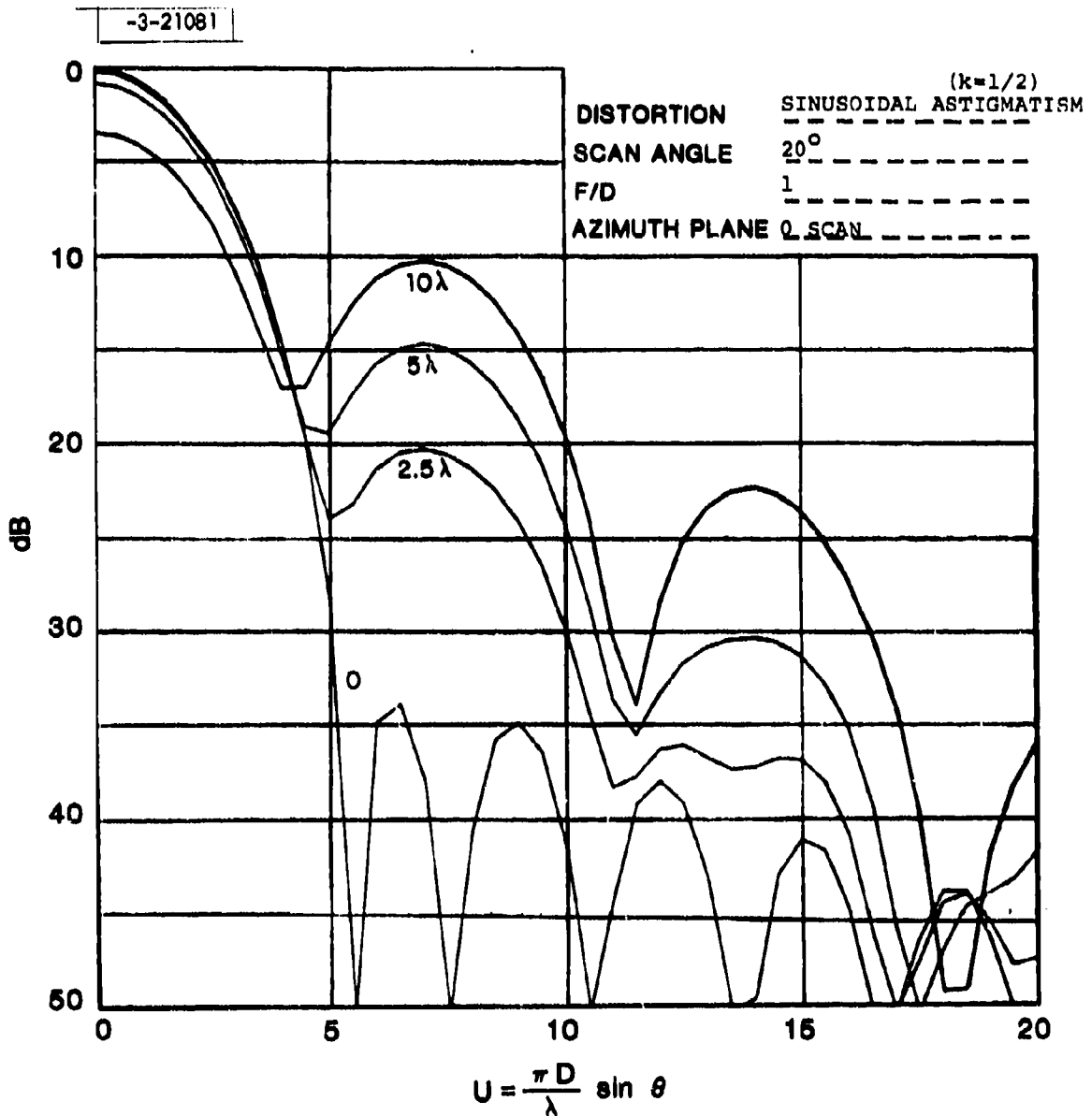


Fig. 44. Radiation patterns of space fed array Gaussian taper  $f(r) = e^{-2r^2}$ .

-3-21082

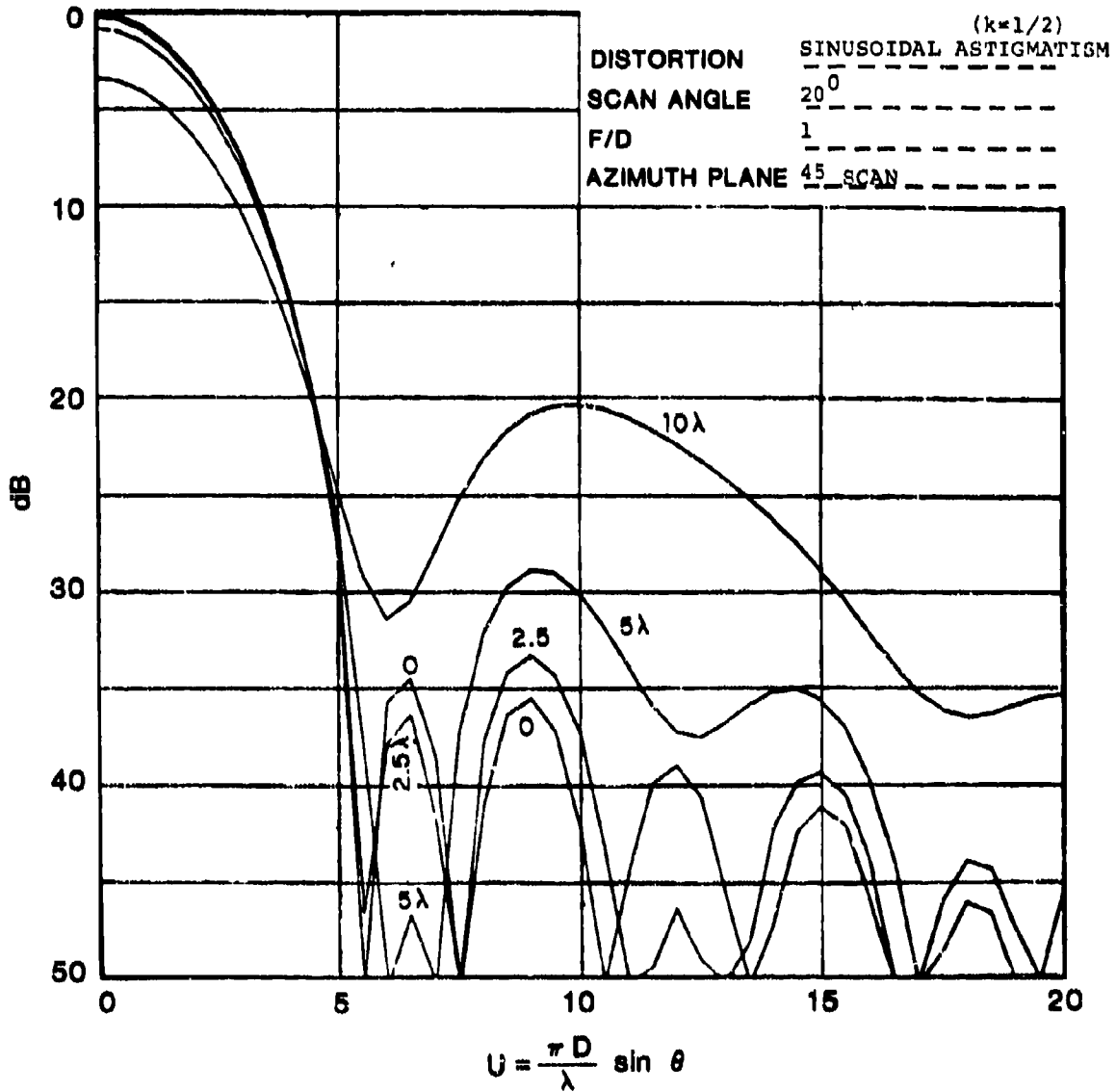


Fig. 45. Radiation patterns of space fed array Gaussian taper  $f(r) = e^{-2r^2}$ .

-3-21083

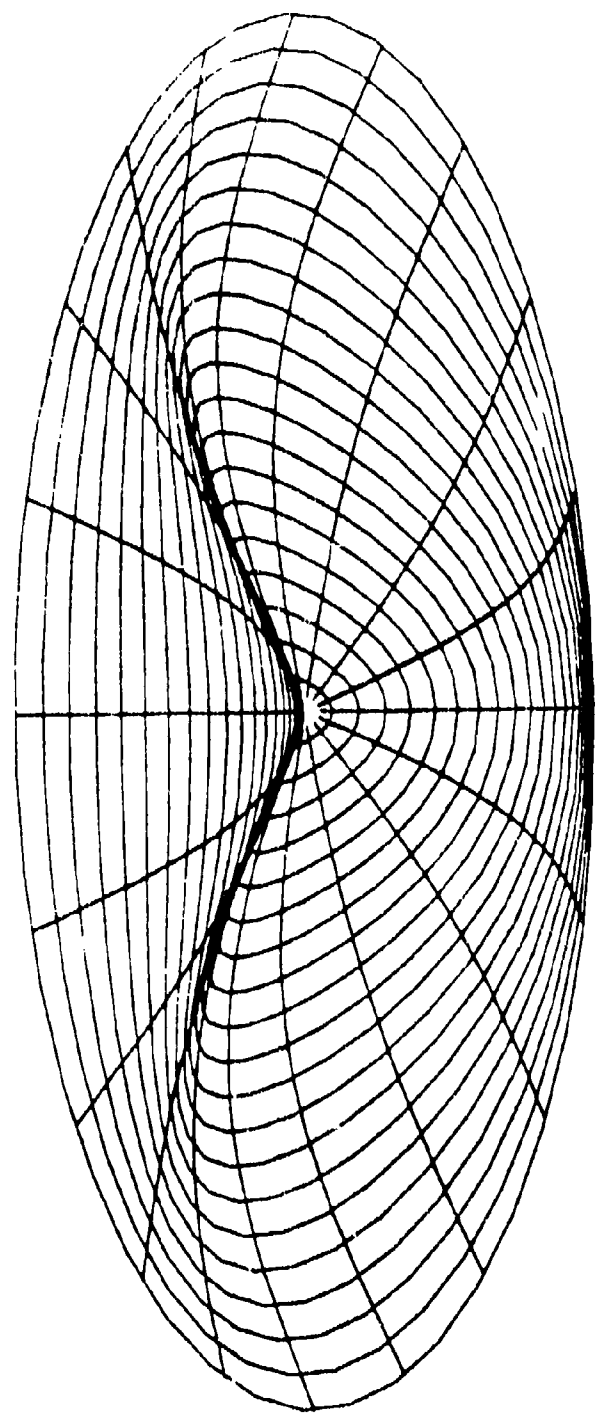


Fig. 46. Sinusoidal astigmatism ( $k = 1$ )  $z = a(\sin nr) \cos 2\phi$ .

-3-21084

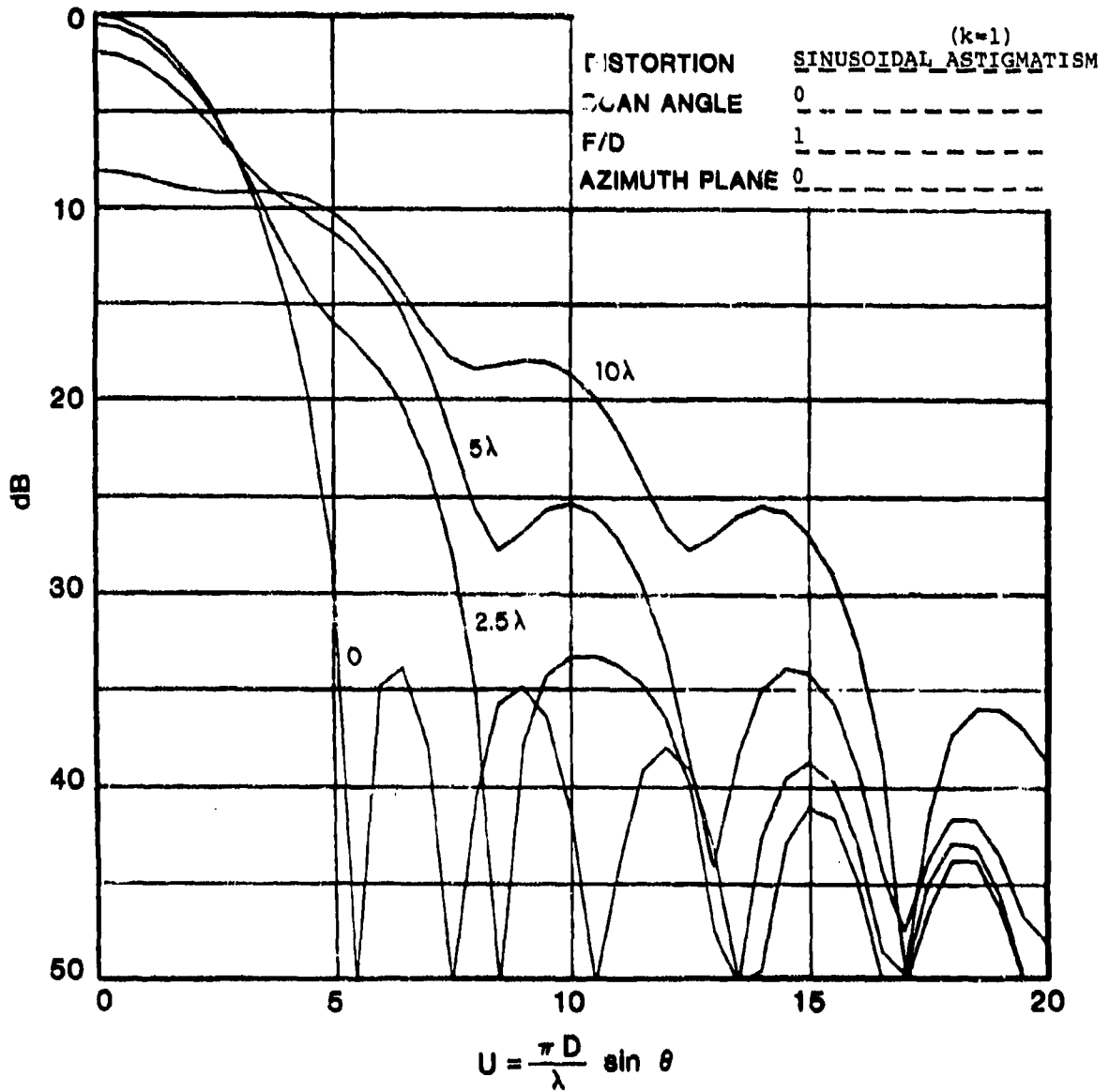


Fig. 47. Radiation patterns of space fed array Gaussian taper  $f(r) = e^{-2r^2}$ .

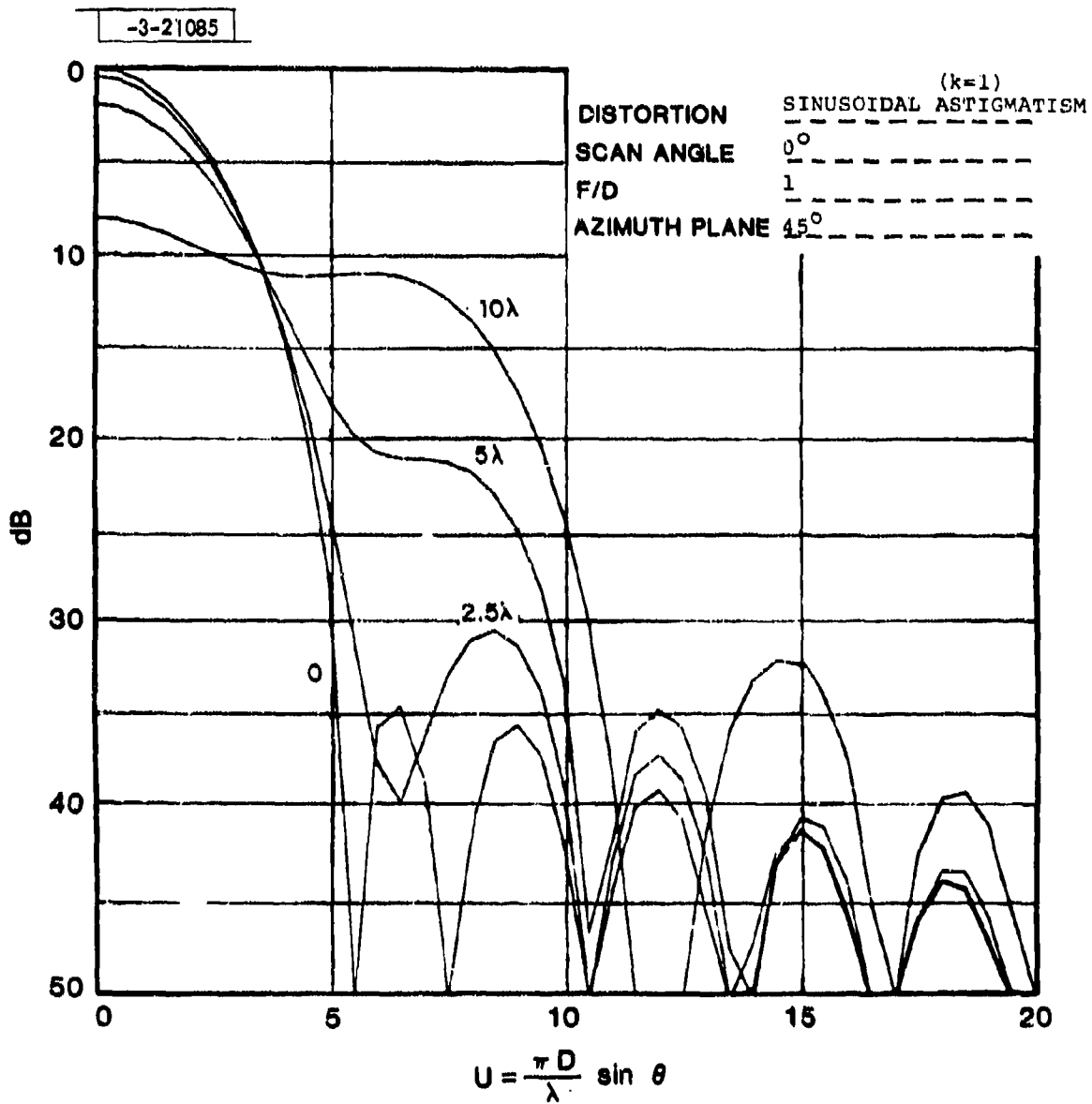


Fig. 48. Radiation patterns of space fed array Gaussian taper  $f(r) = e^{-2r^2}$ .

-3-21086

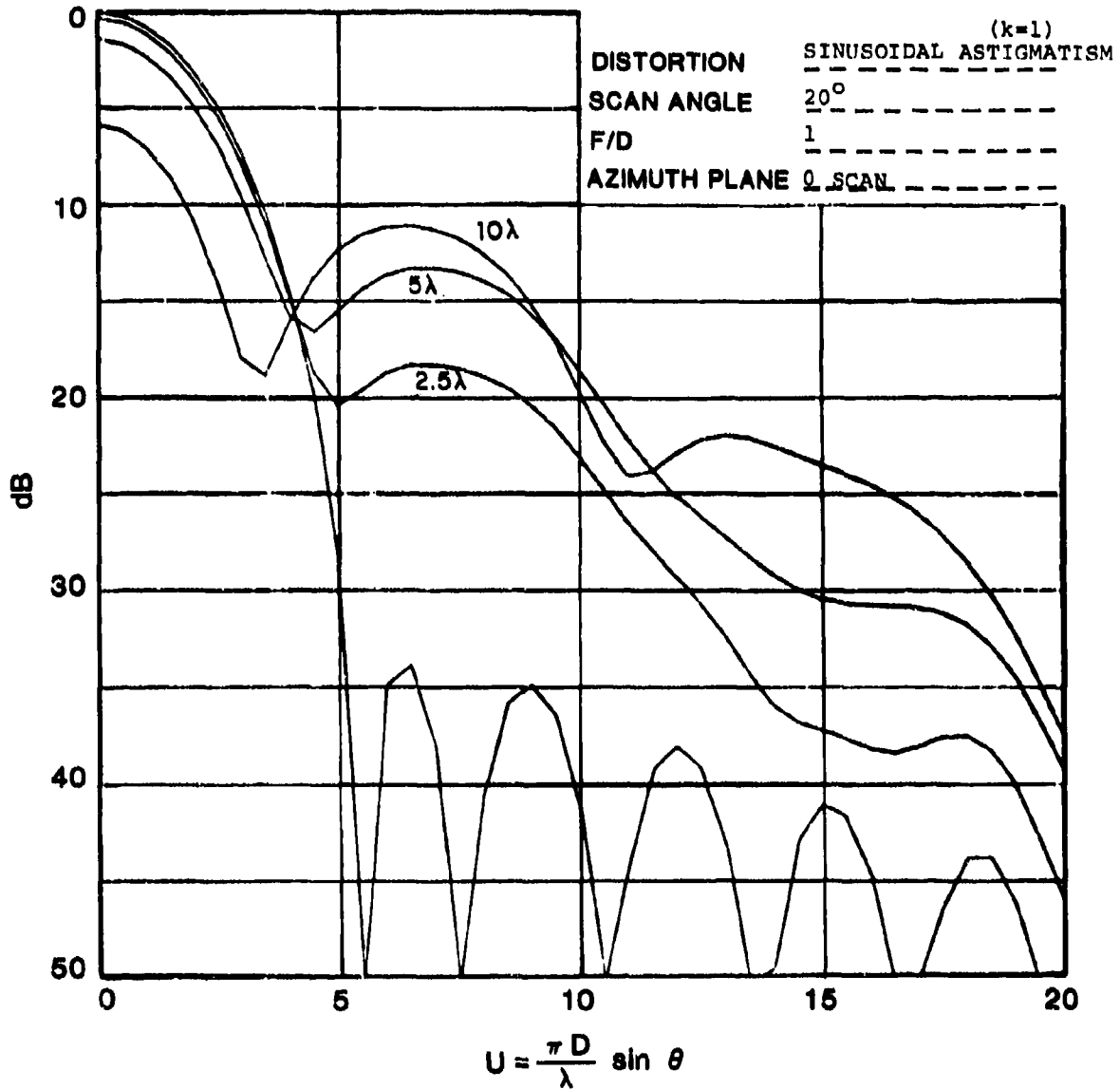


Fig. 49. Radiation patterns of space fed array Gaussian taper  $f(r) = e^{-2r^2}$ .

-3-21087

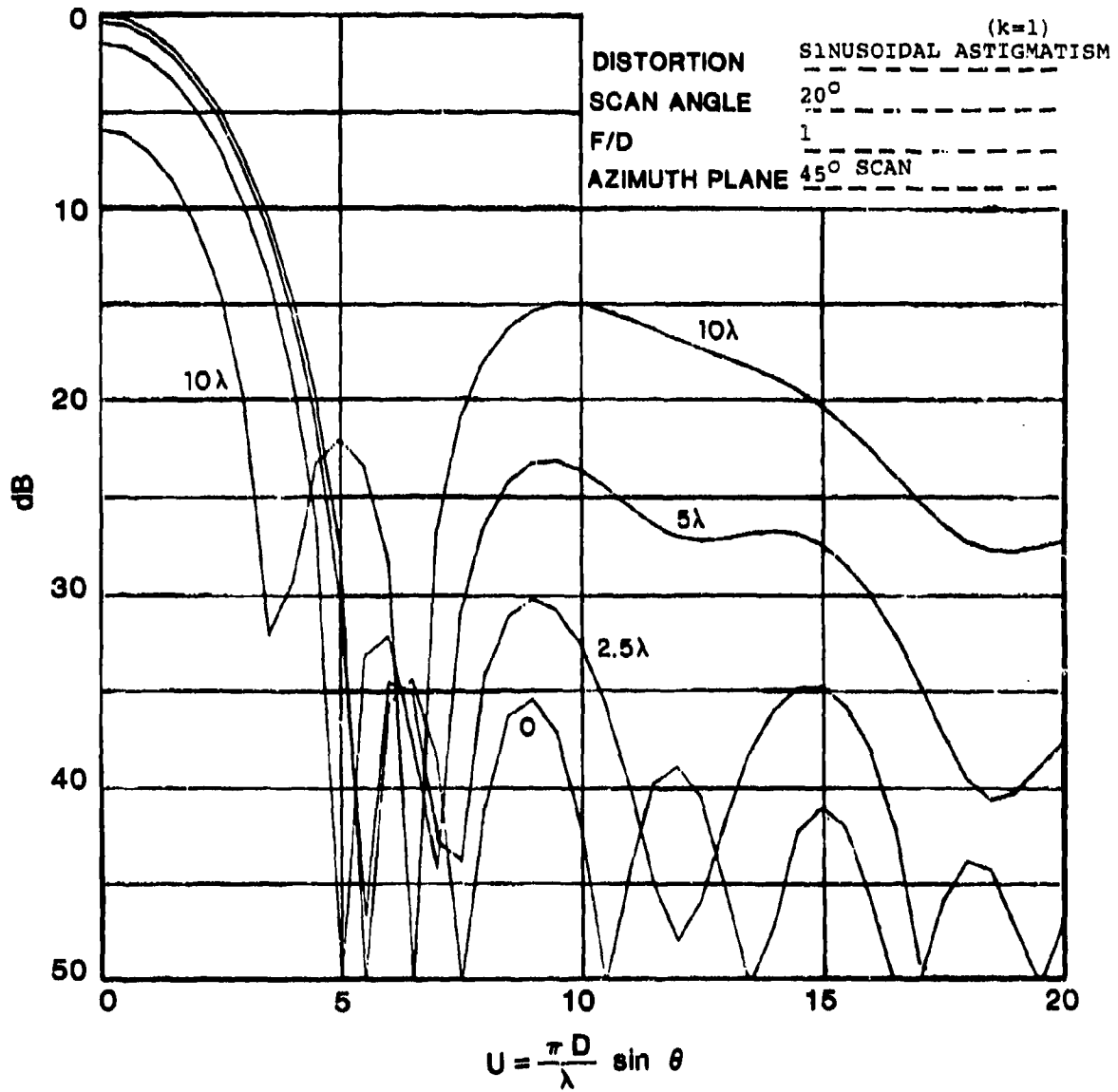


Fig. 50. Radiation patterns of space fed array Gaussian taper  $f(r) = e^{-2r^2}$ .

Fig. 51 shows graphically Eq. 25 for "k=1.5." Fig. 52 to 55 inclusive show the patterns. We note that due to the high distortion near the array center that a 2.5 wavelength distortion is no longer acceptable.

Examination of the pattern degradation in the two astigmatic cases shows that it is more benign in the 45° or seam planes. This is due to the fact that about these planes the phase error has conjugated symmetry. Collapsing the complex illumination function onto the 45° plane results in a modified real illumination function.

#### 6.6 Eight and Sixteen Gore

As the circular space fed lens may be of gore construction pattern calculations were made with increased azimuthal frequency variations. That is axial distortions of the type:

$$8 \text{ Gore} \quad z = a \sin \pi k r (\cos 4\phi) \quad (26)$$

$$16 \text{ Gore} \quad z = a \sin \pi k r (\cos 8\phi) \quad (27)$$

$$k = 1/2, 1, 3/2.$$

Graphics and degraded patterns are shown in Fig. 56-79. Few general comments can be made about these and the "four gore" case of Section 5 above; namely:

-3-21088

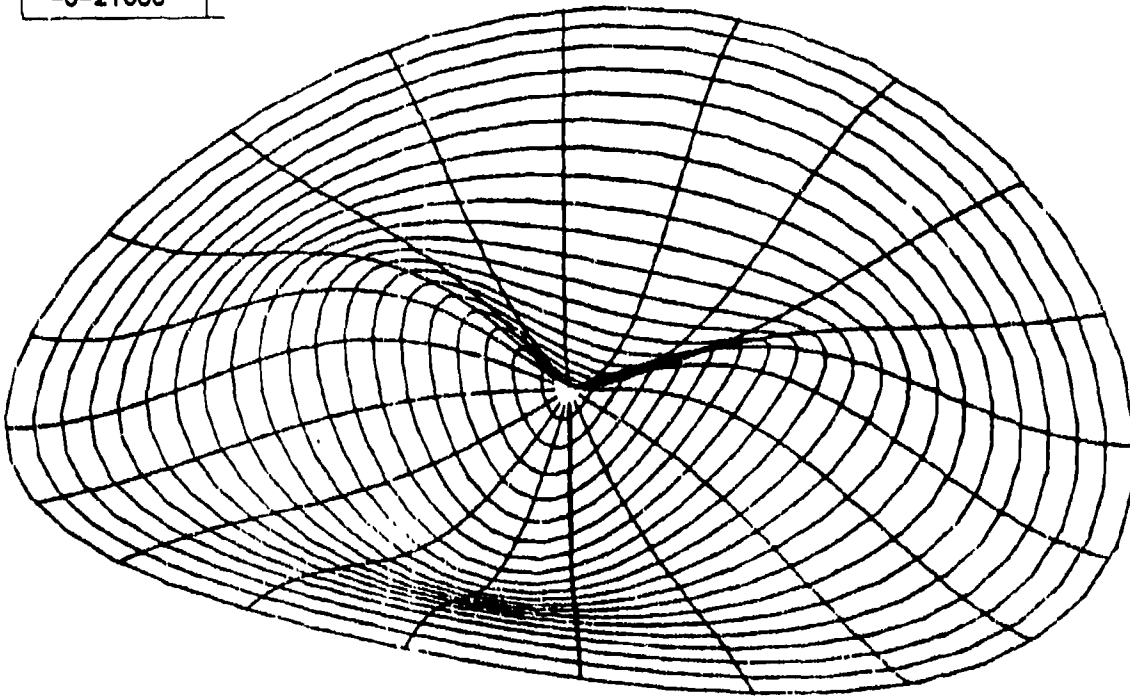


Fig. 51. Sinusoidal astigmatism ( $k = 1.5$ )  $z = a(\sin 1.5\pi r) \cos 2\phi$ .

-3-21089

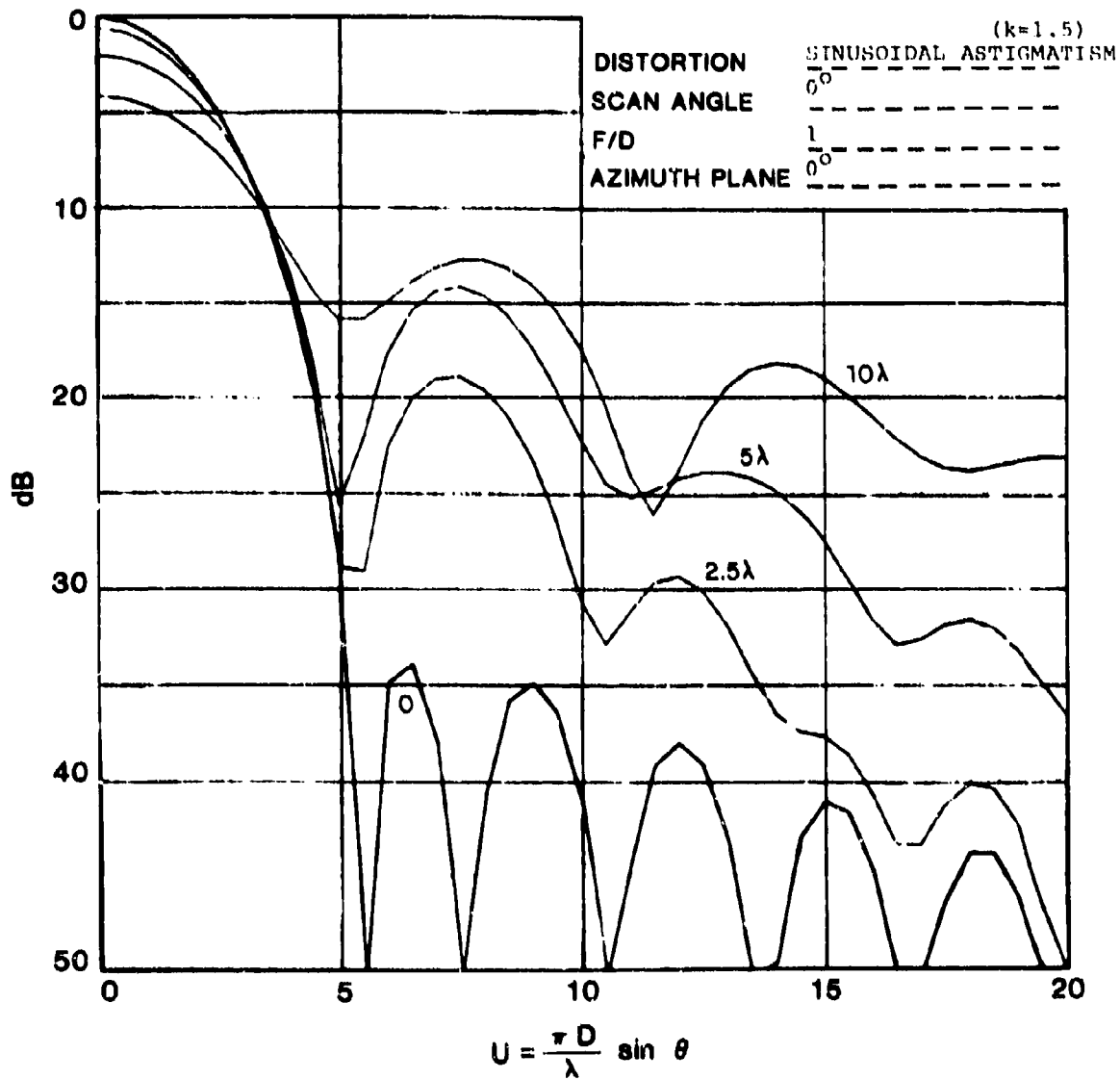


Fig. 52. Radiation patterns of space fed array Gaussian taper  $f(r) = e^{-2r^2}$ .

-3-21090

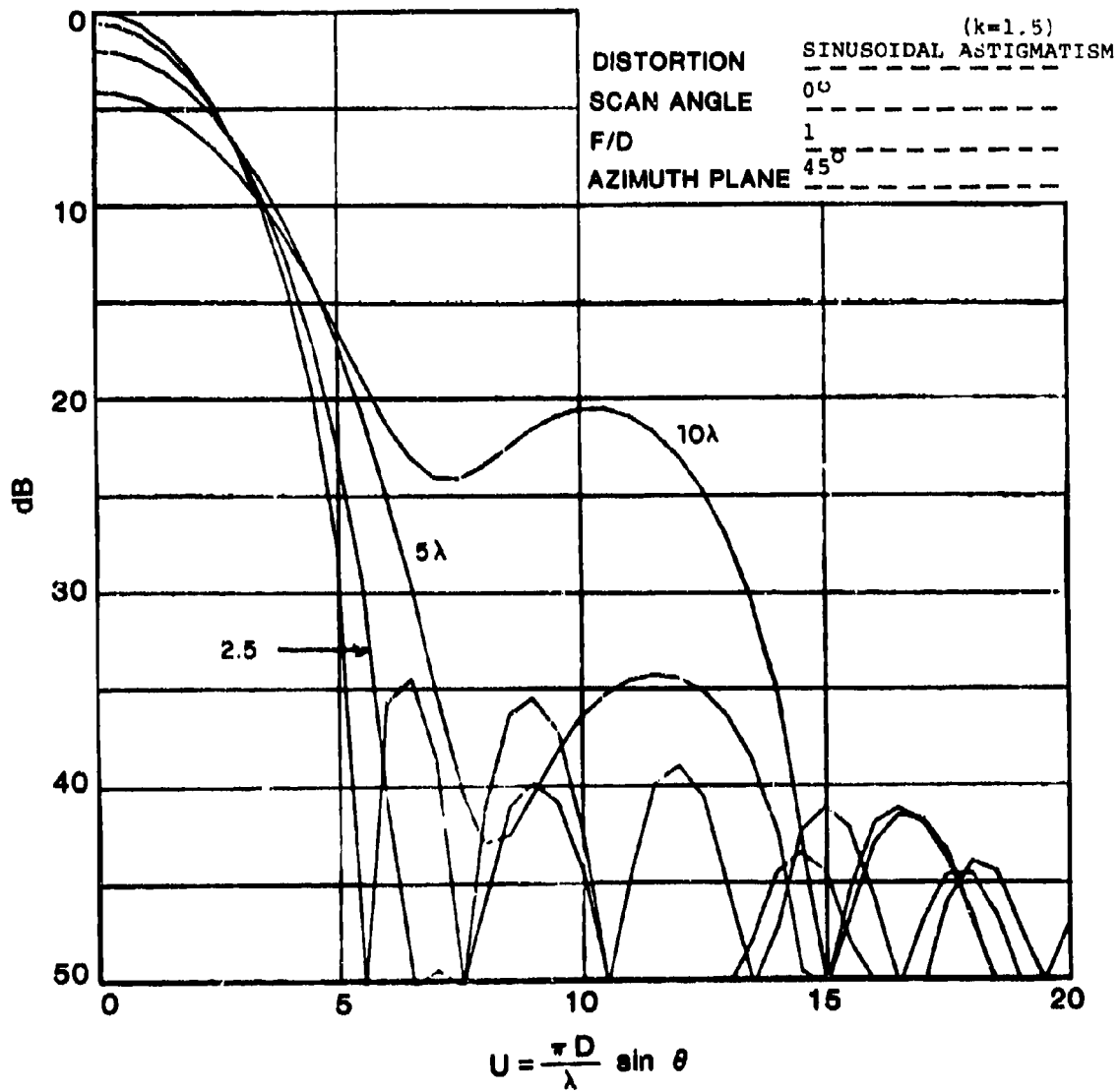


Fig. 53. Radiation patterns of space fed array Gaussian taper  $f(r) = e^{-2r^2}$

-3-21091

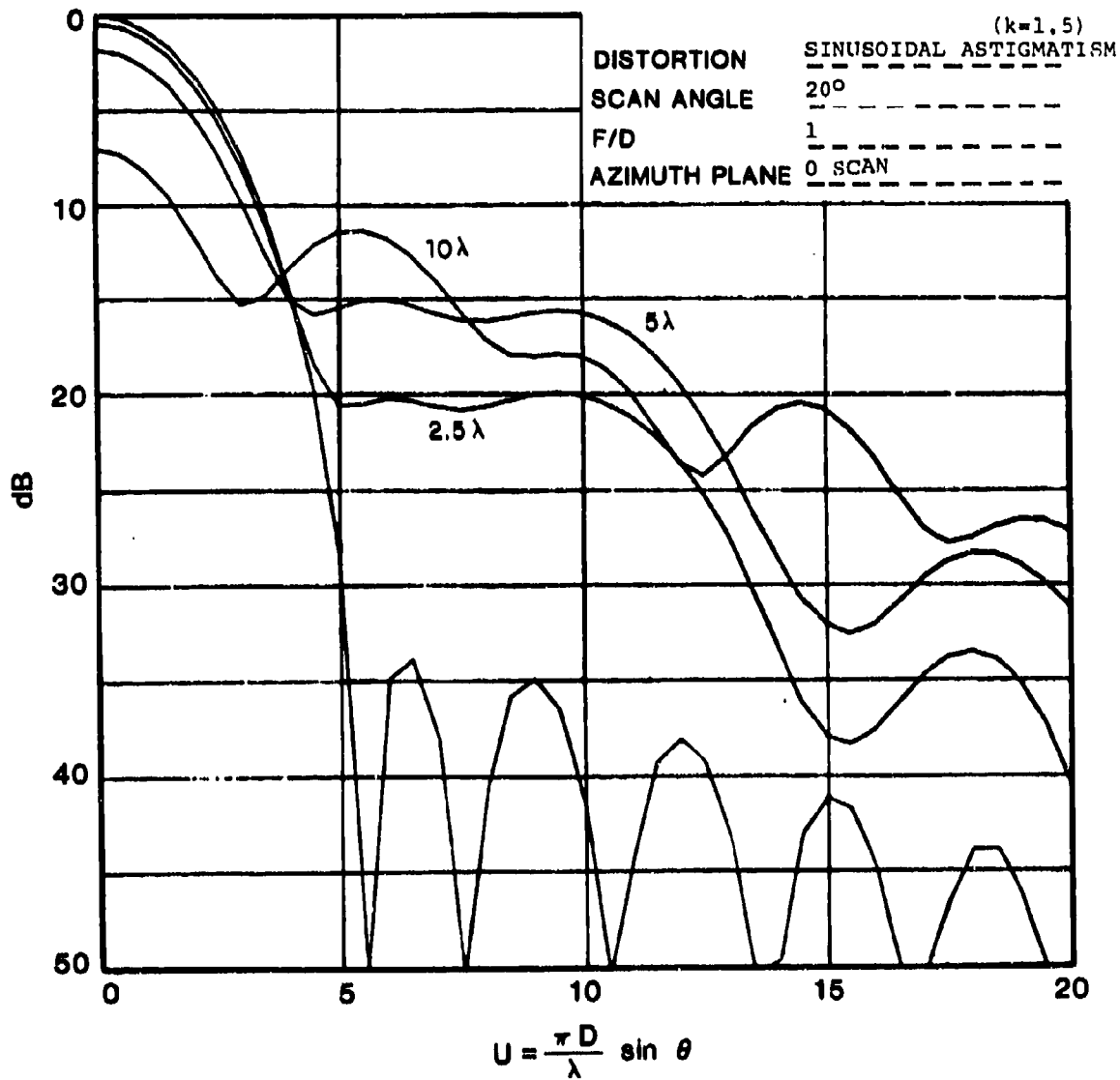


Fig. 54. Radiation patterns of space fed array Gaussian taper  $f(r) = e^{-2r^2}$ .

-3-21092

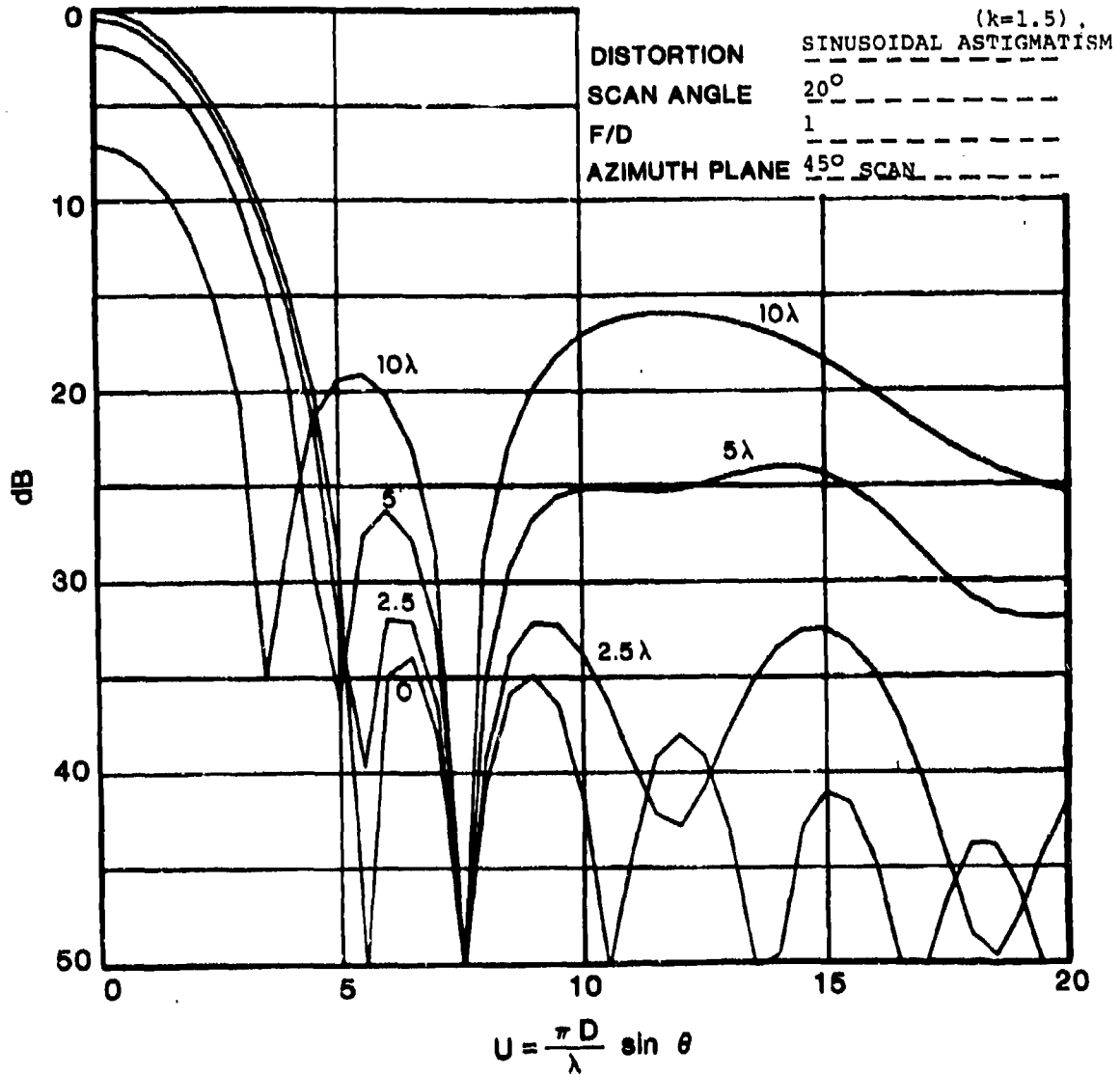


Fig. 55. Radiation patterns of space fed array Gaussian taper  $f(r) = e^{-2r^2}$ .

-3-21093

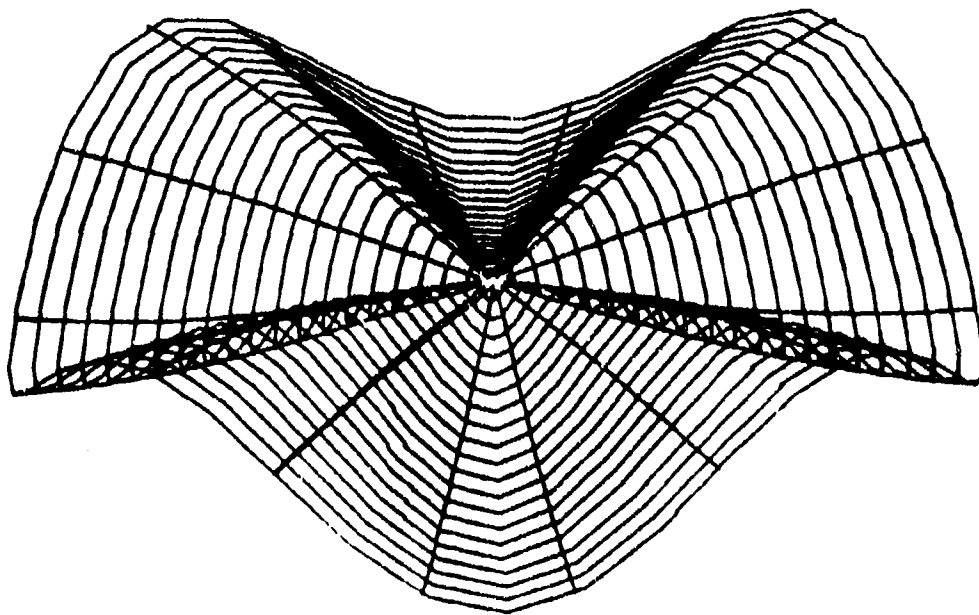


Fig. 56. Eight gore distortion  $z = a(\sin \frac{\pi}{2} r) \cos 4\phi$ .

-3-21094

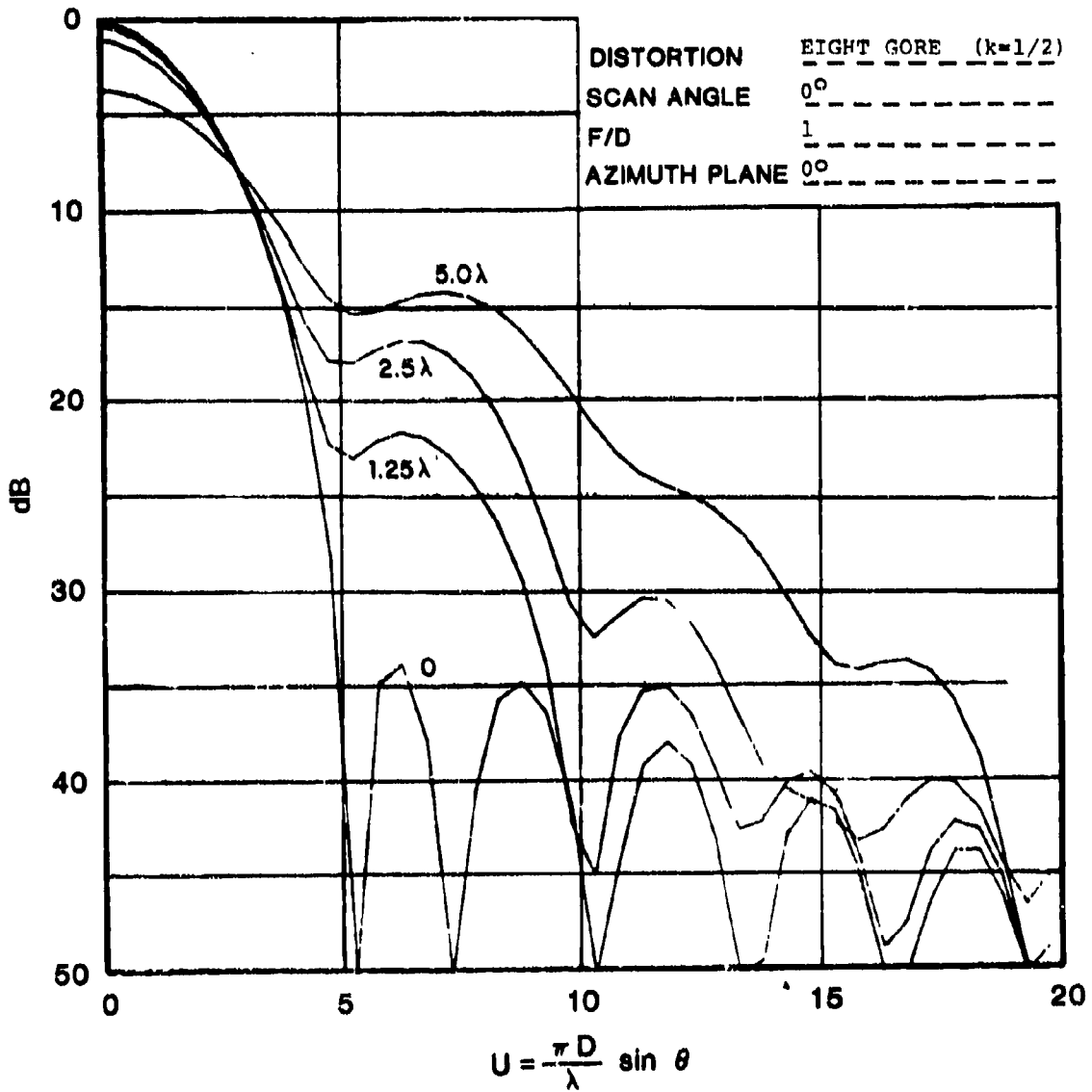


Fig. 57. Radiation patterns of space fed array Gaussian taper  $f(r) = e^{-2r^2}$ .

-3-21095

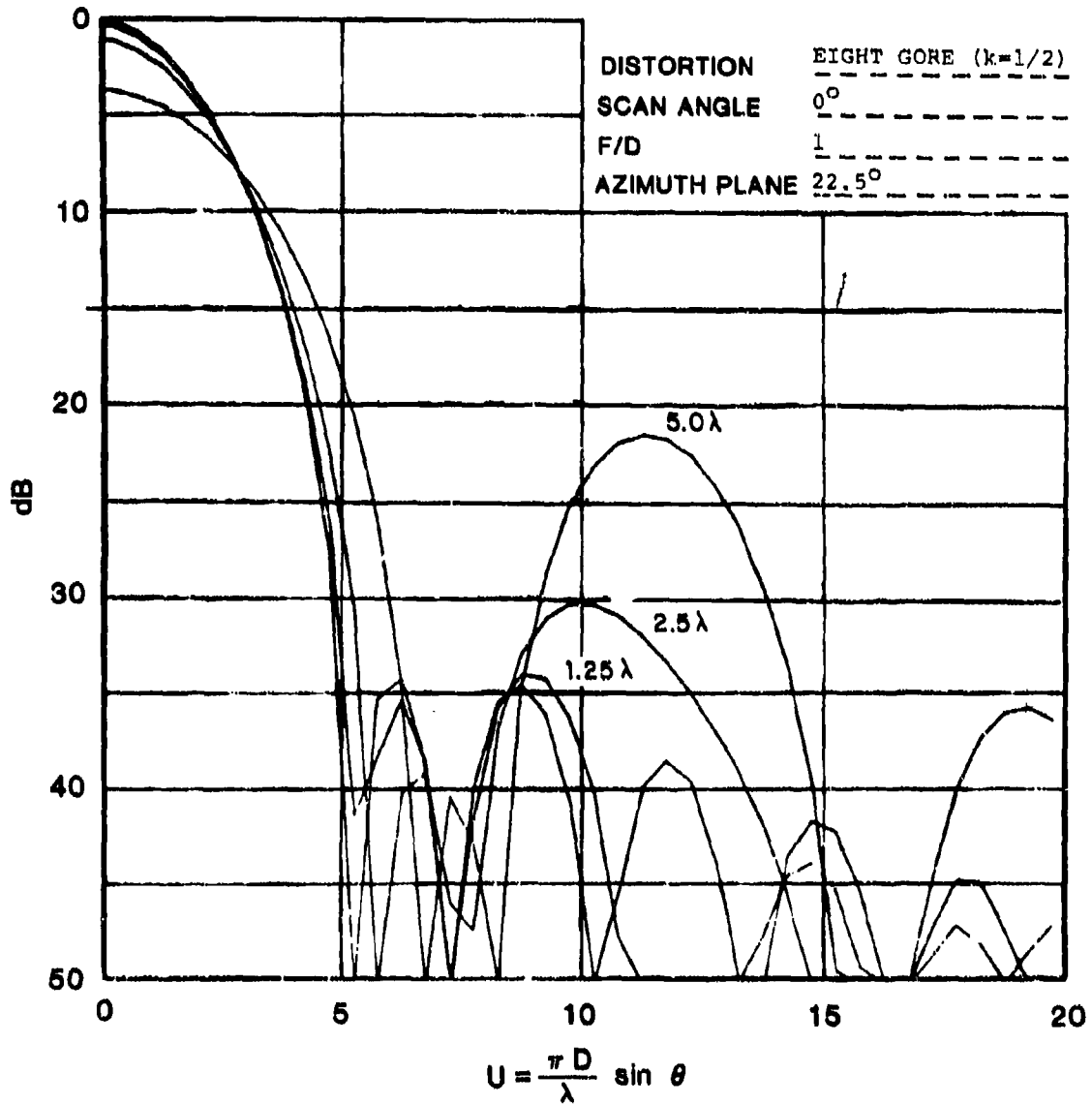


Fig. 58. Radiation patterns of space fed array Gaussian taper  $f(r) = e^{-2r^2}$ .

-3-21096

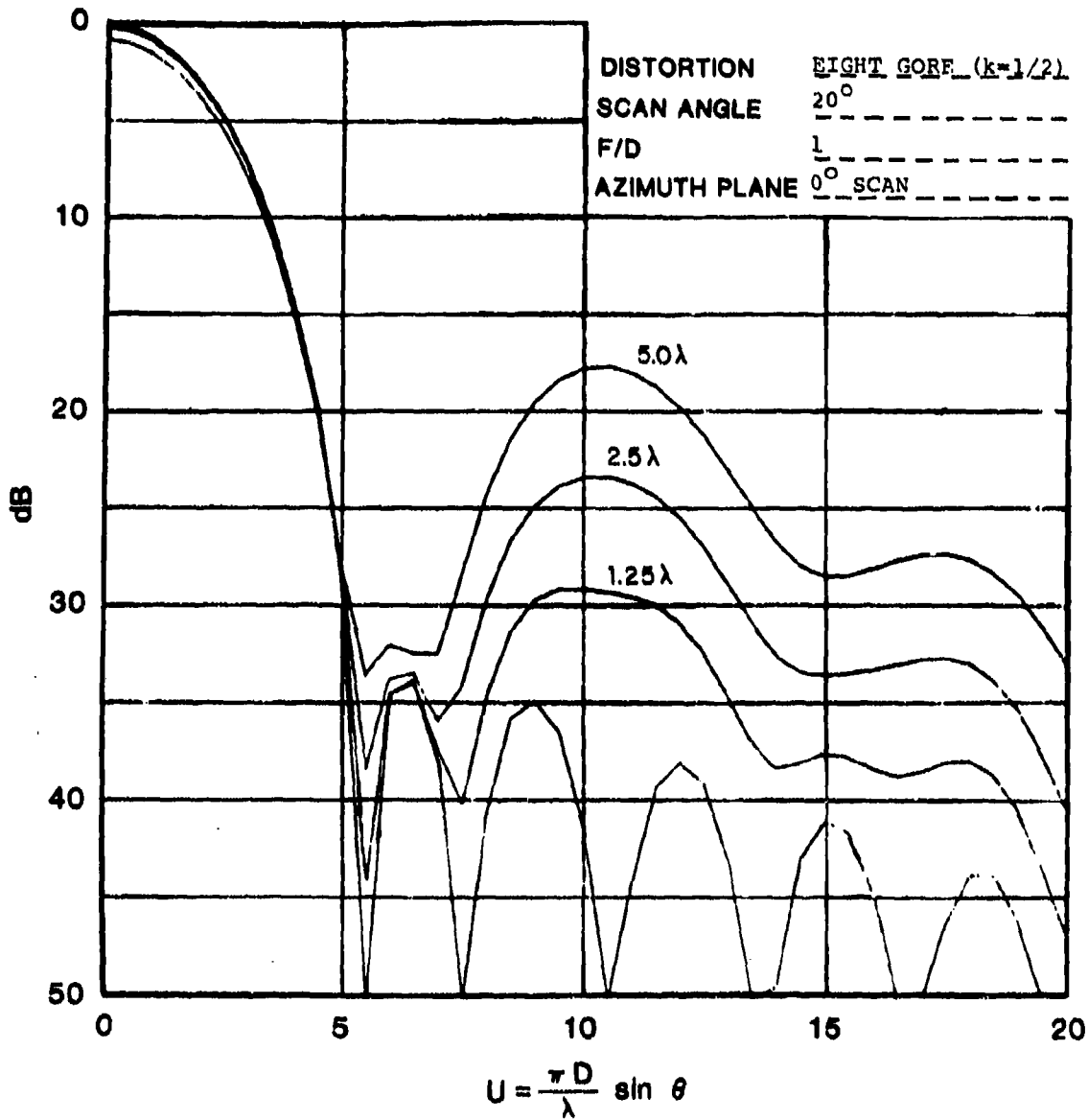


Fig. 59. Radiation patterns of space fed array Gaussian taper  $f(r) = e^{-2r^2}$ .

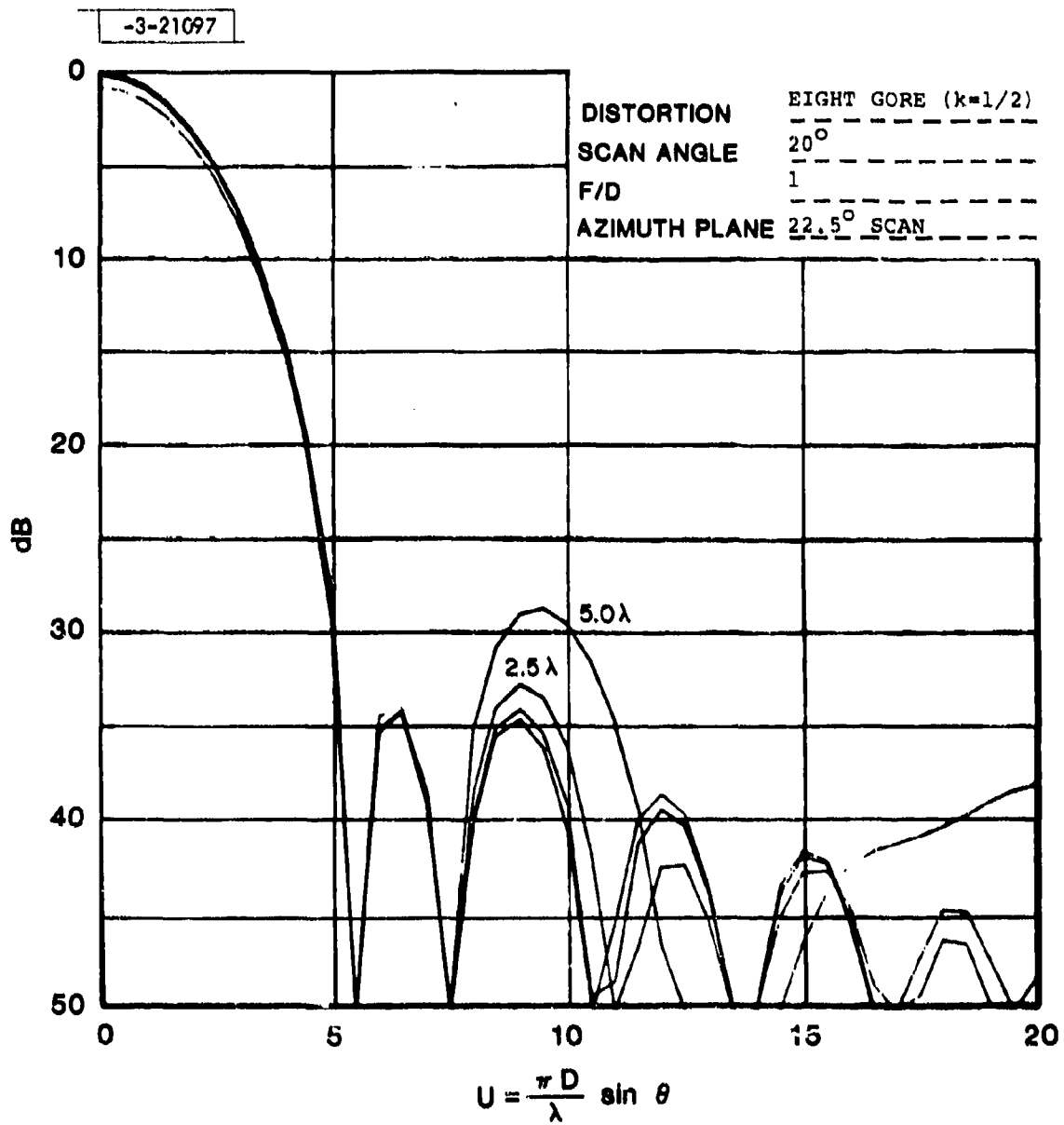


Fig. 60. Radiation patterns of space fed array Gaussian taper  $f(r) = e^{-2r^2}$ .

-3-21098

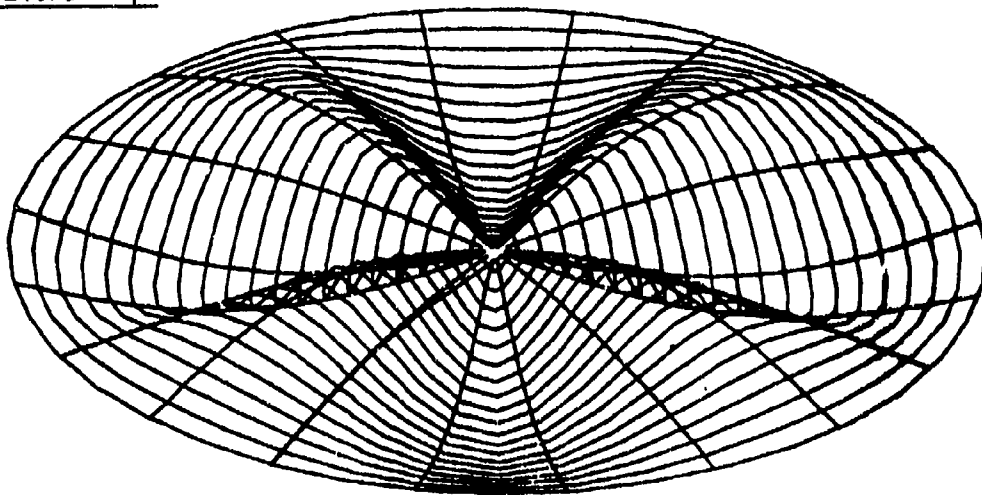


Fig. 61. Eight gore distortion  $z = a (\sin \pi r) \cos 4\phi$ .

-3-21099

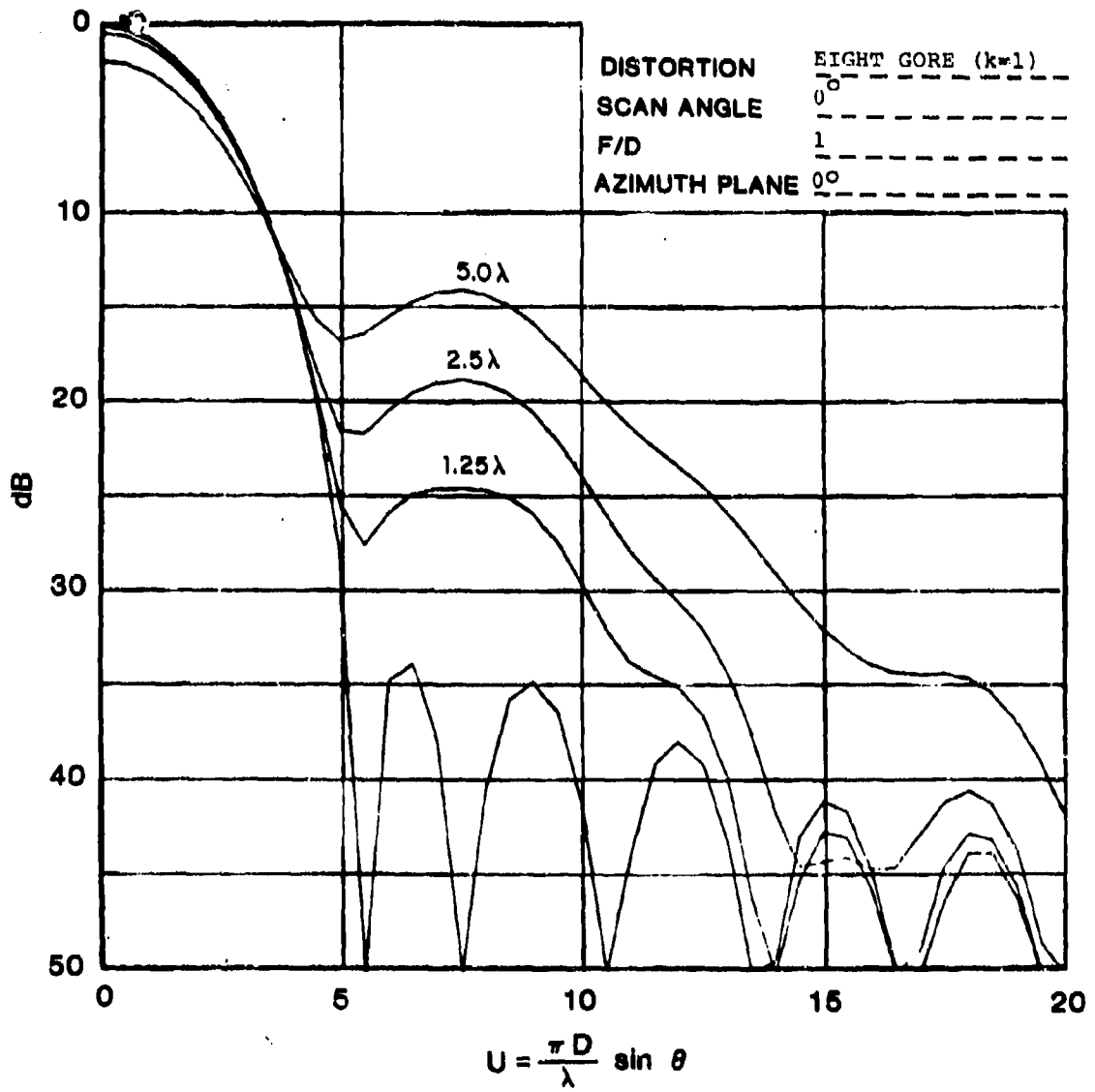


Fig. 62. Radiation patterns of space fed array  
Gaussian taper  $f(r) = e^{-2r^2}$ .

-3-21100

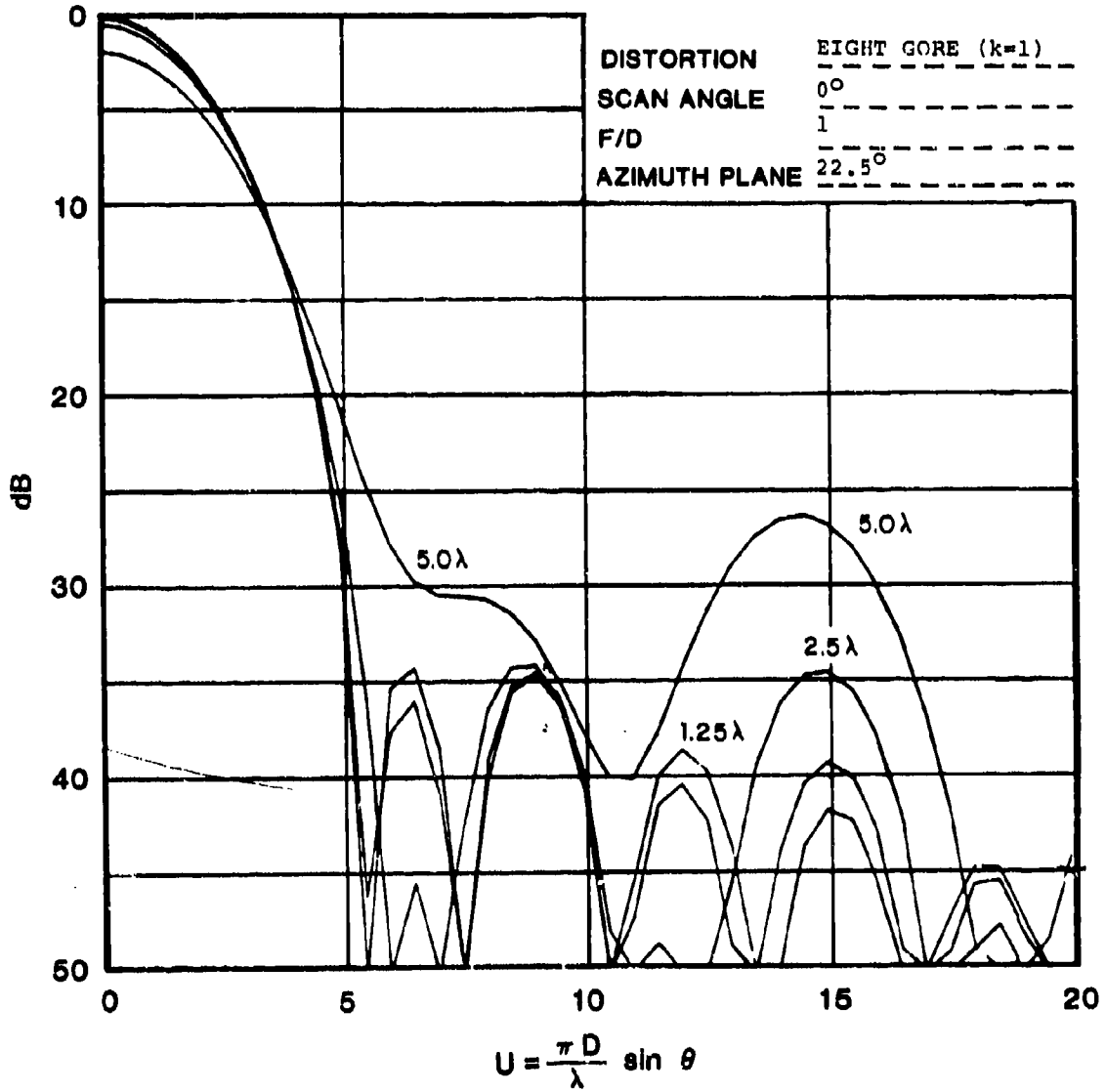


Fig. 63. Radiation patterns of space fed array  
Gaussian taper  $f(r) = e^{-2r^2}$ .

-3-21101

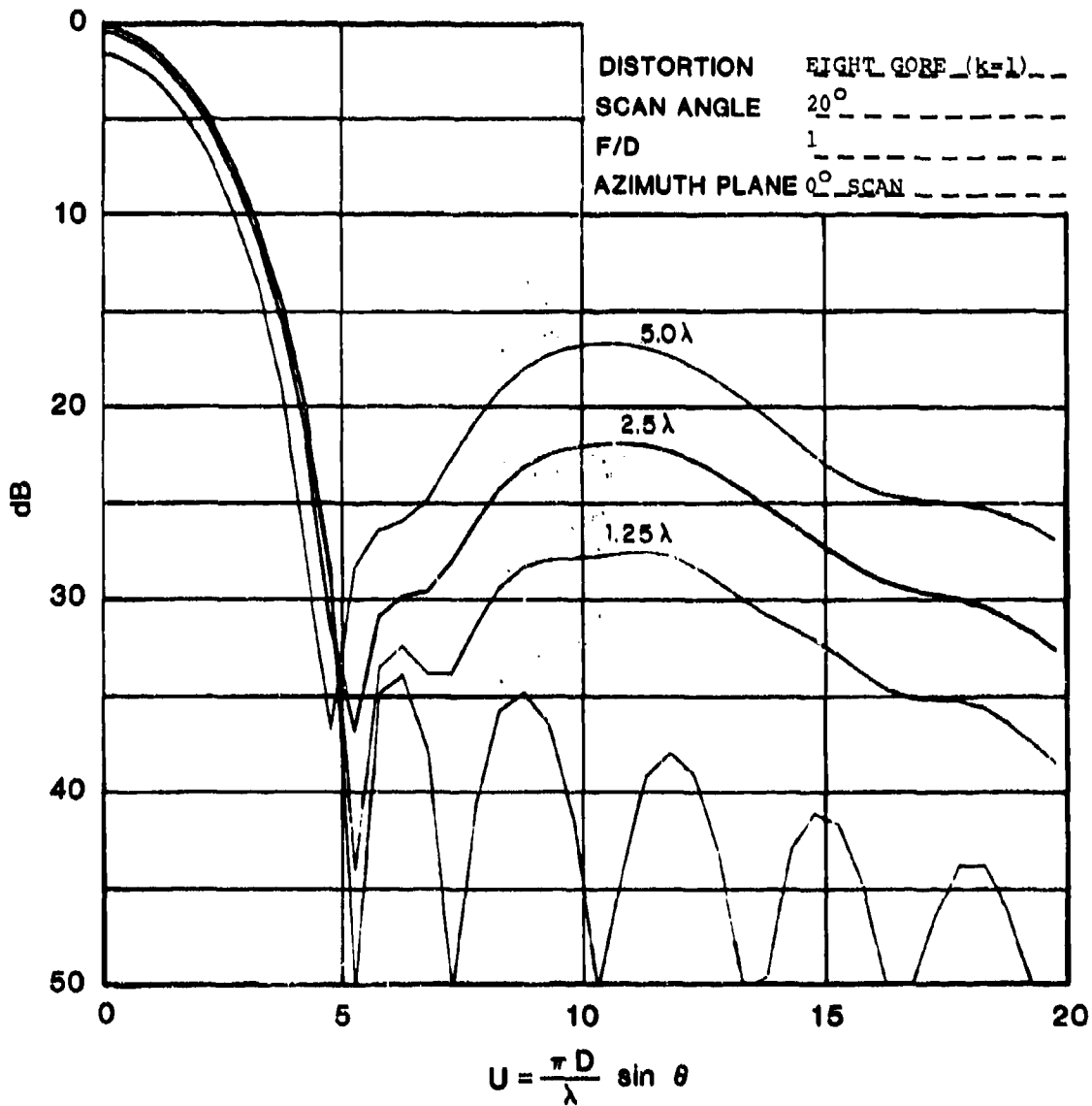


Fig. 64. Radiation patterns of space fed array  
Gaussian Taper  $f(r) = e^{-2r^2}$ .

-3-21102

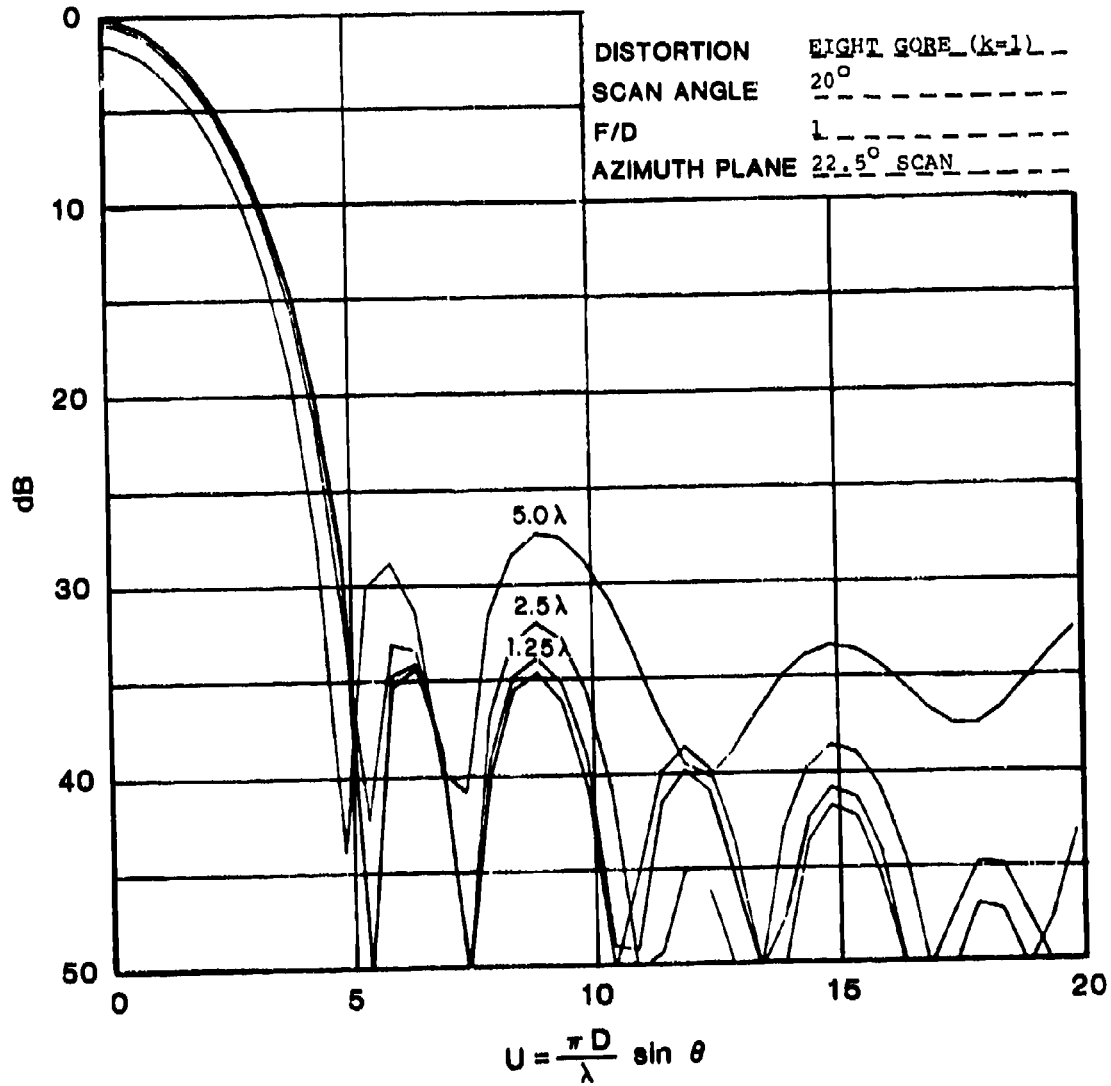


Fig. 65. Radiation patterns of space fed array  
Gaussian taper  $f(r) = e^{-2r^2}$ .

-3-21103

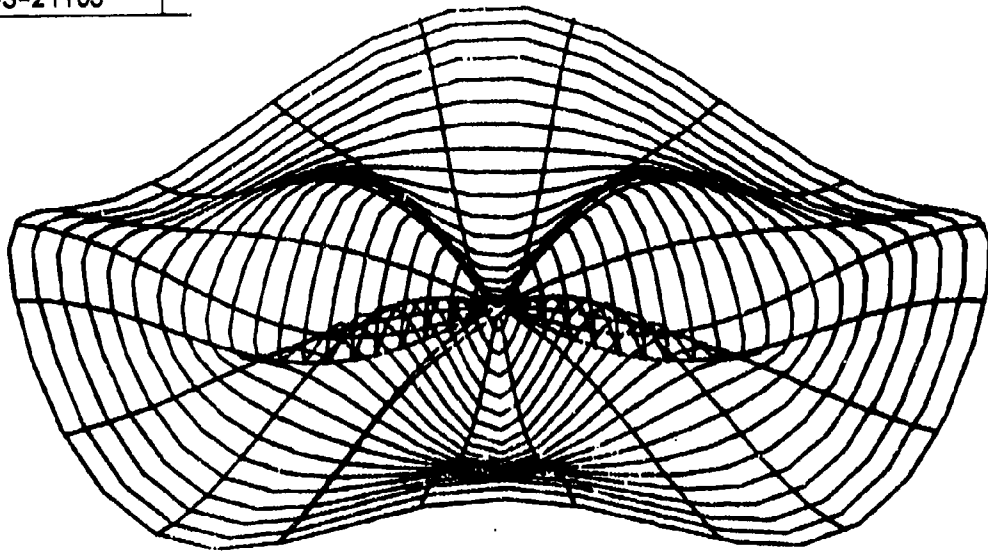


Fig. 66. Eight gore distortion  $z = a (\sin 3/2 \pi r) \cos 4\phi$ .

-3-21104

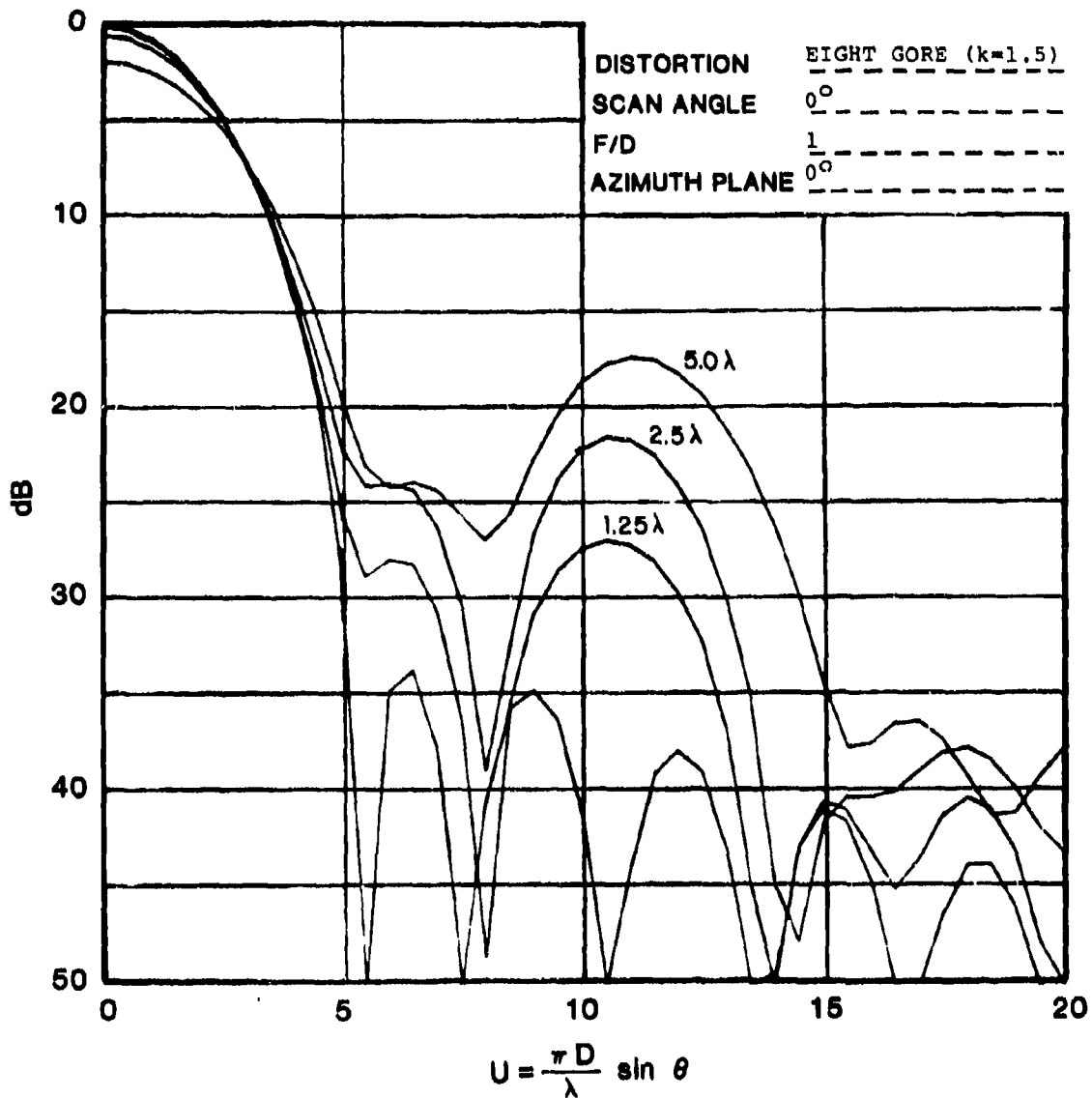


Fig. 67. Radiation patterns of space fed array  
Gaussian taper  $f(r) = e^{-2r^2}$ .

-3-21105

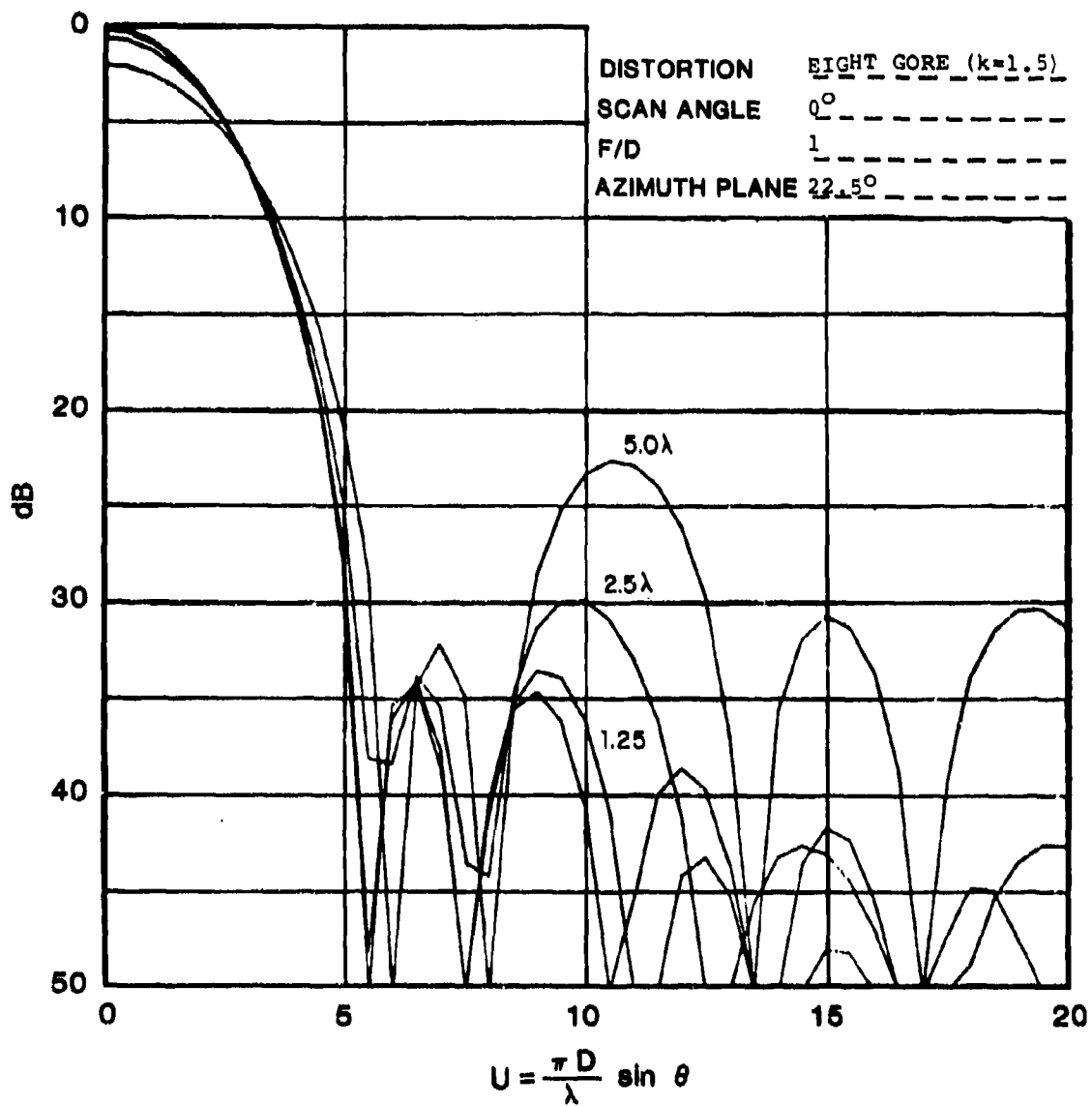


Fig. 68. Radiation patterns of space fed array  
Gaussian taper  $f(r) = e^{-2r^2}$ .

-3-21106

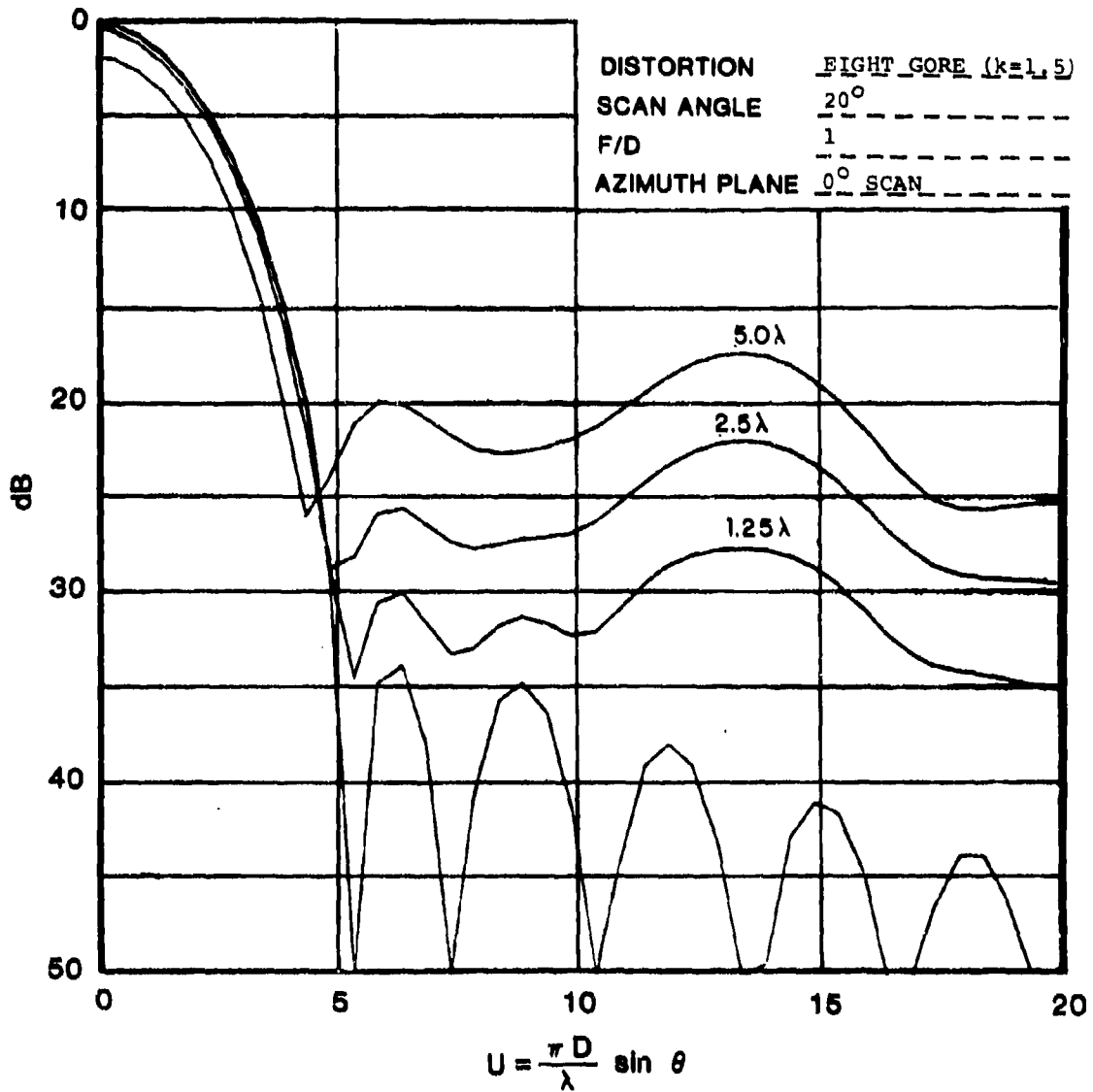


Fig. 69. Radiation patterns of space fed array  
Gaussian taper  $f(r) = e^{-2r^2}$ .

-3-21107

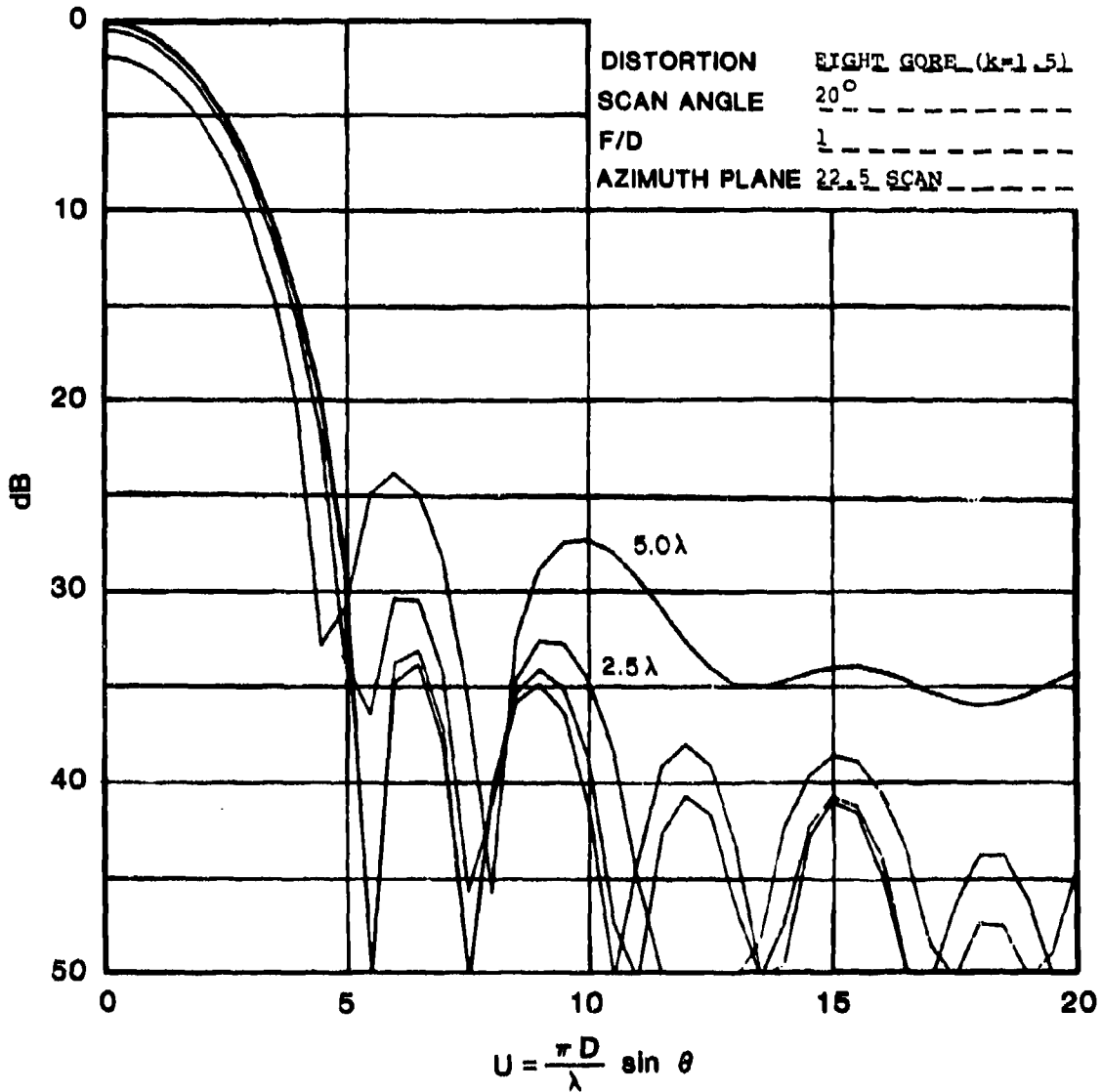


Fig. 70. Radiation patterns of space fed array  
Gaussian taper  $f(r) = e^{-2r^2}$ .

-3-21108

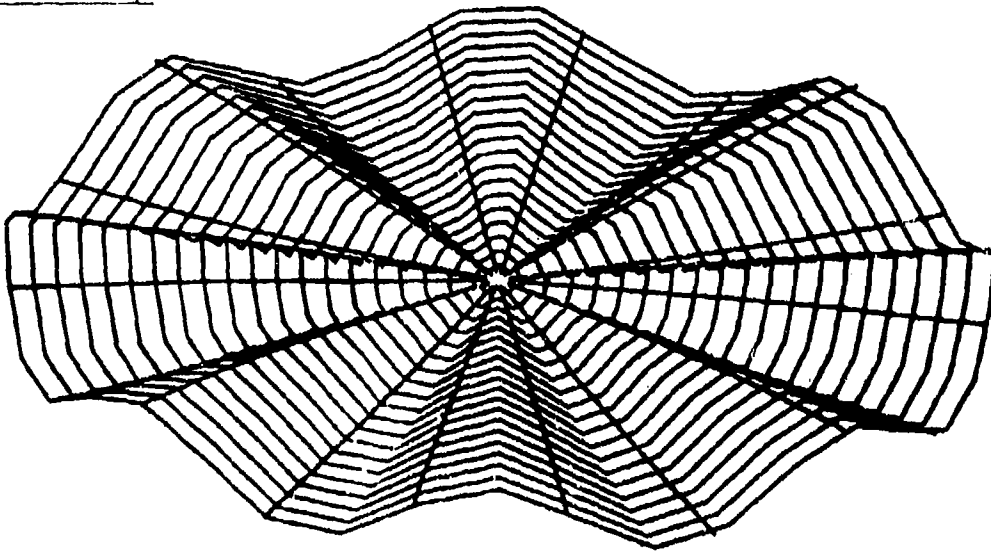


Fig. 71. Sixteen gore distortion  $z = a \left( \sin \frac{\pi}{2} r \right) \cos 8\phi$ .

-3-21109

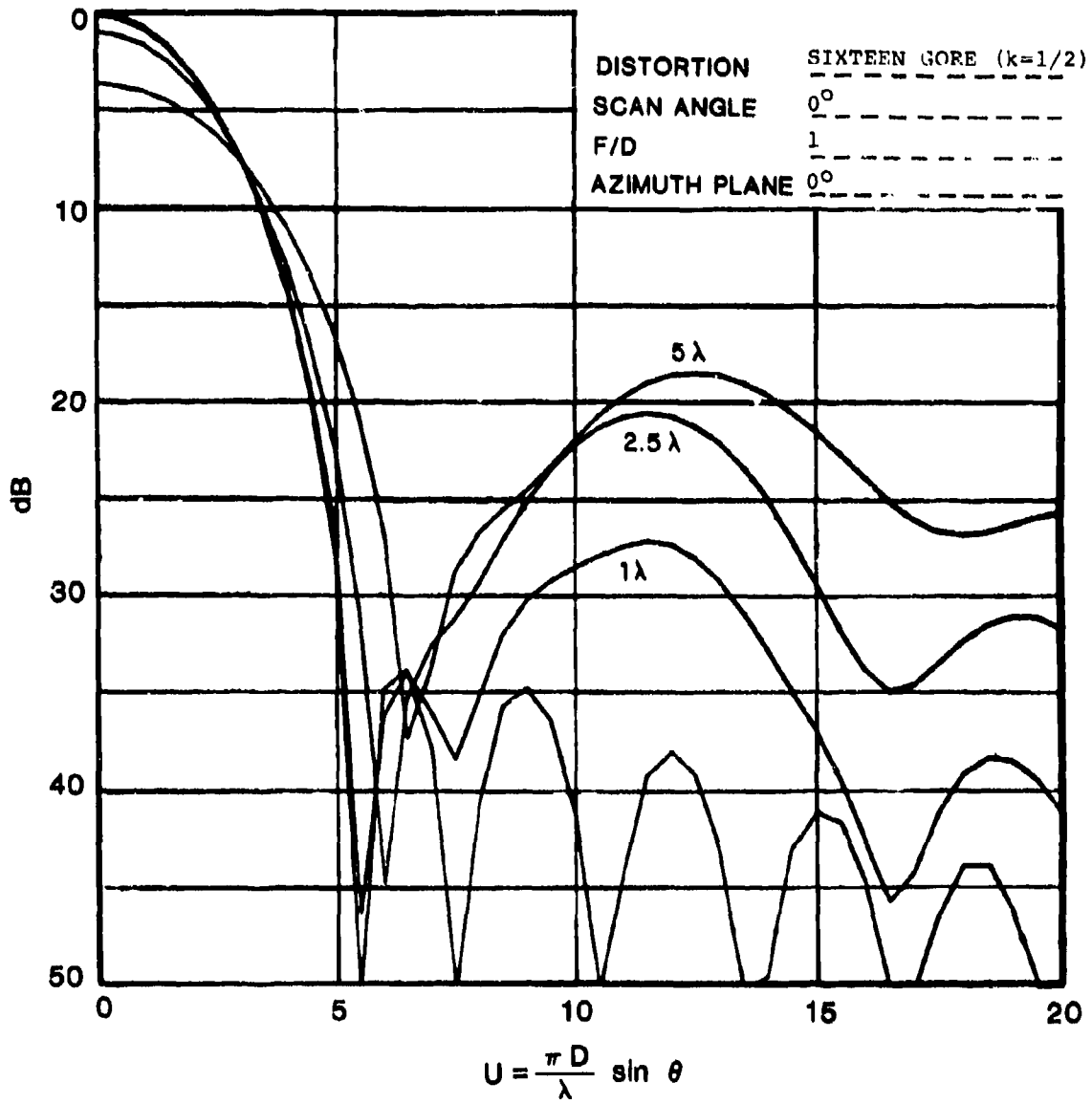


Fig. 72. Radiation patterns of space fed array  
Gaussian taper  $f(r) = e^{-2r^2}$ .

-3-21110

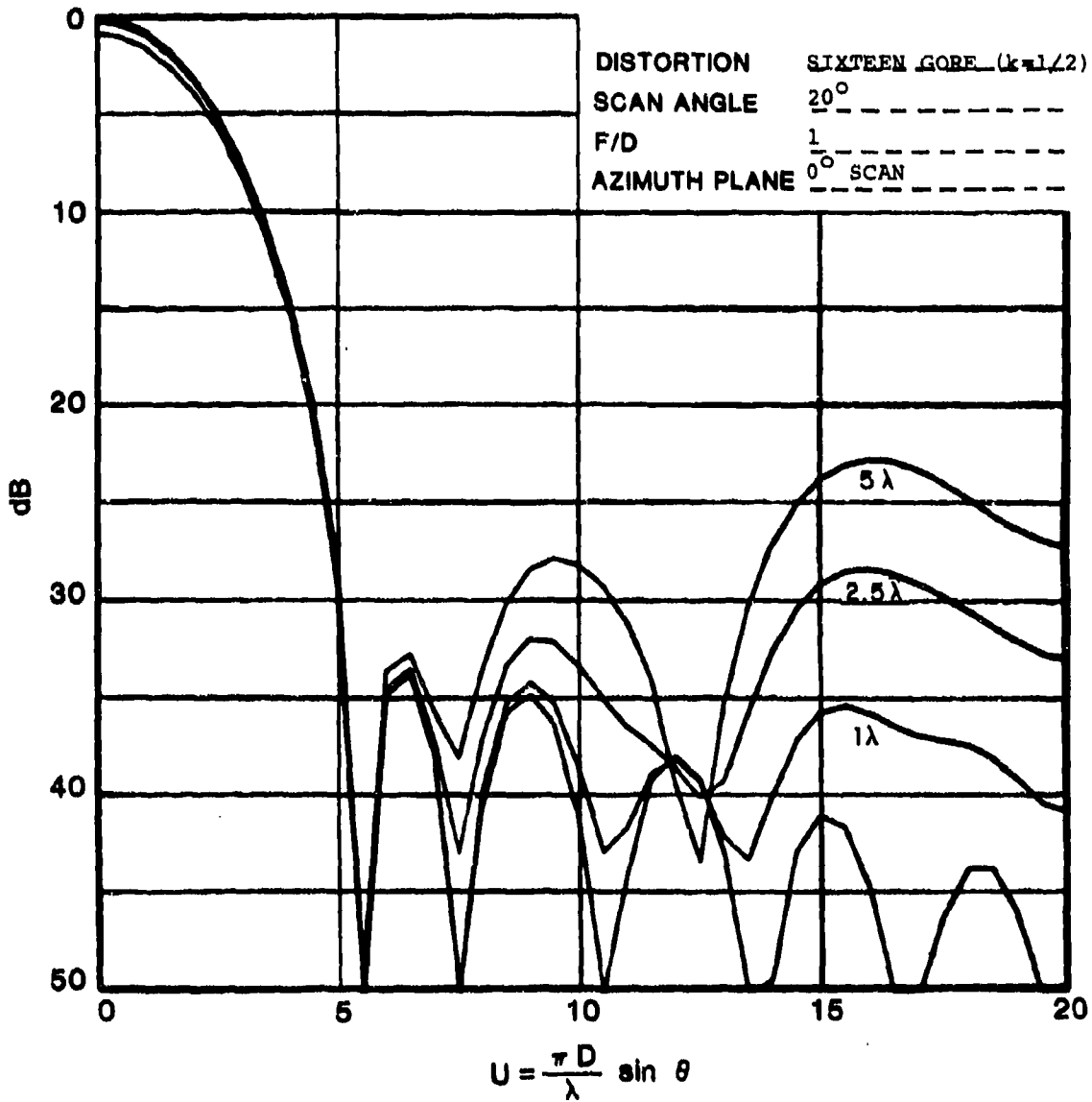


Fig. 73. Radiation patterns of space fed array  
Gaussian taper  $f(r) = e^{-2r^2}$ .

-3-21111

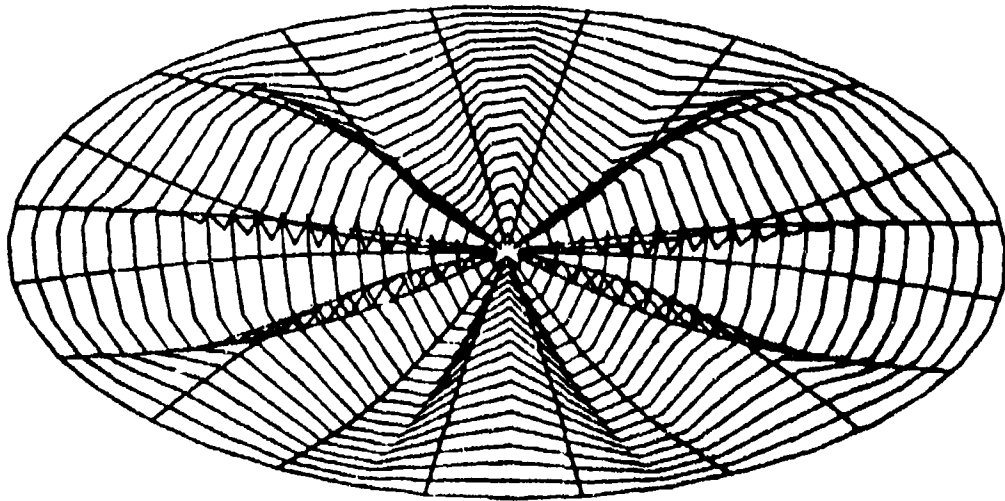


Fig. 74. Sixteen gore distortion  $z = a (\sin^2 r) \cos 8\phi$ .

-3-21112

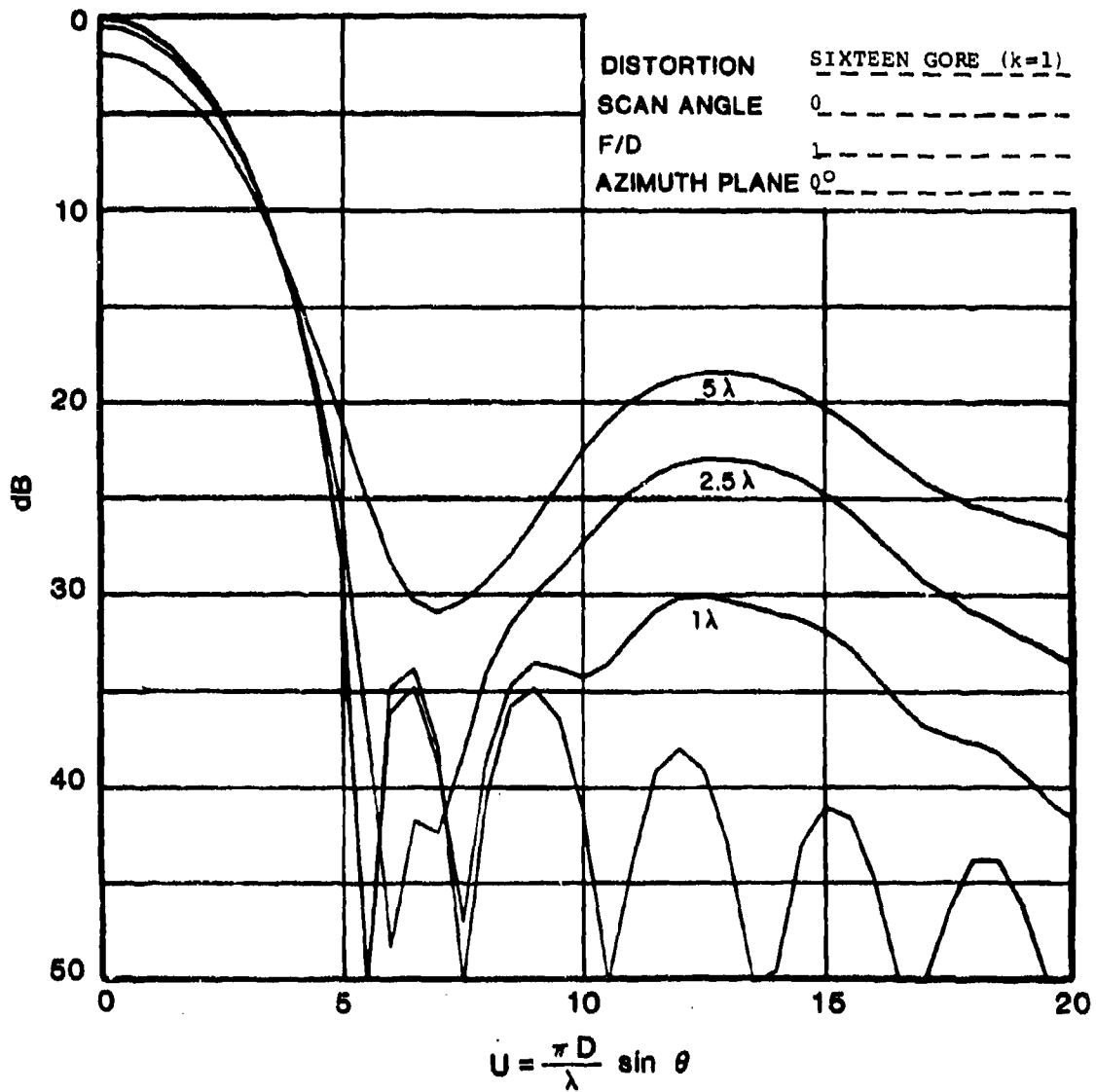


Fig. 75. Radiation patterns of space fed array  
Gaussian taper  $f(r) = e^{-2r^2}$ .

-3-21113

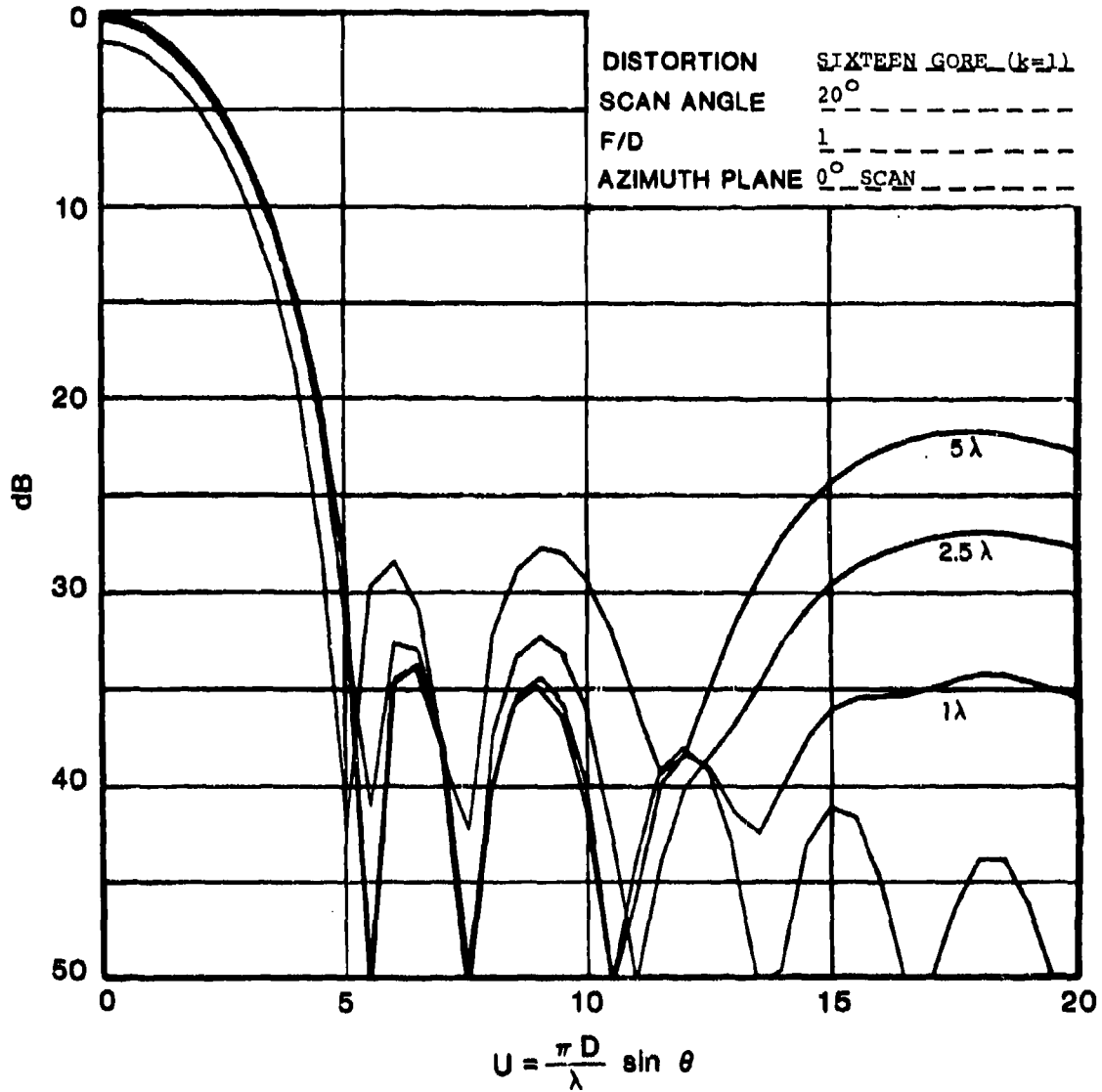


Fig. 76. Radiation patterns of space fed array  
Gaussian taper  $f(r) = e^{-2r^2}$ .

-3-21114

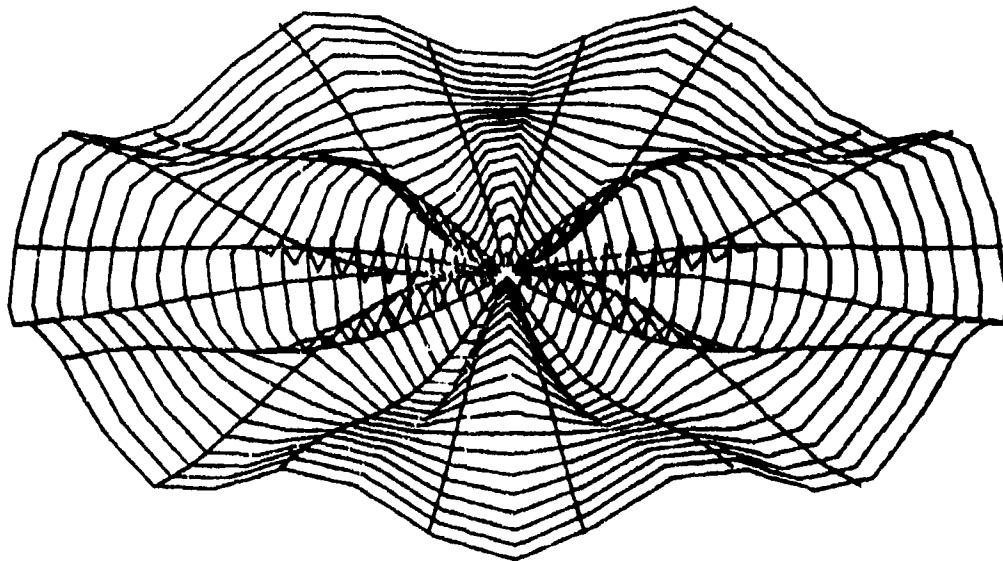


Fig. 77. Sixteen gore distortion  $z = a \left( \sin \frac{3}{2} \pi r \right) \cos 8\phi$ .

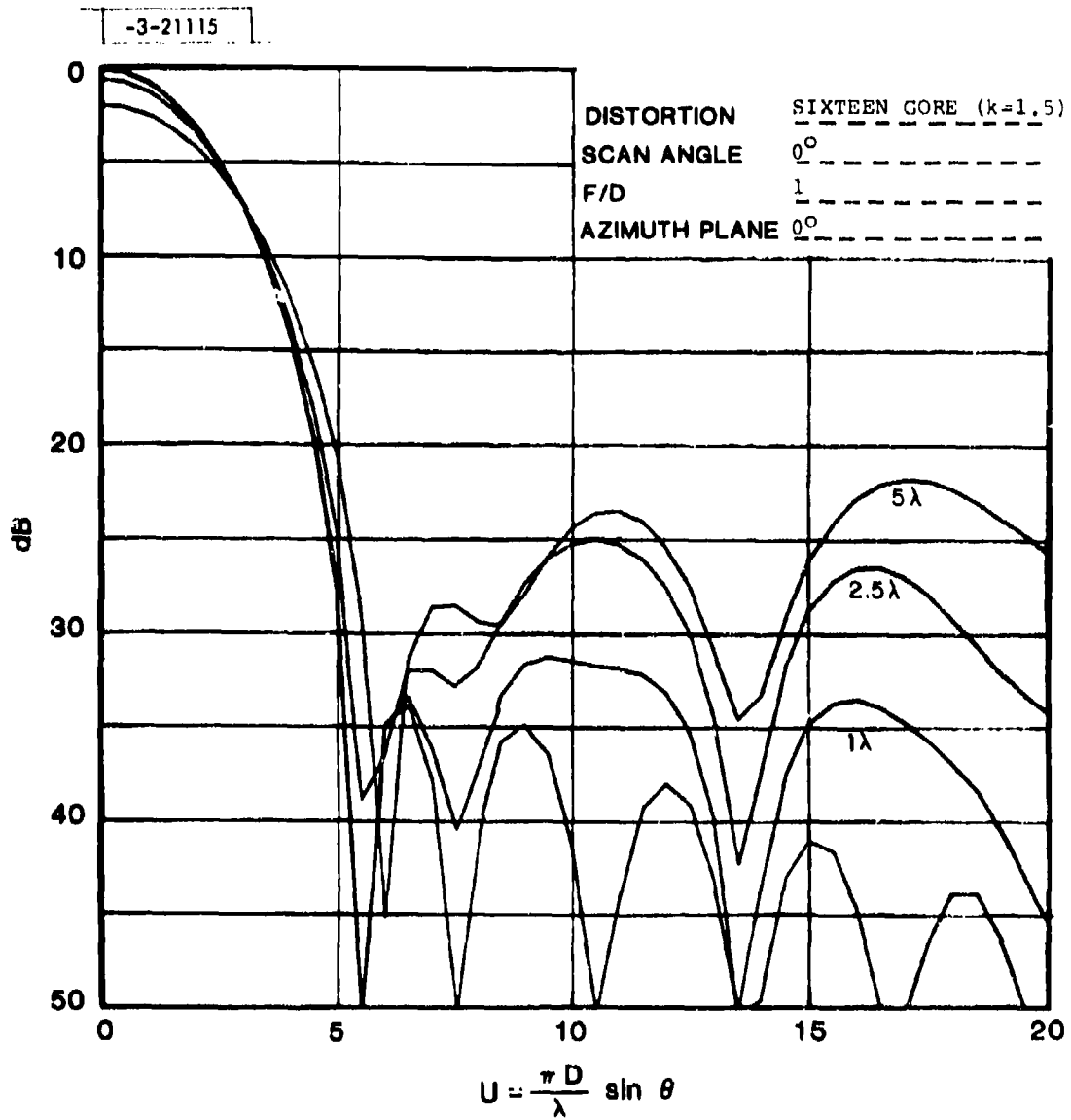


Fig. 78. Radiation patterns of space fed array  
 Gaussian taper  $f(r) = e^{-2r^2}$ .

-3-21116

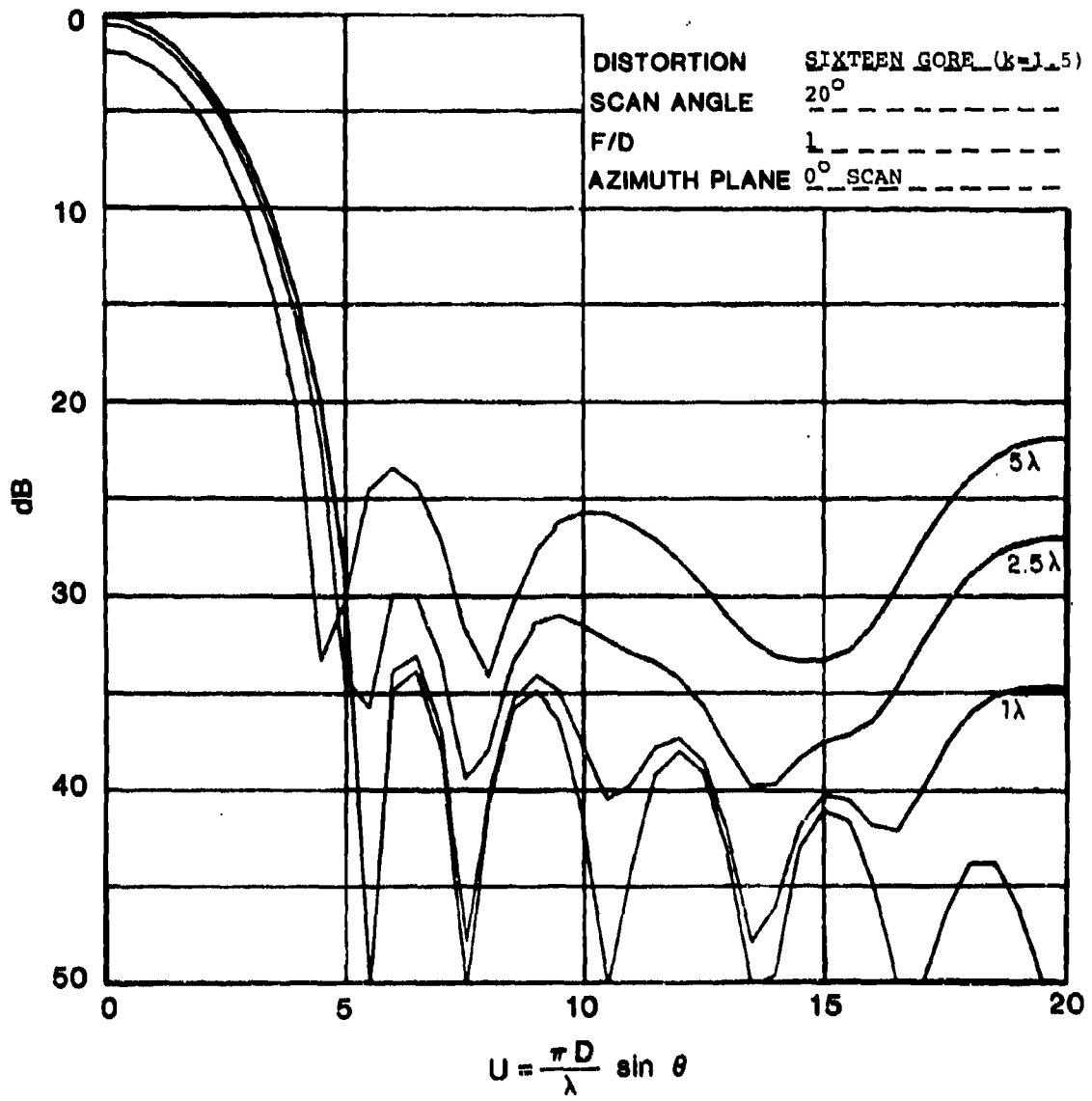


Fig. 79. Radiation patterns of space fed array  
Gaussian taper  $f(x) = e^{-2x^2}$ .

- a) For moderate loss of main beam gain the loss is independent of the number of gores.
- b) The pattern degradation is more benign in the seam plane cut and was not calculated in all cases.
- c) The pattern degradation was markedly dependent on radial axial distortion, that is on the value of "k".
- d) The pattern degradation was more spread out with the larger number of gores, probably as this distortion represents a higher spatial frequency.

The last point mentioned was further investigated, by calculating the patterns over a larger angular interval. Fig. 80 to 83 show the principal and seam plane pattern of a sixteen gore distortion with a five and ten wavelength maximum distortion.

#### 6.7 Half Linear Fold

Next we consider an unsymmetric case where one half of the array experiences a linear distortion, Fig. 84. Fig. 85 and 86 show the radiation patterns across the fold for zero and twenty degree scan angle. The zero scan case clearly shows the expected main beam shift and a coma type degradation.

-3-21117

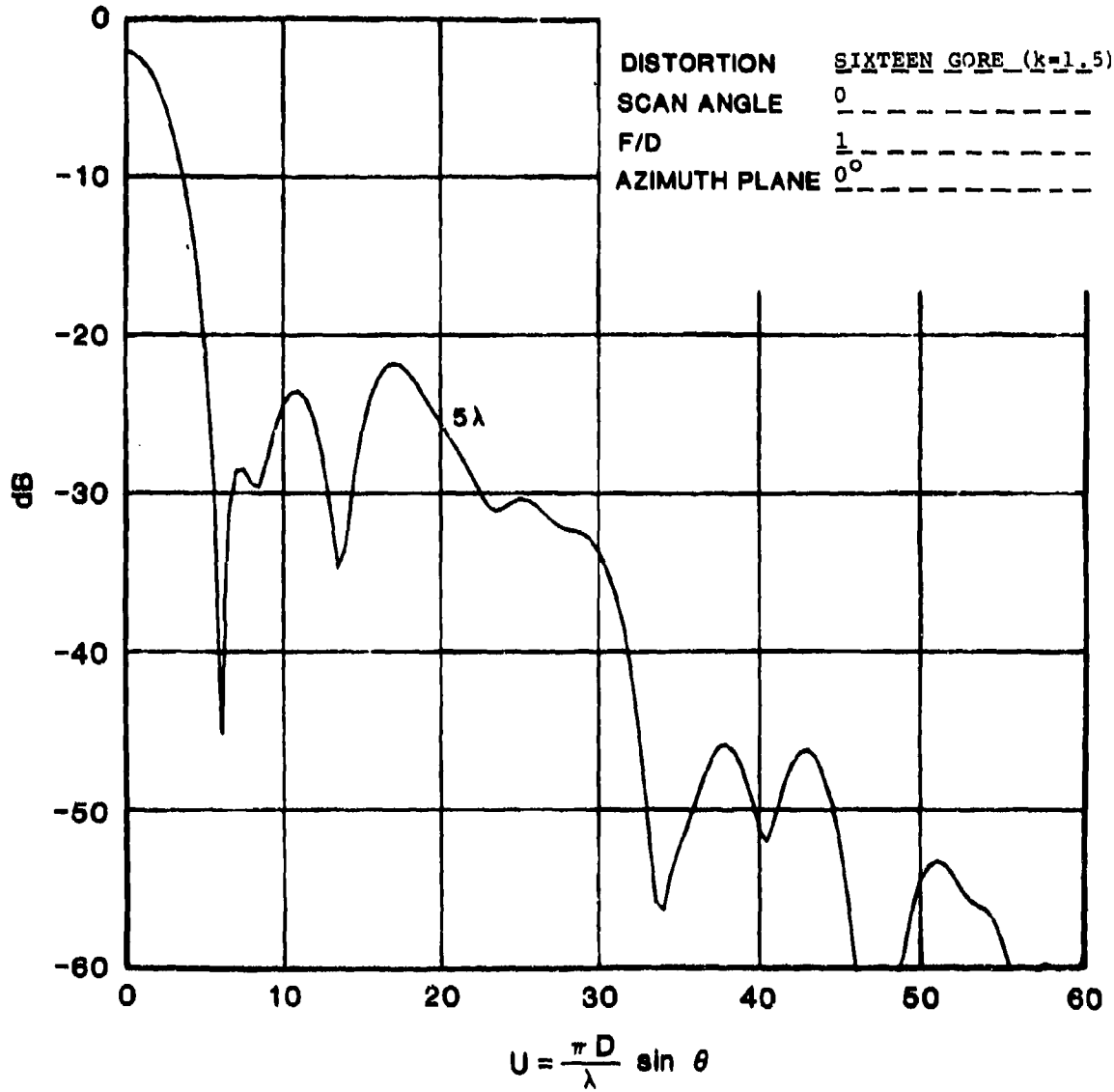


Fig. 80. Radiation pattern of space fed array  
Gaussian taper  $f(r) = e^{-2r^2}$ .

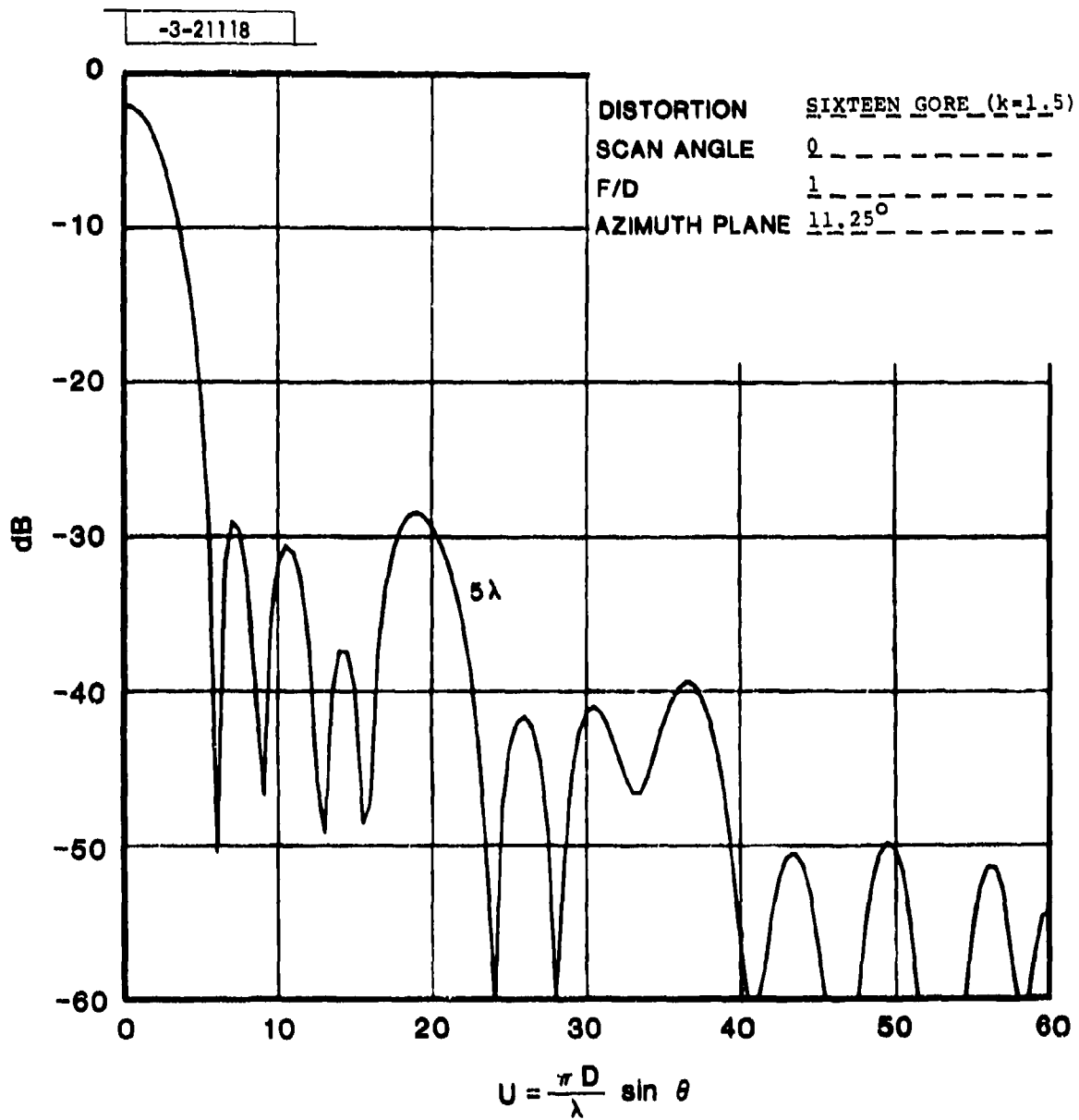


Fig. 81. Radiation pattern of space fed array  
 Gaussian taper  $f(r) = e^{-2r^2}$ .

-3-21119

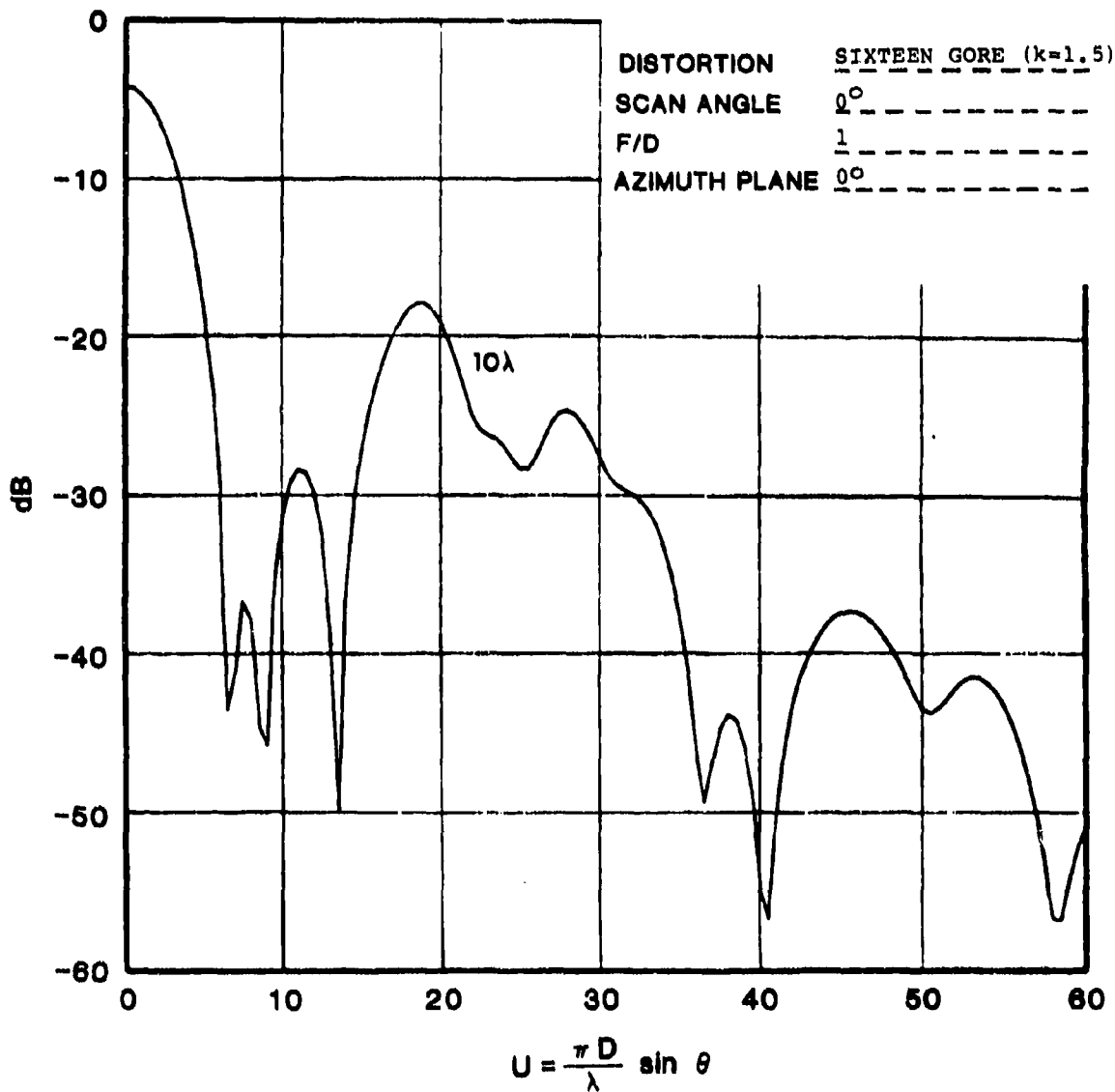


Fig. 82. Radiation pattern of space fed array  
Gaussian taper  $f(r) = e^{-2r^2}$ .

-3-21120

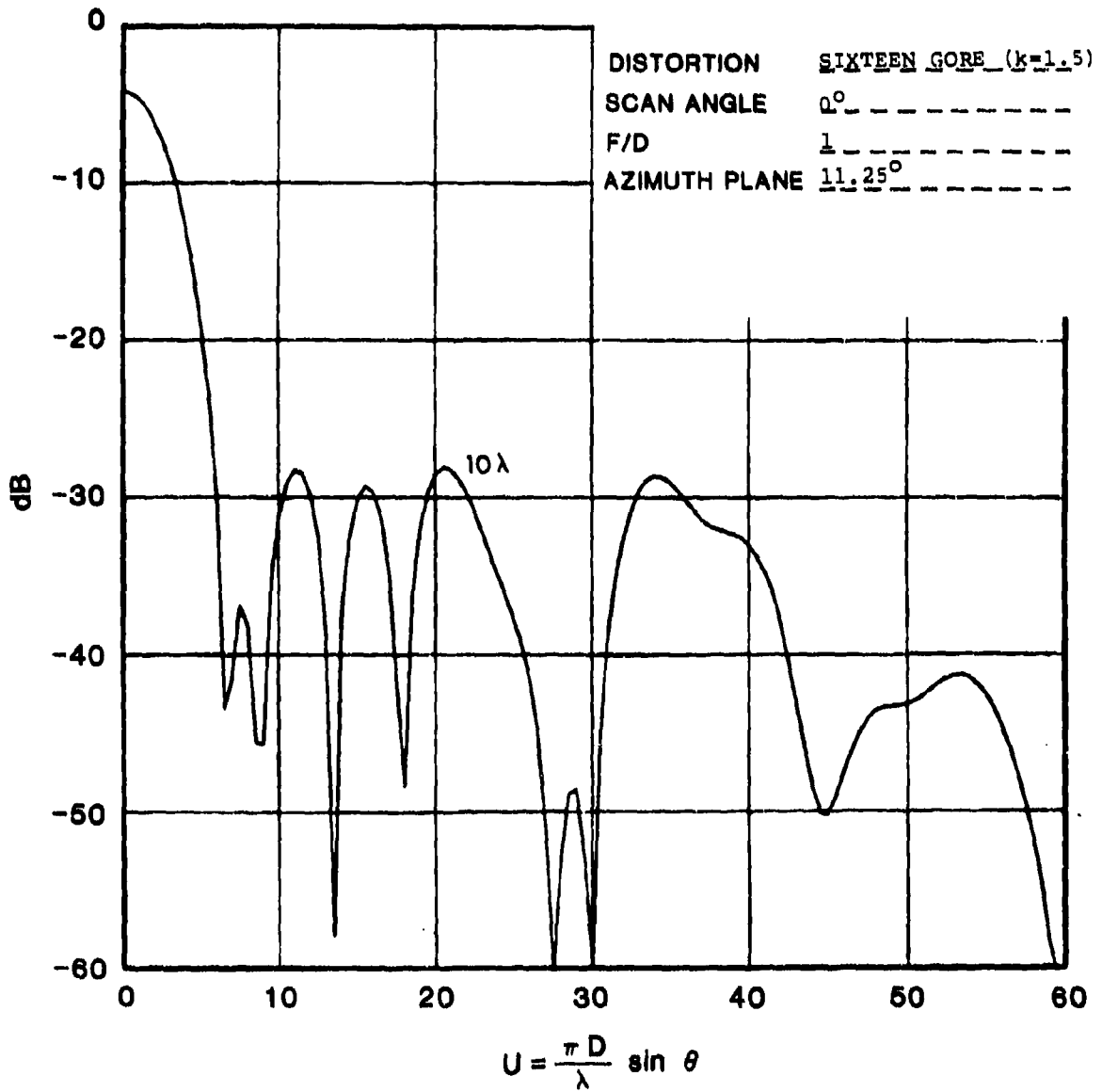


Fig. 83. Radiation pattern of space fed array  
Gaussian taper  $f(r) = e^{-2r^2}$ .

-3-21121

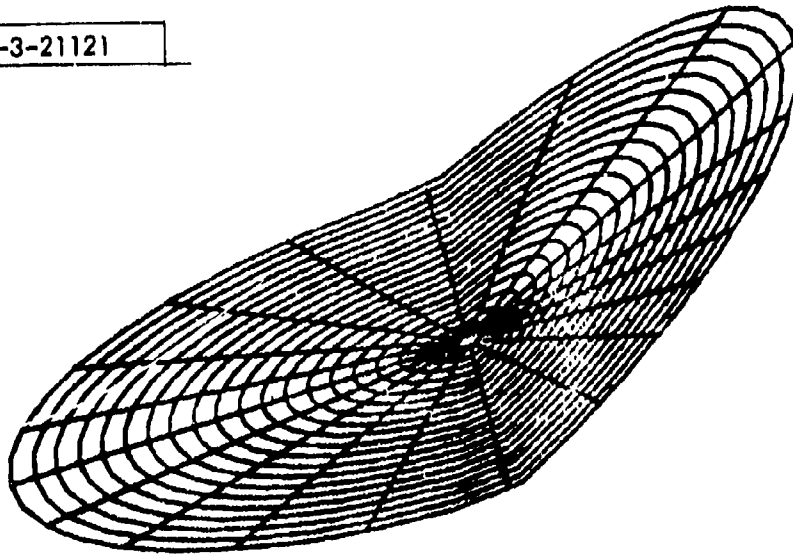


Fig. 84. Half linear fols  $z = ay, y > 0;$   
 $z = 0, y < 0.$

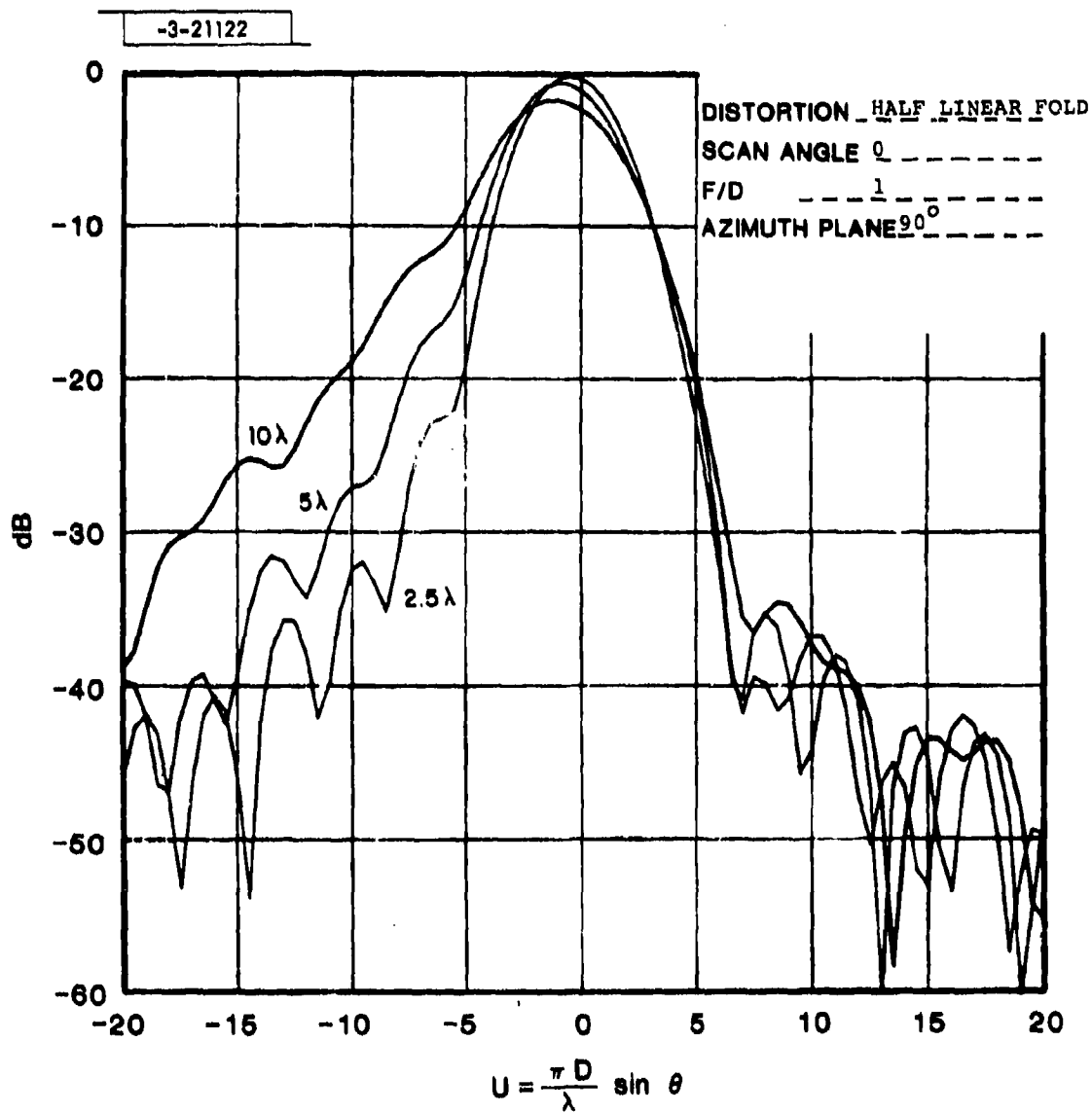


Fig. 85. Radiation patterns of space fed array  
 Gaussian taper  $f(r) = e^{-2r^2}$ .

-3-21123

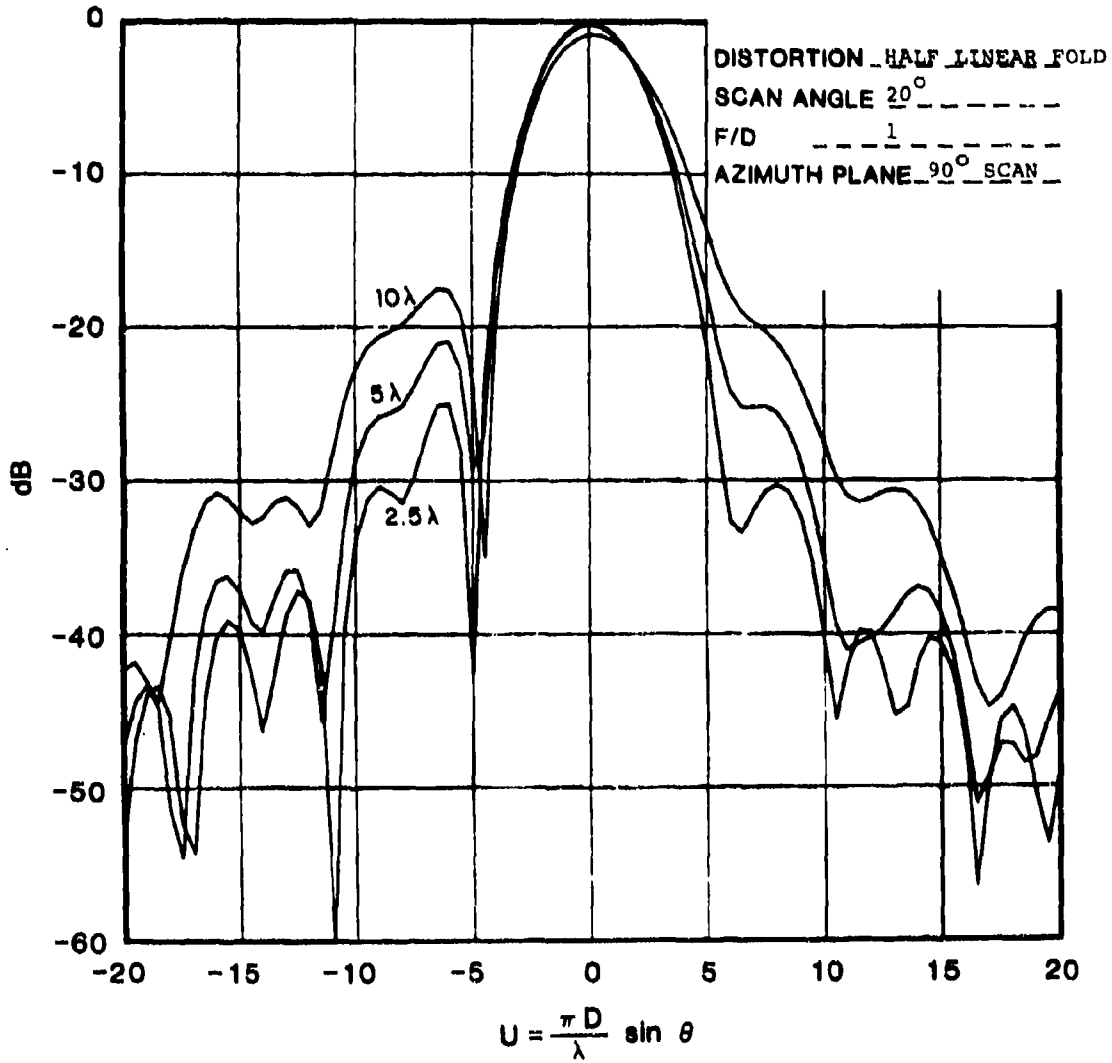


Fig. 86. Radiation patterns of space fed array  
Gaussian Taper  $f(r) = e^{-2r^2}$ .

## 7. RADIAL DISTORTIONS

In Appendix A-2 we derive that the total path length advance due to an element radial displacement  $\Delta_r$  is  $\epsilon_r$ :

$$\epsilon_r = \Delta_r \left[ \sin \theta \cos(\phi - \phi') - \frac{r/2f}{\sqrt{1 + (r/2f)^2}} \right] \quad (28)$$

where  $(r, \phi)$  are aperture coordinates

and  $(\theta, \phi)$  are observational coordinates.

### 7.1 Uniform Thermal Expansion

We consider the case of uniform thermal expansion where a module element at a radial distance " $R_0$ " has expanded to a radial distance " $R$ " given by

$$R = R_0 [1 + e\Delta T] \quad (29)$$

where  $R_0$  is the original radius used for the phase shift commands

$e$  is the thermal coefficient of expansion

$\Delta T$  is the temperature change

The radial displacement is

$$\Delta_r = R_0 e \Delta T \quad (30)$$

The radiation pattern for the circular aperture scanned to  $(\theta_0, \phi_0)$  may be written as

$$g(\theta, \phi) = \int_0^{R_m} \int_0^{2\pi} f(R) e^{jkR\sin\theta_0 \cos(\phi_0 - \phi') - jkR\sin\theta \cos(\phi - \phi')} \times \\ e^{jkRe\Delta T \sin\theta \cos(\phi - \phi')} \times \\ e^{jk\epsilon''} R dR d\phi' \quad (31)$$

where  $k = 2\pi/\lambda$

$$\epsilon'' = -Re\Delta T \frac{R/F}{\sqrt{1 + (R/F)^2}}$$

$f(R)$  = aperture taper function

in the plane of scan  $\phi = \phi_0$  and we have

$$g(\theta, \phi_0) = \int_0^{R_m} \int_0^{2\pi} f(R) e^{jkR[v_0 - v(1-e\Delta t)] \cos(\phi_0 - \phi') + jk\epsilon''} R dR d\phi' \quad (32)$$

where  $v_0 = \sin \theta_0$

$v = \sin \theta$

since " $\epsilon''$ " is a function only of  $R$  the " $\phi$ " integration can be performed with the result:

$$g(\theta, \phi_0) = \int_0^{R_m} f(R) J_0[kR(v_0 - v(1-e\Delta t))] e^{jk\epsilon''} R dR \quad (33)$$

where  $J_0(x)$  is the zero order Bessel Function

The beam maximum occurs at " $\hat{\theta}$ "

$$\sin \hat{\theta} = \frac{\sin \theta_0}{1 - e\Delta T} \quad (34)$$

or at a slightly larger angle than commanded. The pointing error " $\Delta\theta$ " is then

$$\Delta\theta = e\Delta T \tan \theta_0 \text{ radians} \quad (35)$$

a result independent of the HPBW and the "f" number.

Typical space craft materials have expansion coefficients given as:

<u>Material</u>	<u>e</u>
Kapton	$20 \times 10^{-6}/^{\circ}\text{C}$
Aluminum	$28 \times 10^{-6}/^{\circ}\text{C}$

Taking a  $\pm 100^{\circ}\text{C}$  temperature change we have a beam pointing error of  $\pm 2.5$  milliradians ( $0.14^{\circ}$ ) at a scan angle of 45 deg. A 100 meter aperture at L-band has a HPBW of about  $0.2^{\circ}$  so that the effect is not insignificant. The beam pointing error caused by uniform thermal expansion therefore merits consideration for narrow beamwidth arrays scanned to large angles.

We still have to consider the term "ke" in Eq. (33).

This term

$$k_e = \frac{2\pi}{\lambda} (e\Delta T) \frac{R^2/F}{\sqrt{1 + (R/F)^2}} \quad (36)$$

is a parabolic type radial phase error considered in Fig. 9 where a quarter wave rim displacement caused a tolerable gain degradation (about 1 dB). Setting this as a criteria we have the relation:

$$\left(\frac{F}{D}\right)\left(\frac{\lambda}{D}\right) = \frac{e \Delta T}{\sqrt{1 + (D/2F)^2}} \quad (37)$$

where "D" is the array diameter.

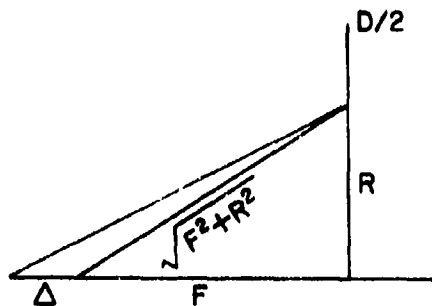
For a 400 wavelength aperture (100 m at L-Band) we have an allowable temperature change of  $\pm 112^{\circ}\text{C}$  for a unity "f" number system. We note larger "f" numbers permit larger antenna diameters measured in wavelengths.

It is evident that thermal expansion will set a limit on the antenna size in wavelengths unless some means of phase correction is employed.

## 8. FEED DISPLACEMENT

### 8.1 Axial

Due to faulty deployment or thermal expansion of the feed supports the feed may not be in its correct axial position. Considering an axial displacement, " $\Delta$ " from the focal point, we have for the path length error (PLE)



$$PLE = \left[ \sqrt{(F+\Delta)^2 + R^2} - (F+\Delta) \right] - \left[ \sqrt{F^2 + R^2} - F \right] \quad (38)$$

where the second bracketed term is the phase shifter correction programmed for the correct focal position. For small displacements:

$$PLE = \Delta \left[ \frac{1 - \sqrt{1 + (R/F)^2}}{\sqrt{1 + (R/F)^2}} \right] \cong \frac{\Delta}{8} \left( \frac{D}{F} \right)^2 \quad (39)$$

which is a quadratic type error for which we can choose the quarter wave criteria at the rim for a 1 dB loss and we have:

$$\Delta = 2\lambda \left( \frac{F}{D} \right)^2 \quad (40)$$

The axial tolerance, therefore, increases as the square of the "f" number and is about two wavelengths for F=D.

## 8.2 Lateral

On the assumption that the unipod feed support (required for deployment) remains straight but is depressed by an angle "α" an aperture phase error is created given by:

$$\psi(r, \phi') = \frac{2\pi f D}{\lambda} \left[ \left\{ 1 + \left( \frac{r}{2f} \right)^2 - \frac{r}{f} \sin \alpha \cos \phi' \right\}^{1/2} - \left\{ 1 + \left( \frac{r}{2f} \right)^2 \right\}^{1/2} \right] \quad (41)$$

The beam shift and pattern degradation can be computer calculated using this expression. However, a tolerance can be set on "α" as it can be shown by expansion of Eq. 41 that the beam pointing error (BPE) is "α" essentially independent of the f number. The allowable BPE, therefore, sets the tolerance on the permitted lateral feed displacement.

## 9. THREE DIMENSIONAL ARRAYS AND PHASE COMPENSATION

A space fed array with axial surface distortions forms a three dimensional array of elements. This is a form of conformal array where the element location conform to the distorted lens surface. Other forms of conformal arrays such as those mounted on a sphere or cylinder frequently exhibit high sidelobes in the farout angular region even though the near in sidelobes show the expected sidelobe behavior. This condition, belately realized, led us to question the assumption, originally made in this report, that the pattern degradation will be confined to the vicinity of the main beam if the distortion spatial period is large. This behavior can be placed in evidence by returning to Eq. 13.

$$\epsilon_a = \Delta_a(r, \phi') \left[ \frac{1}{2} \left( \frac{r}{2F} \right)^2 - 2 \sin^2 \frac{\theta}{2} \right] \quad (13)$$

For small observation angles,  $\theta$ , the effective path length error is considerably smaller than the lens distortion and the lens structure has its alleged distortion insensitivity. However at large observation angles, the effective error approaches the lens distortion and the farout sidelobe level will rise above the low theoretical value. It is, therefore, necessary to examine the complete pattern in the forward half space. To do this a specific array must be examined. To limit computation time we have chosen a 32 wavelength square grid (3217 elements, 38.85 dB gain and  $2.24^\circ$  HPBW) and with our

Gaussian taper.

Another consideration that arises due to our three dimensional array is the problem of array directivity (loss-less gain). The directive gain should be calculated from

$$G = \frac{4\pi p(\theta_0, \phi_0)}{\int_0^\pi \int_0^{2\pi} p(\theta, \phi) \sin\theta d\theta d\phi} \quad (42)$$

where  $p(\theta, \phi)$  is the power pattern in all space

$p(\theta_0, \phi_0)$  is the power pattern at beam peak. The gain reduction shown in all of the previous graphs is the reduction of all the element contributions at beam peak taken as a vector sum. For a discussion of the two methods of gain computation see reference [4].

Conformal arrays are normally phased cohered to radiate a plane wave in the desired scan direction. This technique can also be applied to a distorted lens array if the element locations are known. Their position can be determined by a laser radar located at the focal point or by other means. As the distortions are expected to be smooth and of long correlation length only a reasonable number of survey points are required to determine the distorted surface. To determine the phase compensation required to cohere the distorted array we return to Eq. 11 for the effective phase error.

$$\frac{2\pi}{\lambda} \epsilon_a = \frac{2\pi}{\lambda} \Delta_a(r, \phi') \left[ \cos\theta - \frac{1}{\sqrt{1 + (r/2f)^2}} \right] \quad (11)$$

To cohere the array at an observation angle  $\theta_0$ , we apply a phase correction (function of aperture coordinates and desired scan angle  $\theta_0$  only).

$$\text{Phase Correction} = - \frac{2\pi}{\lambda} \Delta_a(r, \phi') \left[ \cos \theta_0 - \frac{1}{\sqrt{1 + (r/2f)^2}} \right] \quad (43)$$

The residual phase error becomes:

$$\text{Residual Phase} = \frac{2\pi}{\lambda} \Delta_a(r, \phi') [\cos \theta - \cos \theta_0] \quad (44)$$

which vanishes at the cohered angle but which remains significant for angles far from the compensated angle.

To avoid the double integration of the radiation pattern required by Eq. 42, we have chosen an azimuthally symmetric distortion (Radial ripple) specified by

$$\Delta a(r) = a \sin 1.5\pi r \quad (45)$$

We show in Figs. 87, 88, and 89 the radiation patterns for  $a = 0, 2$ , and 5 wavelengths. The two wavelength case shows the degradation of the near-in sidelobes, the five wavelength case we see further degradation and a farout sidelobe near isotropic levels.

The array was then phase cohered for boresight radiation. Fig. 90 ( $5\lambda$  distortion) shows that the undistorted main beam

-3-21124

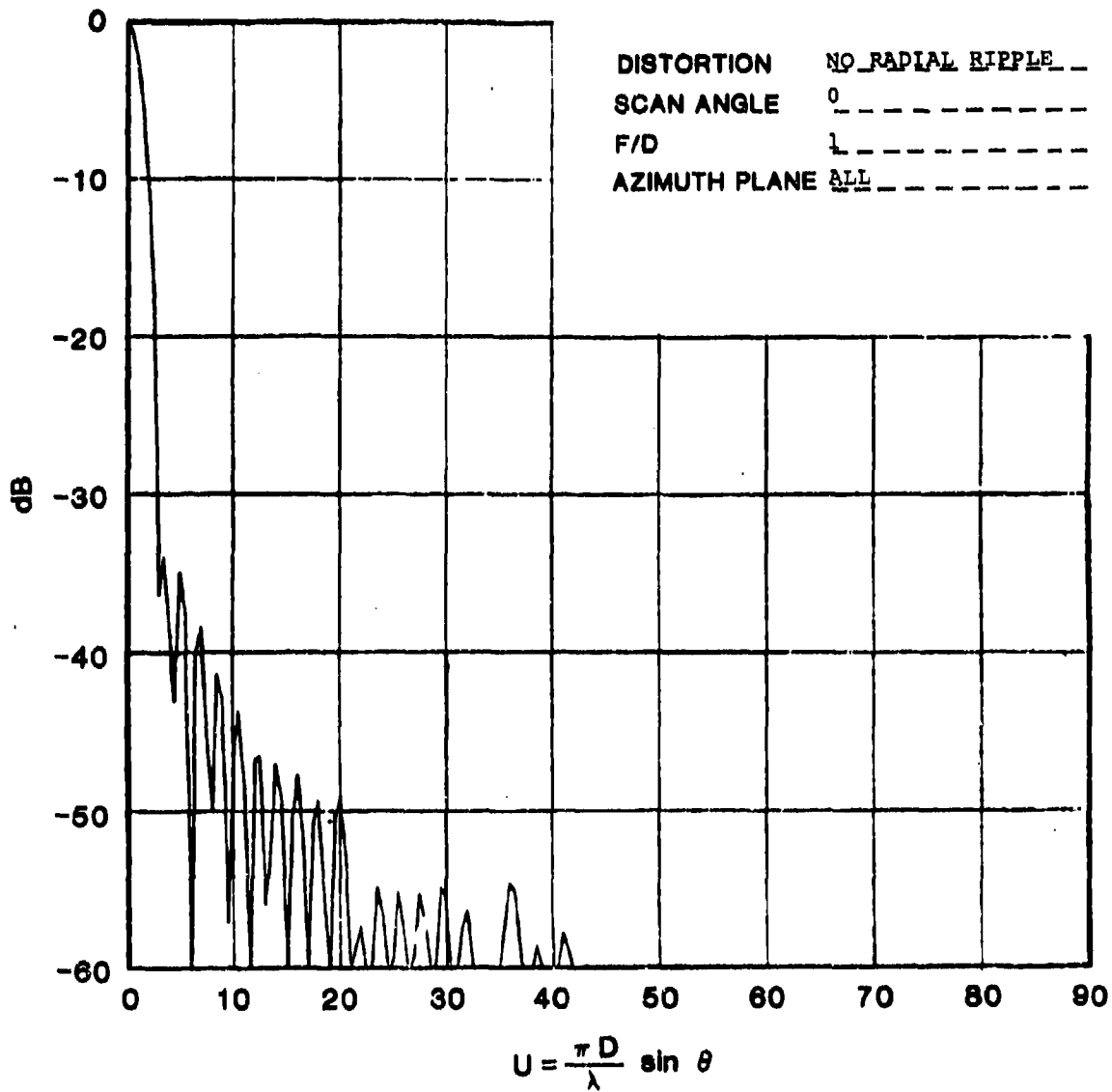


Fig.87. Radiation pattern of space fed array  
Gaussian taper  $f(r) = e^{-2r^2}$ .

-3-21125

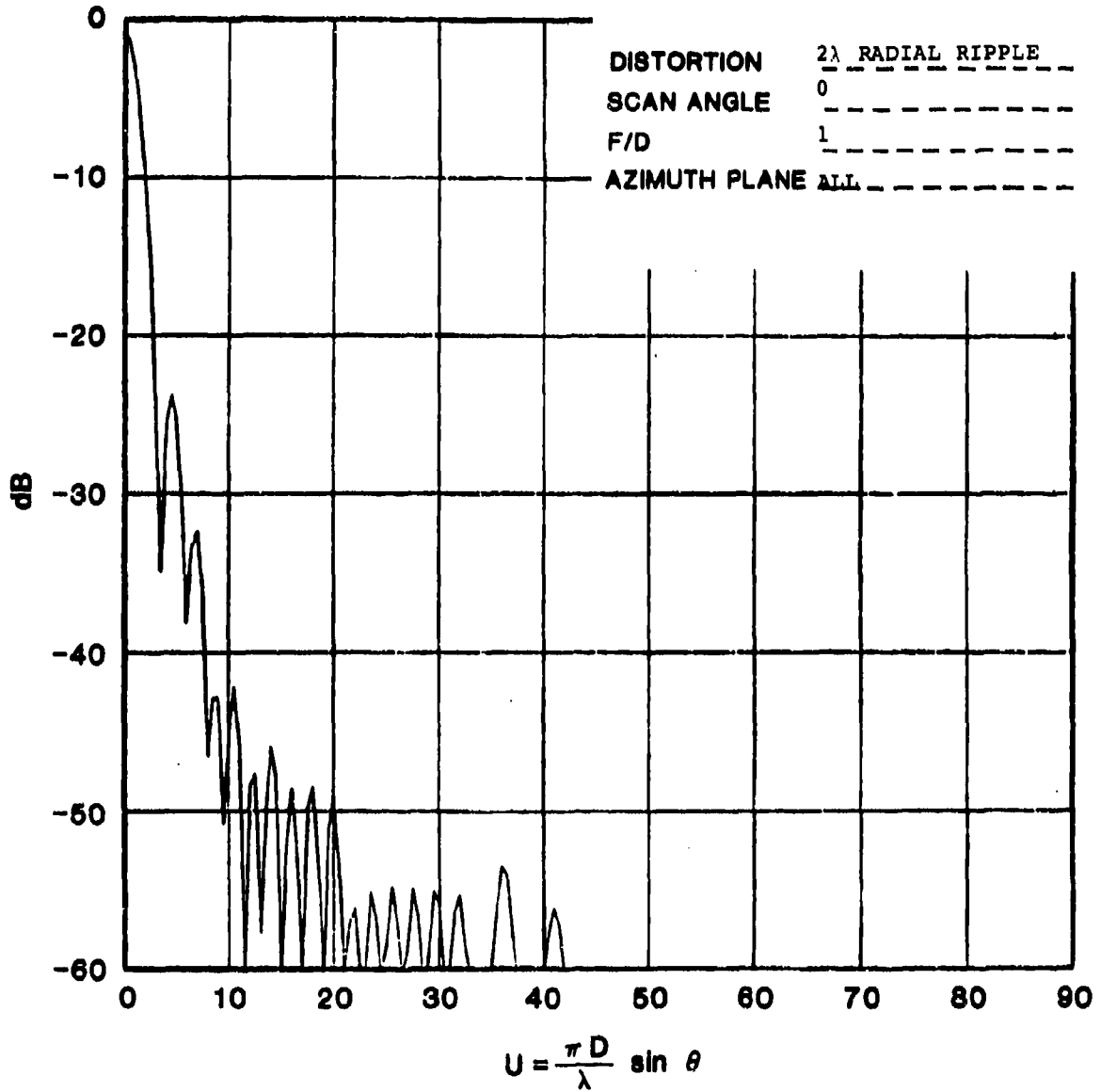


Fig. 88. Radiation pattern of space fed array  
Gaussian taper  $f(r) = e^{-2r^2}$ .

-3-21126

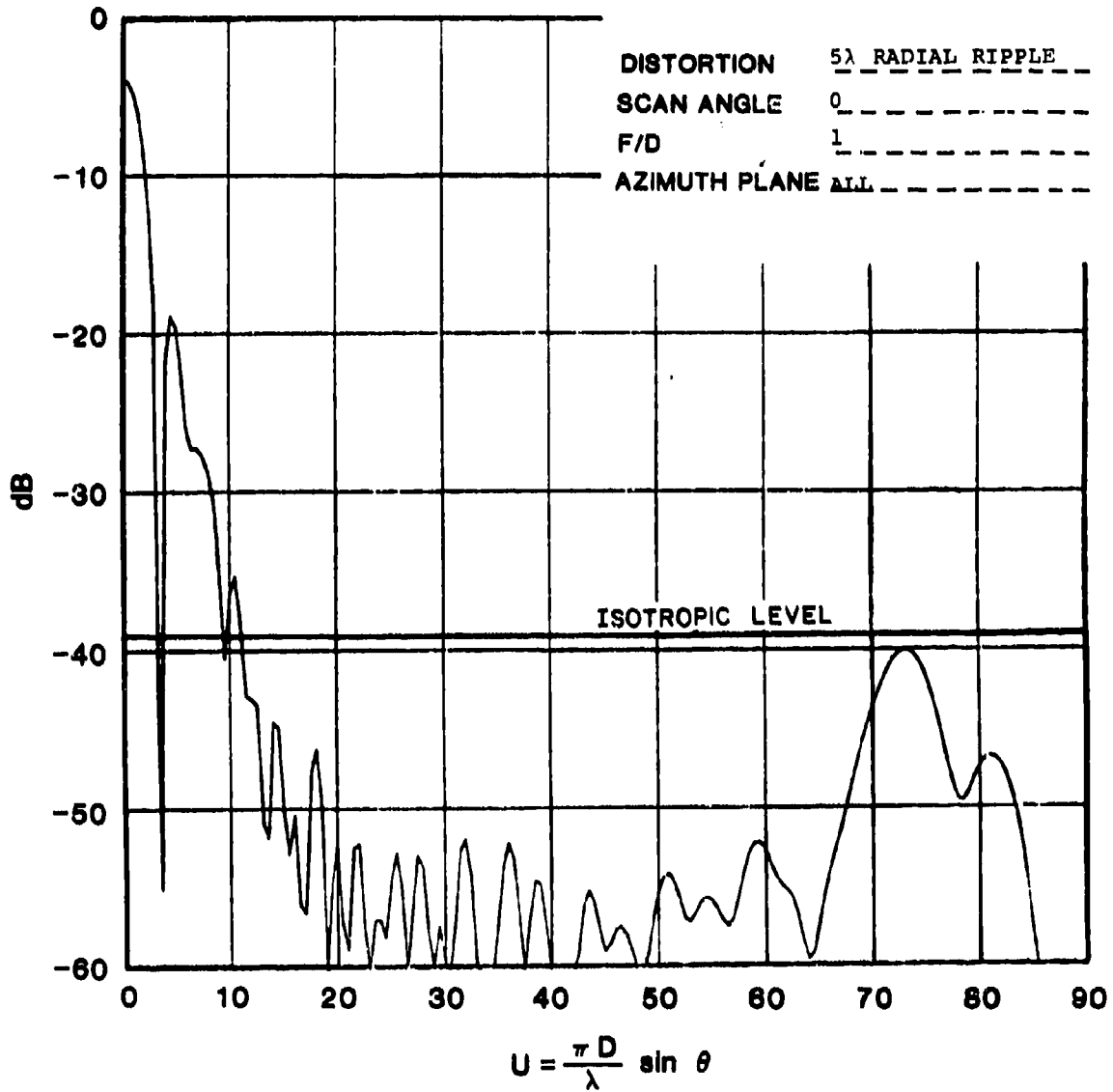


Fig. 89. Radiation pattern of space fed array  
Gaussian taper  $f(r) = e^{-2r^2}$ .

-3-21127

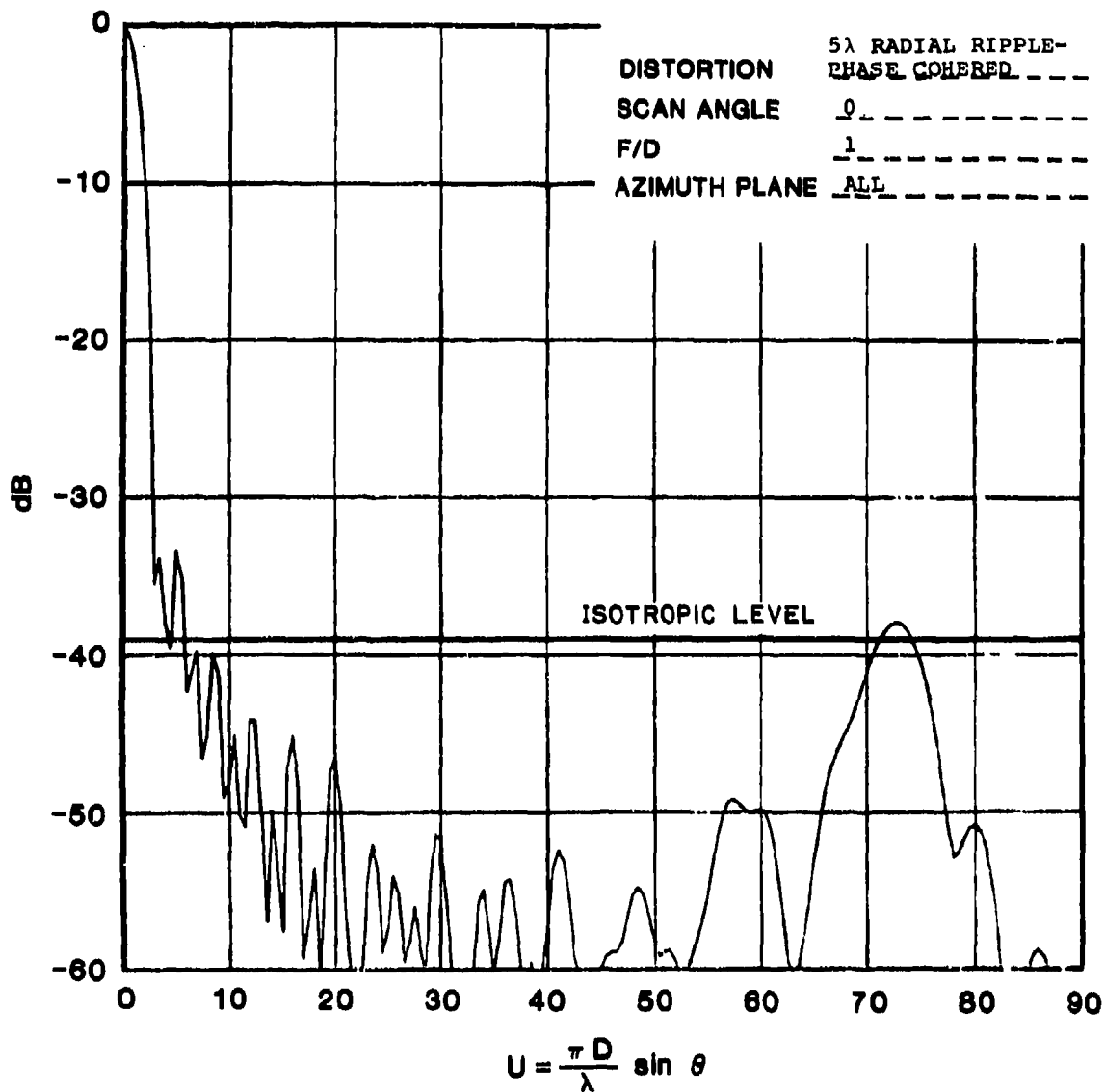


Fig. 90. Radiation pattern of space fed array  
Gaussian taper  $f(r) = e^{-2r^2}$ .

gain and beam shape was recovered but the farout sidelobe degradation remained. A cosine square element power pattern is included in these calculations.

From the computer printouts we summarize some data of interest:

Uncompensated

a	Gain Loss*	Gain**
0	0.00 dB	38.97 dB
1 $\lambda$	0.20	38.77
2 $\lambda$	0.77	38.20
5 $\lambda$	3.85	34.95

Phase Compensated (cohered)

1 $\lambda$	0.00 dB	38.97 dB
2 $\lambda$	0.00	38.97
5 $\lambda$	0.00	38.68

---

\* From summation of elements in phase and magnitude

\*\* From pattern integration

We note that the gain loss obtained by summing the element contributions and that by pattern integration agree rather well, especially for reasonable distortions justifying the previous work in the body of this report. When the array is boresight phase coherent the gain loss is only 0.3 dB with the five wavelength distortion.

Another item of interest is the distribution of the radiated energy shown in Fig. 91. For the undistorted array, due to the high illumination taper, essentially 99% of the energy is in the main beam. With a five wavelength uncompensated distortion this is reduced to about 80%; phase compensation increases this to about 93%.

32λ CIRCULAR APERTURE

TAPER  $e^{-2r^2}$

RADIAL RIPPLE DISTORTION

$Z = A \sin 1.5\pi r$

-3-21128

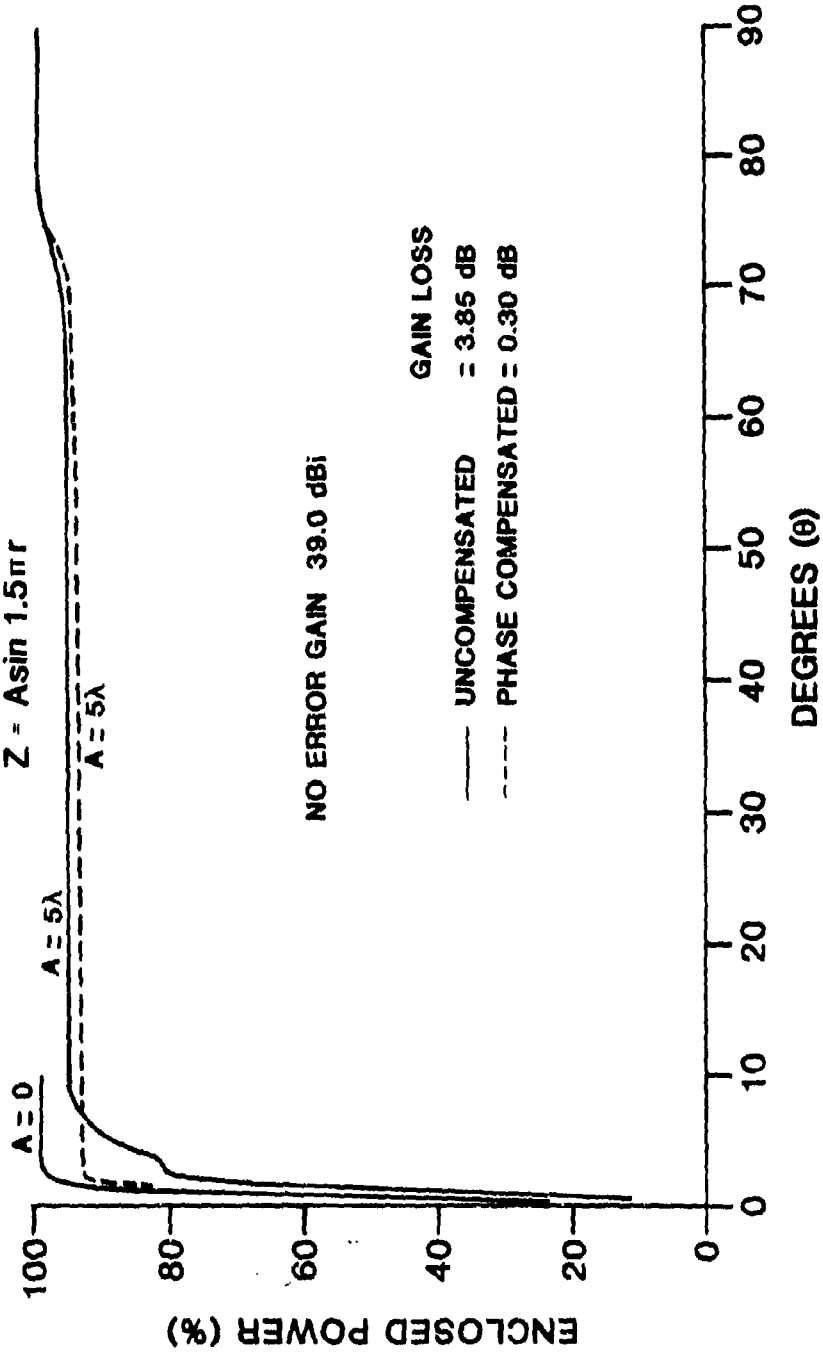


Fig. 9L. Enclosed power vs polar angle.

## 10. CONCLUSIONS

### 10.1 Electrical and Structural Defects

Various electrical and structural defects that cause antenna pattern degradation have been examined. The results may be summarized as:

#### 10.1.1 Electrical

##### 1. Element Excitation Errors

Well known antenna tolerance theory indicated that to achieve a -10 dBi average sidelobe level requires a 10 electrical degree rms or a 1.5 dB amplitude rms tolerance. Combination of errors is indicated in Fig. 4. This desired SLL level will be difficult to achieve.

##### 2. Element Failure

A 3% element failure will cause an average SLL of -10 dBi with no other electrical defects. This degree of reliability may be difficult to achieve over the projected life of the space craft.

#### 10.1.2 Structural

##### 1. Axial Array Distortions

It was shown that a space fed array is comparatively insensitive to axial surface distortions compared to other antenna types. Many canonical distortions were examined. Although the pattern degradations differ, a general tolerance on flatness can be stated as plus or minus one wavelength for unity f numbers. Larger f numbers reduce the main beam and near-in sidelobe pattern degradation.

## 2. Radial Array Distortions

Uniform thermal expansion causes a beam pointing error and a loss of main beam gain. The beam pointing error is proportional to the tangent of the array scan angle and is independent of the array HPBW and the f number. The gain loss is independent of the scan angle but increases with array diameter in wavelengths and decreases with increasing f number. For typical spacecraft material having a thermal coefficient of expansion of  $25 \times 10^{-6}/^{\circ}\text{C}$  temperature change causes a  $+ 25 \text{ mrad}$  ( $0.14^{\circ}$ ) beam pointing error at a  $45^{\circ}$  scan and a 1 dB gain loss for a 400 wavelength diameter array with unity f number.

## 3. Axial Feed Displacement

The permitted axial feed displacement increases as the square of the f number. For a one dB gain loss and unity f number the axial feed tolerance is two wavelengths.

## 4. Lateral Feed Displacement

A lateral feed displacement produces a beam squint or a beam pointing error equal to the angular feed displacement independent of the f number.

### 10.2 Phase Compensation

Element excitation errors or failed elements cannot in general be corrected. Uniform lens thermal expansion or axial feed displacement due to thermal expansion can be corrected with thermal sensors and quadratic phase corrections stored in the module microprocessor memory. Axial lens distortions are more

difficult to compensate as the distorted lens surface must be measured and the element-modules independently addressed with the required phase correction. This phase coherence is a function of the scan angle. It essentially restores the main beam gain and the near-in low sidelobes. It does not affect the farout sidelobe degradation caused by large axial lens distortion.

### ACKNOWLEDGMENTS

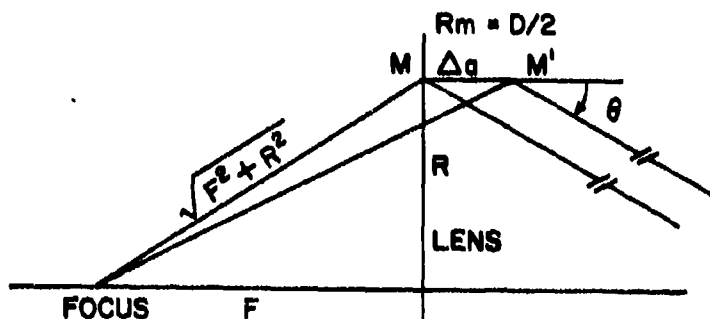
I am indebted to Joseph Zeytoonian for computer programming, to William Steinway for the use of his graphics program, and to David Bernella and Edward Barile for informative discussions. Finally, my thanks go to Linda Theobald for preparing this manuscript.

#### REFERENCES

1. P. M. Morse, Vibration and Sound (McGraw-Hill, New York, 1936), 1<sup>st</sup> edition, pp.147-160.
2. R. C. Hansen, Microwave Scanning Antennas Vol. I (Academic Press, New York, 1964).
3. R. C. Collin and F. J. Zucker, Antenna Theory, Part I, Chapter 6, "Non Uniform Arrays " (McGraw-Hill, New York, 1969) pp. 227-233.
4. R. C. Rudduck, and D. C. F. Wu, "Directive Gain of Circular Taylor Patterns," Radio Sci. 6, pp. 1117-1121 (1971).

APPENDIX

A-1 Axial Displacements



Element module at M provides a phase to:

- 1) Correct the spherical wavefront from the focus; that is provide a phase correction of:

$$\frac{2\pi}{\lambda} \left[ \sqrt{F^2 + R^2} - F \right] \quad (A1)$$

- 2) Scan the beam to  $(\theta_0, \phi_0)$ ; that is provide a phase

$$\frac{2\pi}{\lambda} R \sin \theta_0 \cos (\phi - \phi_0) \quad (A2)$$

When the element module suffers an axial displacement,  $\Delta_a$  the above module functions remain unchanged. However, the module is excited by a path length delay (error) of:

$$\sqrt{(F + \Delta_a)^2 + R^2} - \sqrt{F^2 + R^2} \approx \Delta_a F / \sqrt{F^2 + R^2} \quad (A3)$$

where the expansion is valid for  $\Delta_a \ll F$ .

Eq. A3 may be written as:

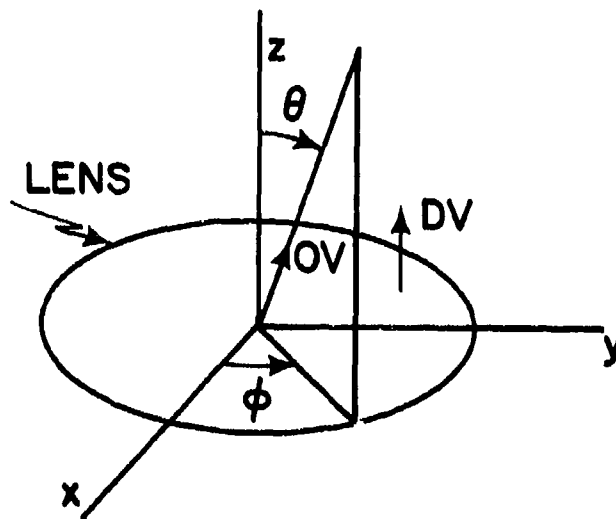
$$\frac{\Delta a}{\sqrt{1 + (r/2f)^2}} \quad (A3)$$

where  $r$  = normalized radial coordinate

$f = F/D$ , the system  $f$  number

There is also an error term in the direction of observation

$(\theta, \phi)$



$\overline{OV}$  is the observation vector =  $\sin \theta \cos \phi \overline{x} + \sin \theta \sin \phi \overline{y} + \cos \theta \overline{z}$

$\overline{DV}$  is the displacement vector =  $a \Delta \overline{z}$

The additional path length advance of

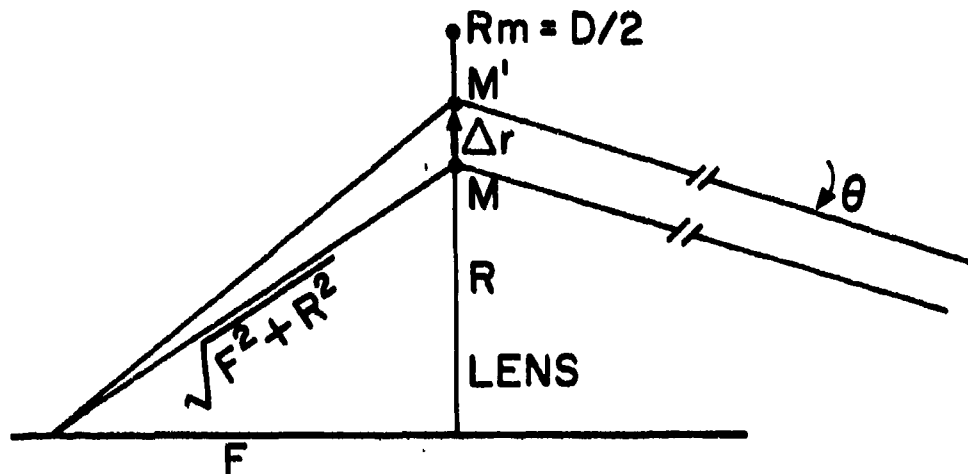
$$\overline{OV} \cdot \overline{DV} = \Delta_a \cos \theta \quad (A4)$$

The total path length advance is then

$$\epsilon_a = \Delta_a \left[ \cos \theta - \frac{1}{\sqrt{1 + (r/2f)^2}} \right] \quad (A5)$$

This result was first derived in the Grumman-Raytheon study.

A-2 Radial Displacements



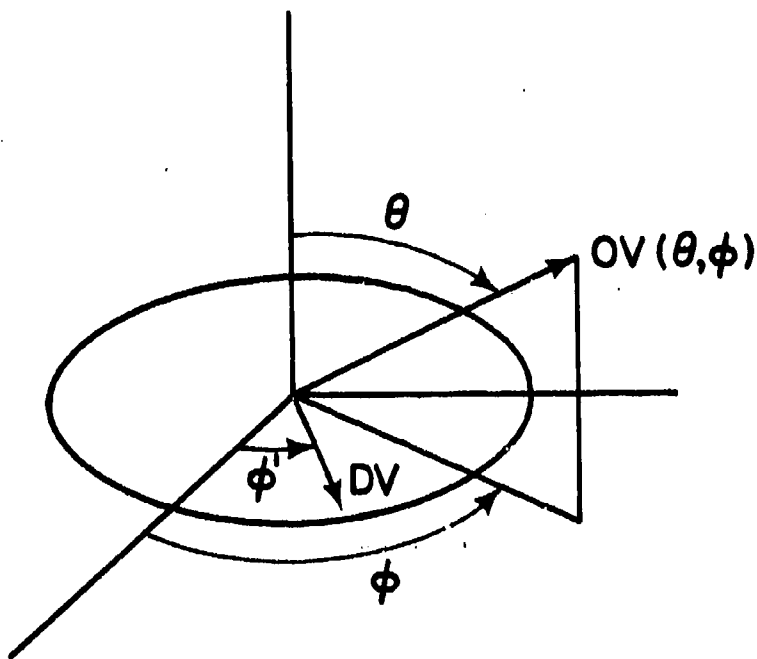
when a module suffers a radial displacement,  $\Delta_r$  a path length delay is incurred of:

$$\sqrt{F^2 + (R + \Delta_r)^2} - \sqrt{F^2 + R^2} \quad (A6)$$

Which may be written, for  $\Delta_r \ll F$  as:

$$\Delta_r \frac{(r/2f)}{\sqrt{1 + (r/2f)^2}} \quad (A7)$$

Similarly to the axial displacement a component in the direction of observation  $(\theta, \phi)$  is incurred.



Observation vector  $\overline{OV} = \sin \theta \cos \phi \overline{x} + \sin \theta \sin \phi \overline{y} + \cos \theta \overline{z}$

Displacement vector  $\overline{DV} = \Delta_r \cos \phi' \overline{x} + \Delta_r \sin \phi' \overline{y}$

path length advance =  $\Delta_r \sin \theta \cos (\phi - \phi')$

The total path length advance is then

$$\epsilon_r = \Delta_r \left[ \sin \theta \cos (\phi - \phi') - \frac{r/2f}{\sqrt{1 + (r/2f)^2}} \right] \quad (\text{A8})$$

